CNEA NT - 3/84

Progress Report
1982 - 1983
Department of Physics

Comisión Nacional
de Energía Atómica

Dirección de
Investigación y Desarrollo

Gerencia de
Investigaciones

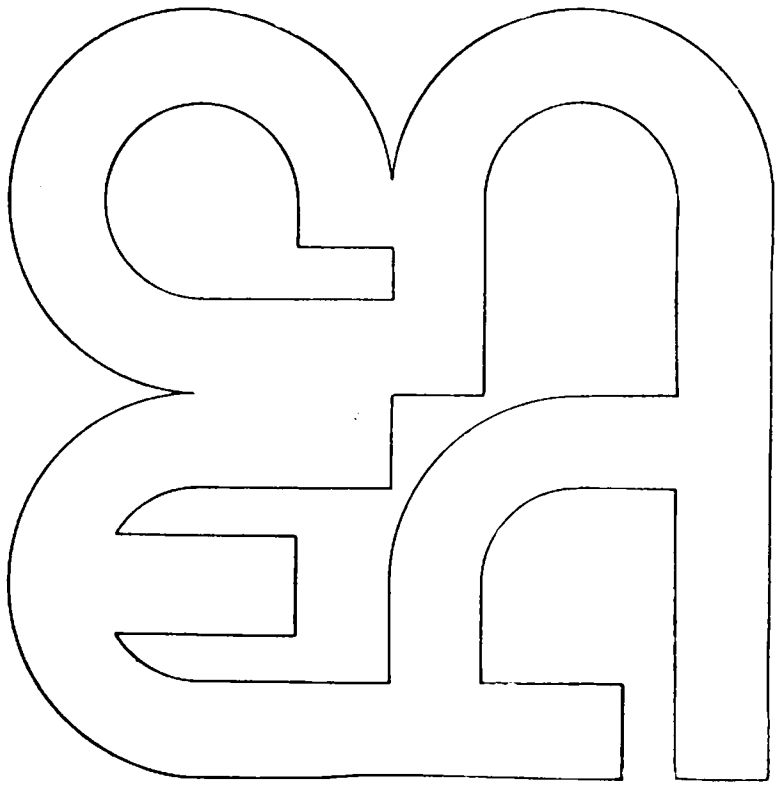

Buenos Aires - Argentina
1984

CNEA NT - 3/84

Progress Report
1982 - 1983
Department of Physics

Comisión Nacional
de Energía Atómica

Dirección de
Investigación y Desarrollo

Gerencia de
Investigaciones

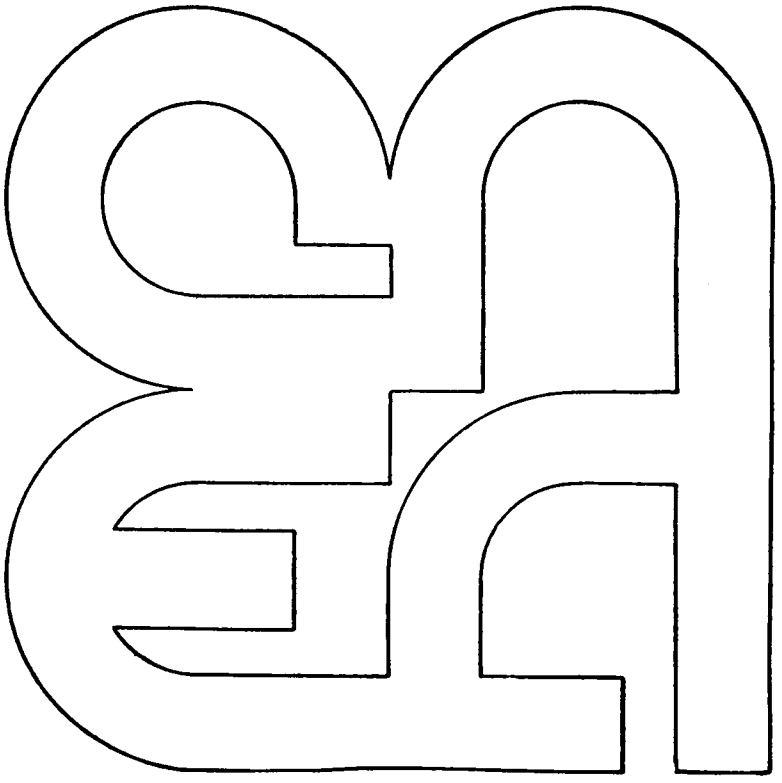

Buenos Aires - Argentina
1984

Introduction

Both 1982 and 1983 have been very particular years for our country and the important events occurred in it have necessarily had an impact on our Physics Department.

The increasing economic difficulties, particularly in the foreign commerce, aggravated by the conflict in the South Atlantic, significantly affected the TANDAR Proyect, since it was still in an execution stage. Nevertheless, during 1982 the local works could be concluded making it possible to perform, in April 1983, the voltage tests. During the tests the interesting value of 24.7 MV at the terminal was reached and that result could be announced to the International Conference on Electrostatics Accelerators taking place at that time at Daresbury, England. Immediately after, the acceleration tubes were assembled and vacuum tested. Some difficulties appeared with components of the pumping stations, in particular regarding the sublimation pumps. At the same time several repairs and improvements were accomplished on equipment located at the terminal, such as the charge selector, and also strong progress was obtained in the installation of the control system.

At the end of December 1983, the last steps were given to have everything ready for vacuum testing the tubes, this time under SF_6 presure in the tank and subsequently repeating voltage tests with the acceleration tubes and the first beam passing throughout the machine.

We are deeply concerned by the present difficulties to import equipment for the implementation of the experimental lines. In the solution of this problem, strong efforts are being applied so as to obtain maximum participation of local industries. An important decision regarding this problem has been to contract with INVAP S.E. the local construction of the magnetic spectrometer whose acquisition from Sweden was impossible to conclude.

The very successful experience offered by the training program mentioned in the Introduction of our last Report, induced the Department to organize on a stable basis, a post-graduate school. The first group of fellowships have been already awarded and the corresponding courses and research work will begin during January 1984.

During the period, the annual nuclear physics workshops continued to be organized with the active participation of Latin-american colleagues and the collaboration in 1982 of J.Ball and J.Axe from Oak Ridge National Laboratory, H.Mang from Münich University, and R.Levine from Hebrew University.

The 1983 workshop, though more limited regarding the external participation, constituted a relevant event since it was in fact the first time the Conference Room at the top of the new building's tower was used. Since March 1983, the majority of the Physics Department moved into the new building with the exception of the Solid State Division, which has to wait until the Sector B of the same building can be constructed. This Division improved its room facilities at the CNEA's main site moving part of its equipment into some of the laboratories left by the nuclear groups.

Despite of the increasing economic difficulties it was also possible to continue the collaboration iniciated during previous years with research groups from local universities and with foreign laboratories.

The result of the efforts developed during these two years can be seen through the following pages. Against our wishes and what was our hope when we were preparing our last Report, we have not been able to present in this one any work done with the Heavy Ion Accelerator. We trust to do it in the next one.

There is a fact occurred during this period which could call the attention to anyone not knowing very well our group. There is a new name at the end of this Introduction, thus meaning a change at the head of the Physics Department. Such a change has no other meaning than a redistribution of duties between its members. There has not been and it will not be a revision of objectives or politics; I only hope that despite the great increment in personnel produced during the last ten years, the spirit of the old Nuclear Physics Department of the 50's and 60's could be mantained and consolidated, spirit of excellence and friendship that Mario Mariscotti knew how to improve during his long and successful performance.

I cannot finish this comment without mentioning the particular meaning for those who have been involved in the TANDAR Project, of the second of the important events occurred in the country in this period. The return to democracy gives support to our permanent faith in the future of our country and in its capacity for recovery. It gives us also the satisfaction of having contributed to the excecution of a project which will offer to the new generations of Argentine physicists the possibility of using a powerful tool for their research just when the creative activity is favoured by the air of freedom that we perceive in every aspect of our public and private lives.

Because of her most efficient performance with the previous Report, the editorial work was again asigned to Martha L. Pérez. Once more the collaboration of Mr. Binda for the printing work is highly appreciated; we are grateful to Mrs. M.T.Carmuega and N.Nuñez, Miss L.Blanco and G.Escriva for typing the manuscripts.

Emma Pérez Ferreira
January 1984

I. Tandar

1. Heavy ion Accelerator
2. Laboratories
3. Nuclear Facilities

I.1 HEAVY ION ACCELERATOR

I.1.1 Electromechanical installations for the Tandar Project

N.Fazzini, H.González, J.Nicolai, R.Requejo, S.Tau and E.Ventura

During the years 1982-1983 all the electromechanical installations for the different services of the Tandar Project were performed. Here we will briefly itemize the most important ones, excluding the SF_6 Gas Handling System which has been described in detail elsewhere[1].

All these installations were performed by several contracted firms, and in every case were entirely supervised by CNEA's personnel. The installations are divided in Electrical and Mechanical Installations.

Electrical Installations.

- Assembly and wiring of three (3) 13.2/0.4 KV transformers of 1,500 KVA each.
- Assembly and wiring of over 400 electrical switchboards.
- Normal and emergency building lights.
- Signal and power cables for the accelerator and experimental target areas.

Mechanical Installations.

- Equipment installation and piping for the following services:
  - (a) cooling water
  - (b) demineralized water
  - (c) compressed air
  - (d) instrument air
  - (e) natural gas
  - (f) air conditioning (warm-cold)
  - (g) telephone systems
  - (h) alarm systems
  - (i) fire prevention systems
- Installation of seven (7) shielding doors giving access to the target areas and accelerator tower.

All of these installations and services have been already tested, and are actually under routine operation.

I.1.2. ASSEMBLY OF THE 20 UD HEAVY ION ACCELERATOR

N.Fazzini, H.Gonzalez, R.Requejo, S.Tau, E.Ventura

The column voltage test of the accelerator have been recently performed (April/83). The experiment was designed as to demonstrate the voltage holding capabilities of the column structure at or near the maximum SF_6 pressure consistent with the vessel design and before installation of the acceleration tubes.

Previous to the experiment the generating voltmeter (GVM) was calibrated using a capacitive divider method. The calibration point was set at 2 Mv with the vessel open to air; the error in the method was estimated to be +5%, -8%.

The vessel was pumped down to 0.5 mb and presurized in ten steps with pure SF_6 from 1.3 kg/cm^{2}a (4.2 psig) up to 9.8 kg/cm^{2}a (125 psig). The terminal potential was then slowly raised up to the point of breakdown.

This procedure was repeated for each SF_6 pressure until a reasonable number of sparks were produced and no higher terminal potential could be attained.

The corona current readings of the 20 UD column grading system were compared, with the data taken by NEC for a single gap of three needles and with extrapolation of the data obtained in the 25UR (ORNL) and 20UR (JAERI) accelerators. The 20 UD terminal potentials established from the plots "corona current vs gradient percentege", were within +7%, -15% of the GVM readings. In these conditions the GVM was considered to be representative of the actual potential.

The maximum voltage achieved was 24.72 MV at 80 psig SF_6 pressure. Fig. 1 shows a plot of the terminal potential at breakdown (MV) as a function of the SF_6 accelerator vessel pressure (psig). the maximum and minimum breakdown potential are indicated for each pressure; for the sake of clearity individual points for each spark are not shown: vertical lines indicate the potential range spread. The average has been calculated taking into account all breakdown potentials. Column conditioning considerations may change the shape of the average line.

After the high voltage tests began the mounting of the beam line and associated equipment.

The machine was divided in three main sectors for assembly porpouses:

1) Low energy beam line: between the injector and the accelerator tank, including the pulsing system.
2) Accelerating tubes and associated equipment inside the tank, including rotating shafts, control rods, etc.
3) High energy beam line: between the tank and the analizing magnet exit.

The beam line, including accelerating tubes, was backed and pumped down with the pumping stations. The vacuum in several parts of the beam line have reached the $10^{-9}/10^{-10}$ region.

Acceletator Control:

At the beginning of 1982, 3 out of 7 racks of the main control console were installed at level 53 of the accelerator tower. It was then possible to carry out the column high voltage test and running of the injector with one of the ion sources. Once the test were finished, the racks were moved to their final position in the control room. After that, the console hardwire, general assembly and installation of beam line components took place.

At the present time the injector, most of the beam line components external to the pressure vessel and control rods are fully operational from the control room.

The micro-computer based control ssytem which makes it possible to control parameters that are inside the pressure vessel and bring us the status of the whole accelerator. was bench tested completely. We are now mounting its components and expect to have the entire system running in a few weeks.

Five experimental beam lines have been assembled in the experimental areas. Some equipment was developed at the laboratory for being used in those lines.

Right now the accelerator is ready for conditioning and beam tests.

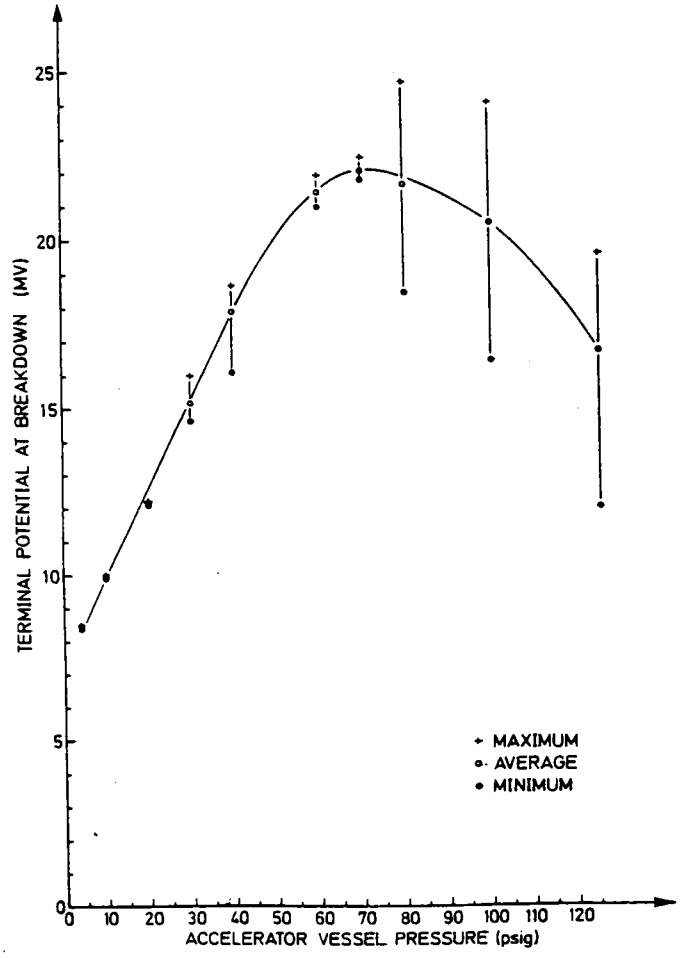

I.1.3 The injector

A.Tersigni and M.González

The injector is a set of instruments enclosed in a cylindrical shape, to obtain and conform negative ions beams which will be later accelerated in the Tandem accelerator.

In order to obtain these beams, the injector is equipped with: the ion source itself, the proper optic to extract, focussing and acceleration of the beams, deflectors steers, Faraday cup and the electrostatic lens to let the beams pass through a 90° analizer magnet.

All these components are polarized with a potential of -300 kV approximately. Finally, there is a preaccelerator tube that accelerates the ions with a final energy of 330 keV after having been separated according to its mass and charge, before entering the Tandar accelerator.

Because of the variety of accelerable ions in this kind of accelerator, it is necessary to count with more than one ion source to obtain a large quantity of ions.

At present the Tandar project is equiped with three sources. Their performance are shown in Table I.

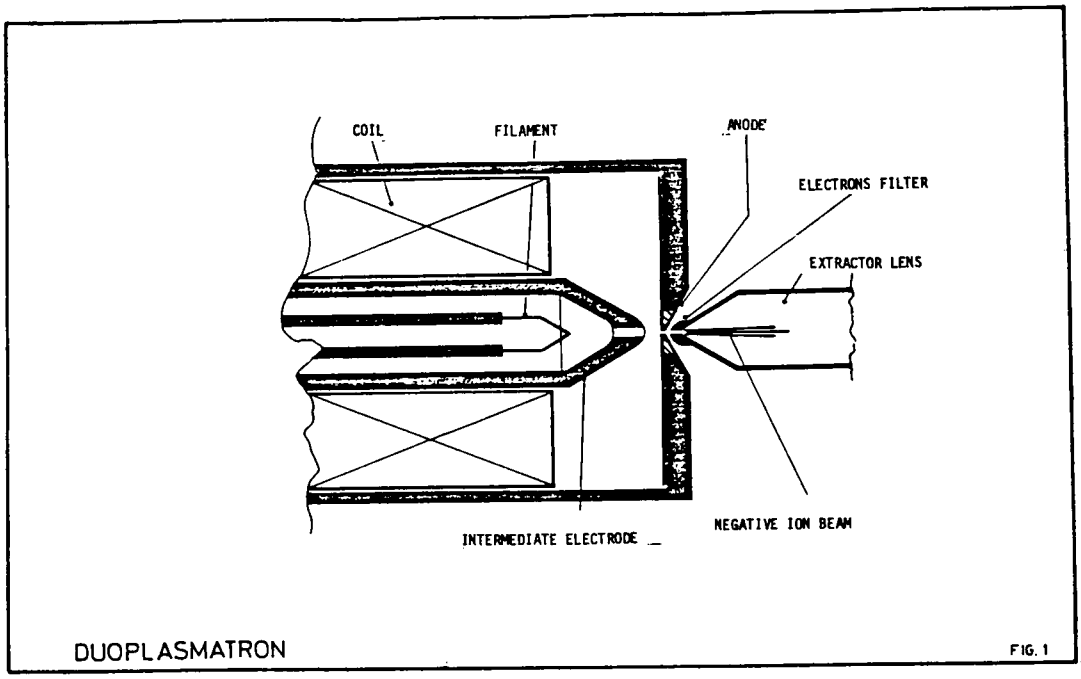

In these three negatives ions sources it is used the conventional principles of ionization, such as:

a) By means of an interchange channel of charges where positive ions can go through the Rb steams.
   The Rb is an element that let free electrons making easier the exchange of charges.
   This source is the Alphatross one (see fig. 2).

b) By means of the sputtering process of Cs positive ions on a conic surface which contains the material to be ionized (see fig. 3).

c) Finally, the direct extraction source or Duoplasmatron, extracts the negative ions from the plasma (see fig. 1).

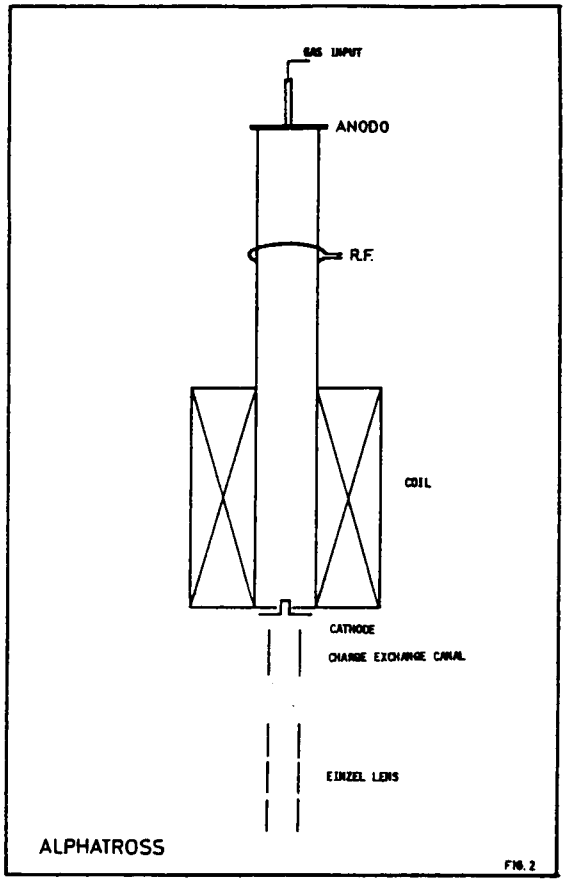

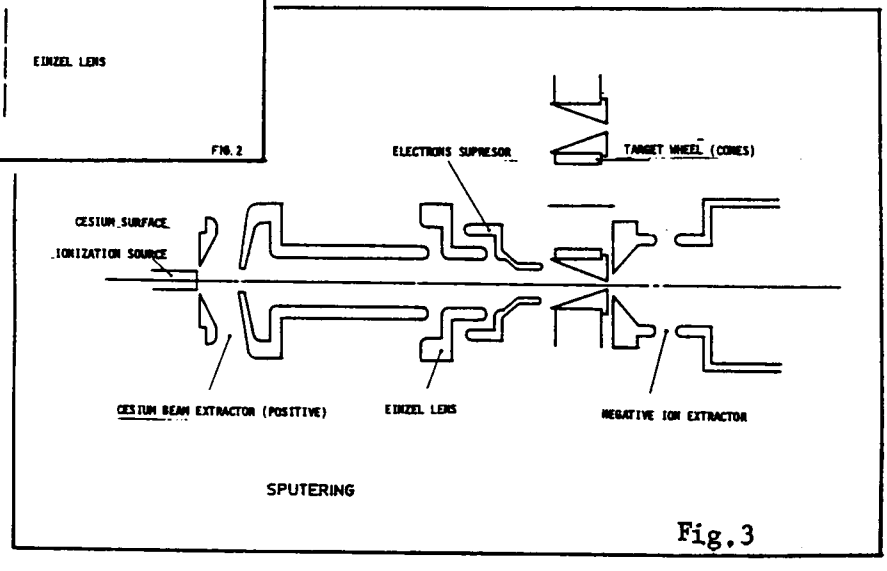

Fig.3

The injector present state and its ions sources:

The alphatross source is assembled mechanically and electrically. At the moment is on the testing bench to the starting of the vacuum system and to prepare the necessary electronic for its right operation.

The Sputtering source is set up in its final place (the injector) to test the performance. At the present time it has been possible to obtain some mA of ^{63}Cu and ^{12}C, with which we hope optimize their parameters and test the different elements shown in Table I since these are the ions expected.

The duoplasmatron source was firstly tested on the testing bench and then in the injector, from a provisional console from the level 53. This source has been tuning with H^-.

The control console was taken to level 0.

Once we obtained the 9 mA beam through the magnetc, we tried with fluor and some mA fluor were obtained, as well as several moleculars beams.

These tests were enough to decide its replacement with the sputtering source, considering that because of the variety of expected ions, this source will be the most required one by the engine users.

WANTED ION BEAMS

ION SOURCE		
Duoplasmatron	Sputtering	Alphatross
H^-	H^-	He^-
O^-	O^-	
F^-	F^-	
I^-	I^-	
Cl^-	Cl^-	
Br^-		
	Li^-	
	S^-	
	B^-	
	C^-	
	Si^-	
	Ni^-	
	Cu^-	
	Au^-	
	NH^-	
	MgO^-	
	AlO^-	
	CaH^-	
	MnO^-	
	FeO^-	
	ZnO^-	
	Ge^-	
	Se^-	
	MoO_3^-	
	CdO^-	
	InO^-	
	WO_3^-	
	ReO_2^-	
	OsO_2^-	
	BiO_2^-	

Table I

I.1.4. SF_6 GAS HANDLING PLANT, ASSEMBLY AND START UP

N.Fazzini, H.González, J.Nicolai, R.Requejo, E.Ventura

During 1982, power and signal wiring of the whole system was performed, as well as panels ans console installation.

The plant was ready for tests by the end of August, and them were carried out during the following two months.

Operation with dry air:

The system was first operated with dry air. The inicial SF_6 inventory was stored in one of the tanks; the other was pressurized with dry air. The test allowed verification of the control pannel including the protection logic which prevents incorrect openings of the electro-pneumatic valves, calibration of all control instruments and elimination of notoroius leaks in the system.

Running of the test was not particulary troublesome: some water accumulations were found in the piping lines and leaks in several blocking valves due to spoiled teflon seals. They are all traced back the cleaning process of the installation. The moisture sensors used in the storage tanks demonstrate to be inadequate and have to be replaced. Only one NORWALK compressor was available for the test: rusting in the cylinders of the other during transportation prevent its operation.

Operation with SF_6:

The first SF_6 transfer test showed a design malfunction of the compressor. Being rated for a suction pressure variable between 1-10 atm the maximum power current was attained at only 4 atm. The solution to this problem consisted in a sequential operation of the three stages of the compressor. Obviously this procedure turned the SF_6 transfer longer than foreseen.

The waste heat of the pumping system and compressor during the SF_6 test was lower than in the case of the operation with air. The safety system consisting of an automatic sequential sensor of SF_6 leaks and O_2 level was calibrated. The second compressor was repaired and made operational with the same restrictions pointed for the other. The installation was ready to run the first SF_6 transfer for the high voltage test of the column structure of the accelerator which was successfully performed on April 1983. The accelerator vessel was first pressurized with SF_6 in 10 steps from 0.35 kg/cm^2 (5 psig) up to 7.0 kg/cm^2 (100 psig). The pressure was then lowered to 5.6 kg/cm^2 (80 psig) and finally raised up to 8.8 kg/cm^2 (125 psig).

The recirculation system was not operated at 8.8 kg/cm^2 (125 psig) because of lower safety calibration values of some of its components.

Conclusions:

The operation of SF_6 gas handling system during the two weeks high voltage column structure test has demonstrated the reliability of the installation.

Its performance fulfills to a large extent the three basic design premises of the system: that is to conserve the SF_6 purity, to be free of significant leaks, and to accoplish a full transfer cycle in about 24 hours.

I.2 LABORATORIES

I.2.1 Target laboratory

A.Ceballos, H.Grahmann and A.Filevich

In the time period covered in this Report the activity in this laboratory has been initiated. About 125 m^2 of room area are being used to install a facility for accelerator target production. The development of a technique to make solid carbon stripper foils is also being carried on by this laboratory.

The laboratory will have commodities for vacuum evaporation electroplating and etching, rolling, and usual laboratory material such as scales, microscopes, high purity water, chemical lab and glass hardware, small cutting and machinning tools for delicate work, measuring instruments, etc. , Most part of this material is available for use but, unfortunately, the main pieces of equipment mentioned above, as well as the separated isotopes stock, are delayed because of difficulties in importation.

At present the basic infraestructure is completed in approximately 70%. However some important pieces are still missing, for instance the fume hood.

Priority has been given to produce solid carbon stripper foils. Because of the high mechanical strength of foils produced by the glow discharge cracking technique in low pressure ethylene it was decided to use this method. The vacuum chamber was designed and built and the auxiliary equipment, such as gas supply and handling system, vacuum pumps, high voltage power supplies, vacuum gauges, safety systems, etc., was acquired.

The first tests yield a number of foils which, we believe, are adequate to be used in the accelerator. The thickness, measured by alpha-particle attenuation, was found close to the required values. Several foils were irradiated in the alpha-particle external beam of the synchrocyclotron to test their mechanical strength. Some foils were sent to the Tandem accelerator, Brookhaven National Laboratory, to be tested in conditions which are closer to those in Tandar terminal.

Standard procedures are being devised for stripper foil production in order to obtain carbon foils in the quality and quantity required by the accelerator.

The main tasks performed in this period were:

- Laboratory and equipment planning and design
- Paperwork for puchasing furniture, equipment and accesories
- Installation of part of the basic infraestructure
- Design and set-up of a vacuum chamber to produce carbon foils
- Fabrication of the first targets made in the laboratory: T10, Tl, ^{121,123}Sb by deposition on adhesives and thin Ta foil by cold rolling.

I.2.2 ΔE-E telescope for the identification of heavy ions

D.E.Di Gregorio, M.C.Berisso, G.Martí and A.J.Pacheco

One of the most common techniques for particle identification is the ΔE-E method where the energy loss, ΔE, and the energy, E, of the products of heavy-ion nuclear reactions are measured. A position sensitive ΔE-E telescope has been designed and constructed. This counter consists of an ionization chamber for the ΔE element and a position sensitive silicon detector for the E element. The elements are housed in a rectangular brass container of approximately 8x9x13 cm^3. An inlet and outlet for the gas flow system and independent electrical feed-through connections for the cathode, Frish grid, anode, and for the energy and position signals of the solid-state detector are provided. Particles enter the detector through an entrance window 0.7 cm high and 3.0 cm long consisting typically of 100 $\mu g/cm^2$ strechted polypropylene.

I.2.3 The design and construction of a system to evaluate Lithium precipitation in germanium detectors

C.Giménez, A. La Terra*, G.Martí

One of the non destructive methods most employed to investigate Lithium precipitation in Germanium detectors, is based on the use of the "thermoelectric probe" (1). This is a hot point of Tungsten that makes contact with the Ge crystal. A thermocouple is then formed between Ge and the Tungsten point. The e.m.f. produced is directly proportional to the thermoelectric power of Germanium since that of Tungsten is negligible. If the point is small enough that power is determined for the impurity concentration in the nearest neighborhood of the probe, then measuring the e.m.f., moving it over the crystal surface changes in the impurities concentration may be determined.

In this form we can precisely find junction positions, their variation, Lithium precipitation localized zones, concentration decreases, etc.

In our particular case it was used to find Lithium diffusion depth in planar HP Ge detectors and to evaluate localized precipitation in the N^+ contact on that detectors and in Ge(Li) detectors also.

The system has a stainless steel support over which slide the crystal holder. It is made of the same material and is in contact with the crystal and advance together.

The movement is controlled with a precision micrommeter screw. The Tungsteng point is located in the extreme of a specially adapted solder to heat the point and this was connected to a high impedance electrometer for the e.m.f. measurements.

Fig.1 shows a diagram plate of the apparatus.

Fig.2 shows two impurities concentration profiles obtained with one of the HP Ge detectors a) inmediately after a Lithium diffusion and b) after a period of time spent at room temperature.

Fig.3 shows a secuence of curves obtained with a Ge(Li) detector after a Lithium diffusion and after succesive periods of time spent at room temperature.

From curve a) of Fig.2 we can obtain lithium diffusion depth and curve b) shows that there were no impurities concentration variation, we then can conclude that there were not Li precipitation despite the fact that it had been more than 3 months at room temperature. We also observed no variation of N^+ I junction position.

In contrast, profiles from Fig.3 shows junction deterioration because of Lithium precipitation and also the shift at the junction position with time.

* Actually address, Dto. Técnico CITEFA

(1) Drift Rate and Precipitation of Lithium in Germanium, IEEE Trans on Nuclear Science NS-13 N° 3 (1966) 245

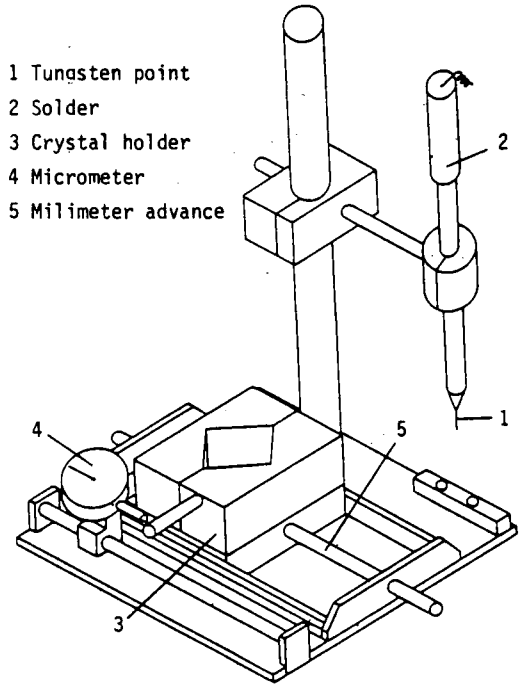

Fig.1: The apparatus to evaluate Lithium precipitation on Germanium detectors.

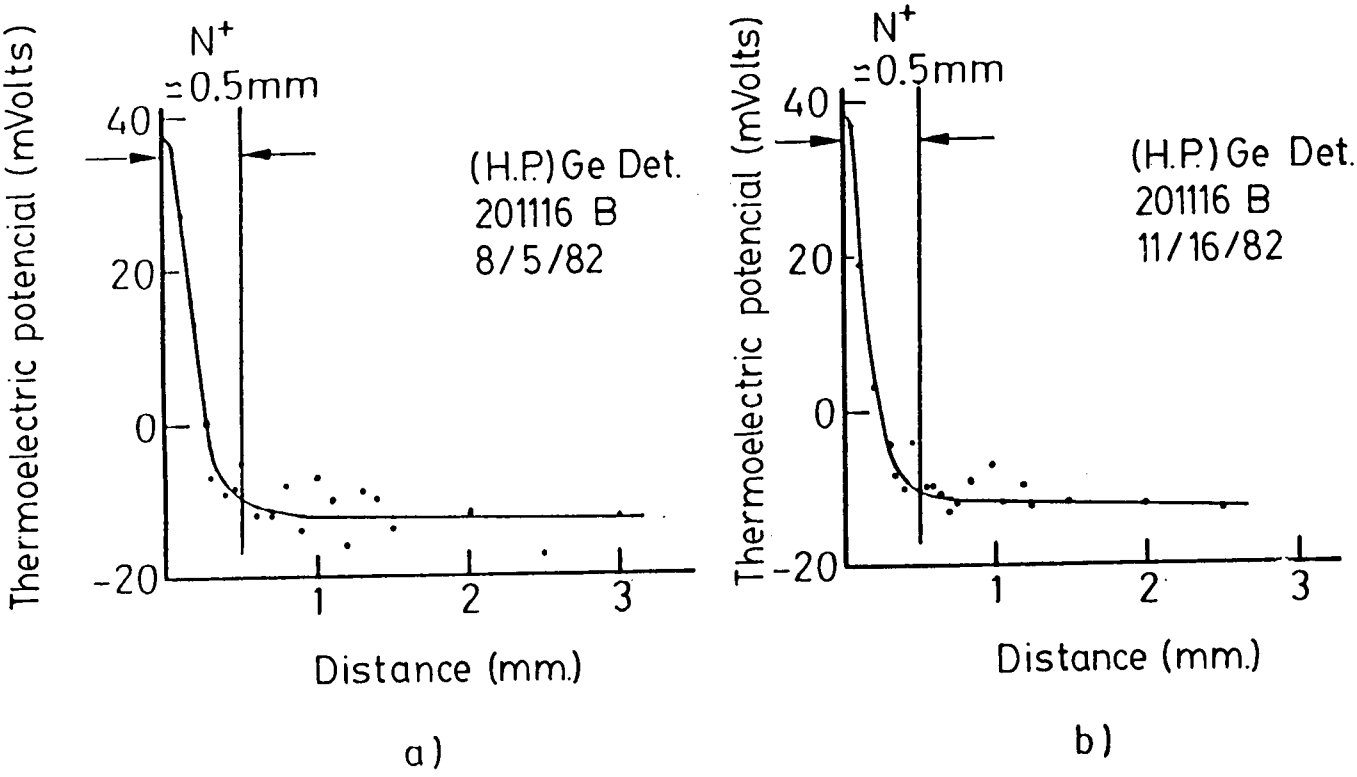

Fig.2: Thermoelectric potential measurements versus distance from crystal surface showing impurities concentration ($N_D - N_A$) profiles on the N^+ contact of a (HP)Ge detector.
a) after a Li^+ diffusion at 330°C
b) after being spent more than 3 months at room tempeture.

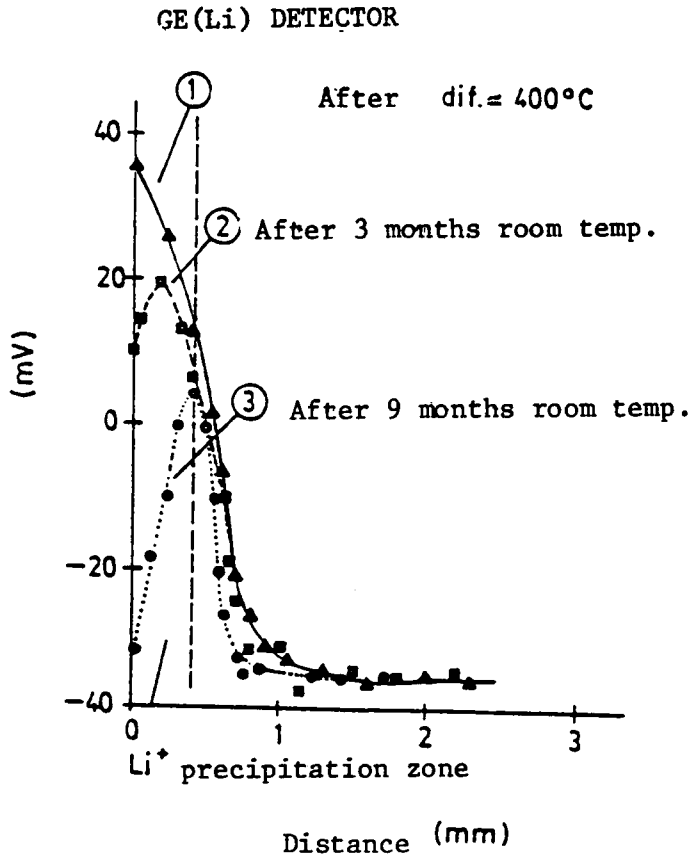

Figure 3:

Thermoelectric potential measurements versus distance from crystal surface showing the variation of the impurities concentration $(N_A - N_D)$ profiles in a Ge(Li) detector with time spent at room temperature.

I.2.4 GENERATING VOLTMETER CALIBRATION USING A CAPACITIVE DIVIDER

D.V.Camin

During the column voltage strength test of the 20 UD tandem accelerator, a calibration of the GVM was required. Formerly the terminal voltage was measured using either resistive dividers or known relationships between the high voltage and corona probe current. In this occasion a capacitive divider formed by the CPO plate and the terminal and a polyestyrene capacitor was used.

The capacitance C_1 existing between the CPO and terminal was determined using the circuit shown in Fig.1.

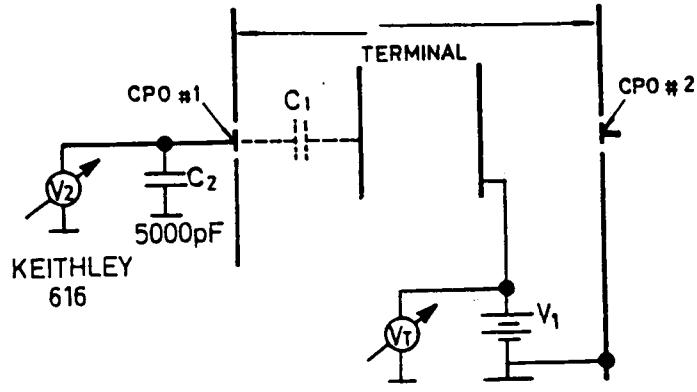

Fig.1

A high voltage power supply V_1 biased the terminal and a very high impedance voltmeter showed an indication V_2 related to C_1 as follows:

$$C_1 = V_2 \ C_2/V_1$$

as C_1 is much smaller than C_2.

Once the value of C_1 was determined (C_1 = 0.0815 pF), the high voltage power supply was disconnected and the terminal potential was raised using the charging system.

A plot giving the indication of the GVM versus V_2 was recorded. Since V_2 is proportional to the true terminal potential, the correction factor for the GVM was determined. The plot is given in Fig. 2.

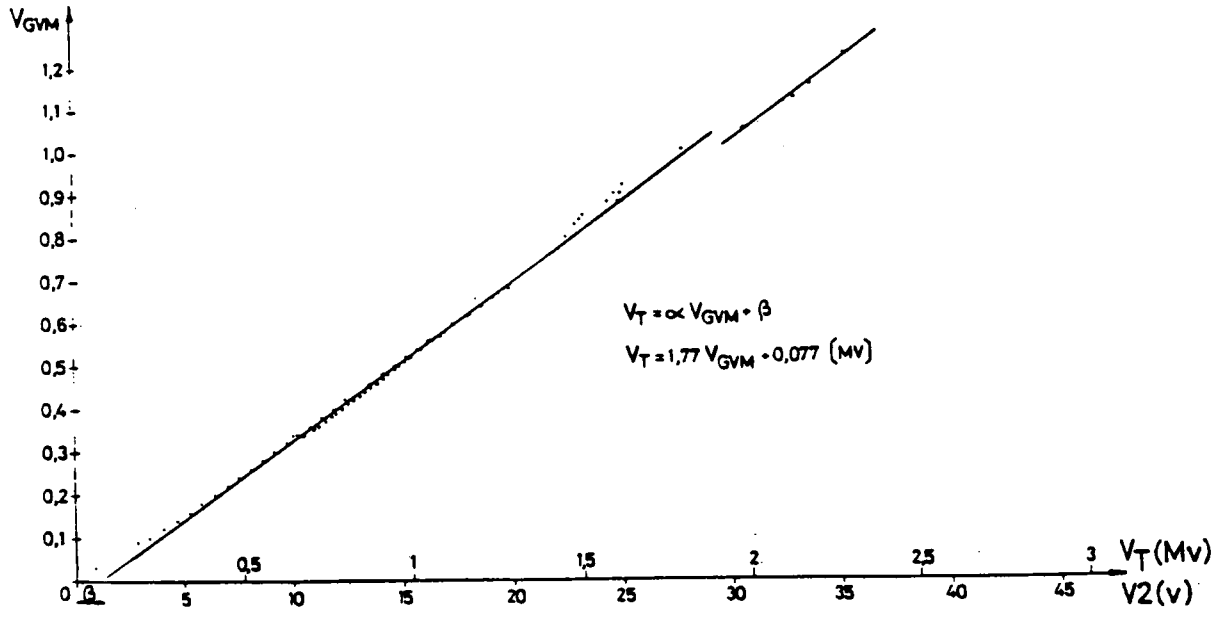

Fig.2

The method showed to be simple and reliable.

The results obtained were very close to those obtained by measuring the corona probe currents. Once the GVM calibration is determined through the measurement of the field strenght of the analyzing magnet, the actual accuracy of this method will be established.

I.2.5 ANALOG TO DIGITAL CONVERTER FOR NUCLEAR SPECTROSCOPY

P.Bianchini*, D.V.Camin, C.Gervai*, A.Kligman*, O.I.Lombardi*, A.López*, M.Satinosky.

A first version of an ADC intended for nuclear measurement ~~have~~ been developed. In the near future a correction using sliding-scale method will be added in order to achieve good diferential linearity.

The ADC consist mainly of two different blocks: the peak stretcher and the conversion block.

The block diagram of the peak stretcher is indicated in Fig.1.

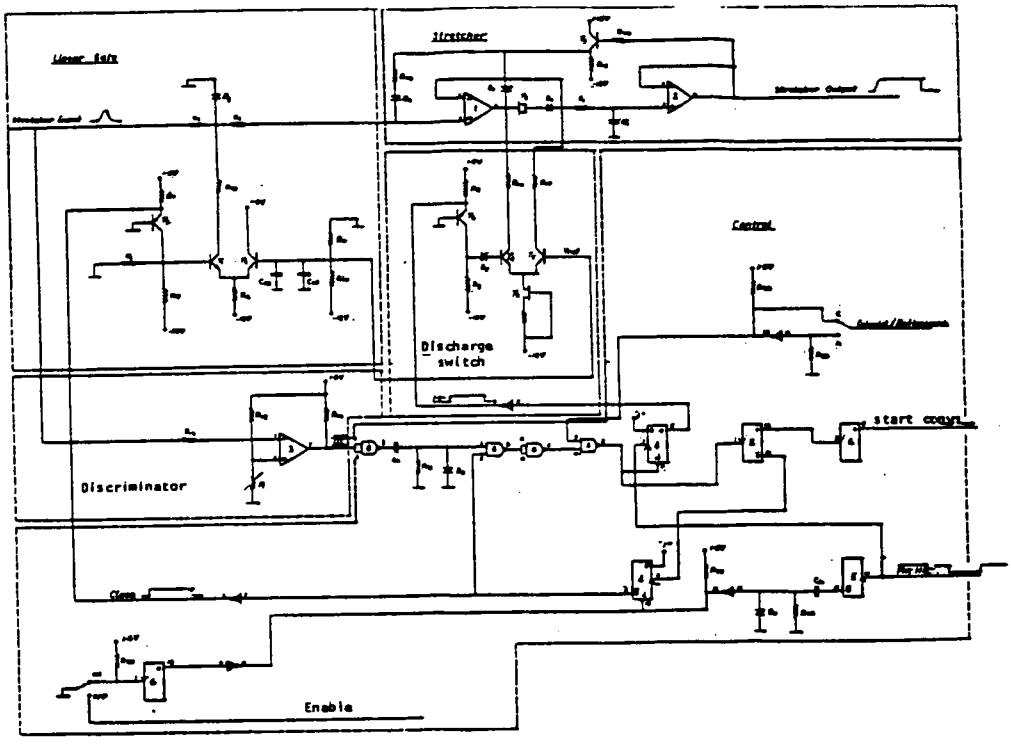

Fig.1: Peak stretcher

* Facultad de Ingeniería, UBA

The stretcher was implemented using LF356 operational amplifiers. The results obtained are satisfactory as a pulse with a 1 μs shaping time can be processed and the stretching time may extend up to 30 μs with no measurable peak drop. The input level extends from 200 mV up to 10V. A coincidence/anticoincidence circuit permits external gating.

The second block, the converter itself was implemented using a 12 bit monolitic converter AD578 which employs succesive approximation technique and a conversion time of 3 μs.

The conversión range can be selected from 5 to 12 bits. A digital back bias extending from 128 to 4K channels can also be selected with a front panel push-button switch. A saturation switch is also located in the front panel.

Fig. 2 shows the block diagram of the conversion block. This block will be subjected to further improvement in the near future to obtain a uniform channel width. For this purpose a sliding scale correction circuit will be added.

The ADC comprises two PCB and is mounted in a double width NIM module.

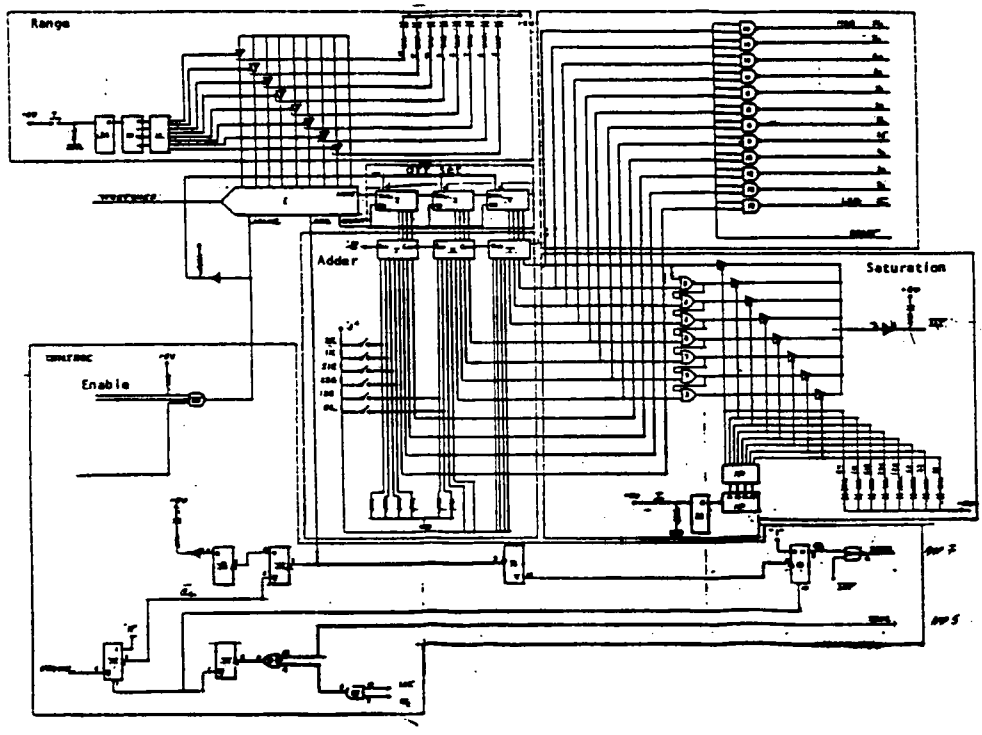

Fig.2: Conversion Block

I.2.6 CAMAC CRT Controller

D.S.Camin and T.Schmukler

This CAMAC CRT controller is intended for displaying alfanumeric information into a commertial TV set. The module has a 2K buffer memory in which the ASII characters entering through the CAMAC dataway are stored in.

In order to avoid the use of CAMAC dataway for refreshing purposes, this task is accomplished by the module.

The CRT controller has two registers used to keep track of a light pen position. These registers can be read from the CAMAC dataway. A shaft encoder is asigned to the parameter pointed to by the light pen.

By this way using only one shaft encoder and the light pen the whole system can be controlled.

Arbitrary zones of the video image can be altered using special characters (reverse video, underlined, blinking, intensified).

This controller, that was fully developed in the Electronics lab, was built in a double CAMAC module. It is used on the visualisation of the mass separators project parameters (NAVE), up to a maximun of 64 rows with 80 characters each. An 8085 microprocessor and an 8275 CRT controller were used to develop this module.

A total of 37 CAMAC comands were implemented, and the decoding is made by hardware and/or by software.

There are five fundamental blocks (Fig.1):

- The control unit: Controls the proper function of the module.
- Screen memory: Stores the ASCII characters to be displayed.
- Video generation: The purpose of these block is to produce the proper signal to drive a commercial TV set which has to be modified to permit access to video amplifier.
- Light pen and Keyboard block: detects when a key is depresed or when the light pen is on forcing the control unit to run the corresponding routine.
- CAMAC interface: This block mantains proper handshake with the CAMAC dataway decoding all the comands and executing those that do not require the microprocessor action.

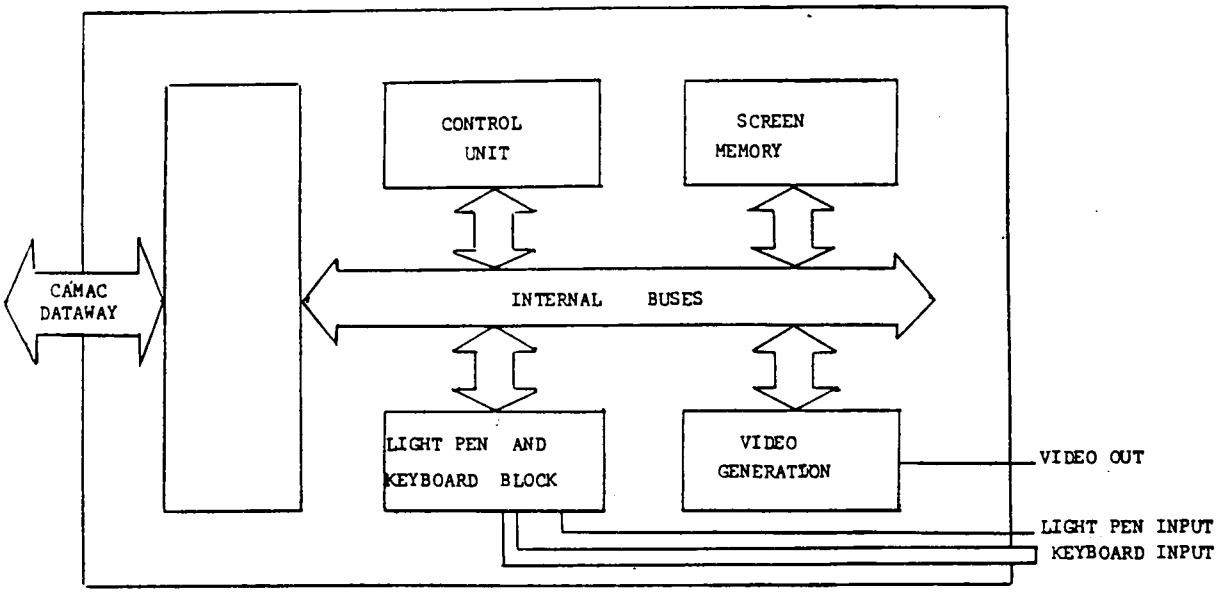

Fig.1: Block diagram of the CAMAC Controller

I.2.7 PARTICLE IDENTIFIER

D.V.Camin, M.Gonzalez Segura*, M.Melón*, A.Sdrigotti*, D.Skiarsky*

One of the requirements made by the experimental physicists of TANDAR Project was to count with a set of coarse particle identifiers intended for reducing the overhead of the data acquisition system.

In order to get fast PID output to E and ΔE signals, the classical time shared approach was disregarded. Instead, a two parallel processing channel method was adopted. Using monolithic components as op-amps, transistor arrays and resistor networks, two identical logarithmic channels have been implemented.

The specifications upon which the circuit was designed are the following:

Inputs: E and ΔE, both gaussian shape with a minimun of 1 μs time to peak and 100 mV up to 10V amplitude.

Outputs: a) PID = $(E + \Delta E)^x - E^x$ with exponent x continously adjustable from 1,5 to 2. Gain control adjustable from 1 to 10 and maximun amplitude 10 V.
b) $E + \Delta E$, 10V amplitude. Gain adjustable from 0,1 to 10. The particle identifier will be built into a single width NIM module and at the moment a prototype was tested with satisfactory results. Fig. 1 shows the circuit diagram of the identifier.

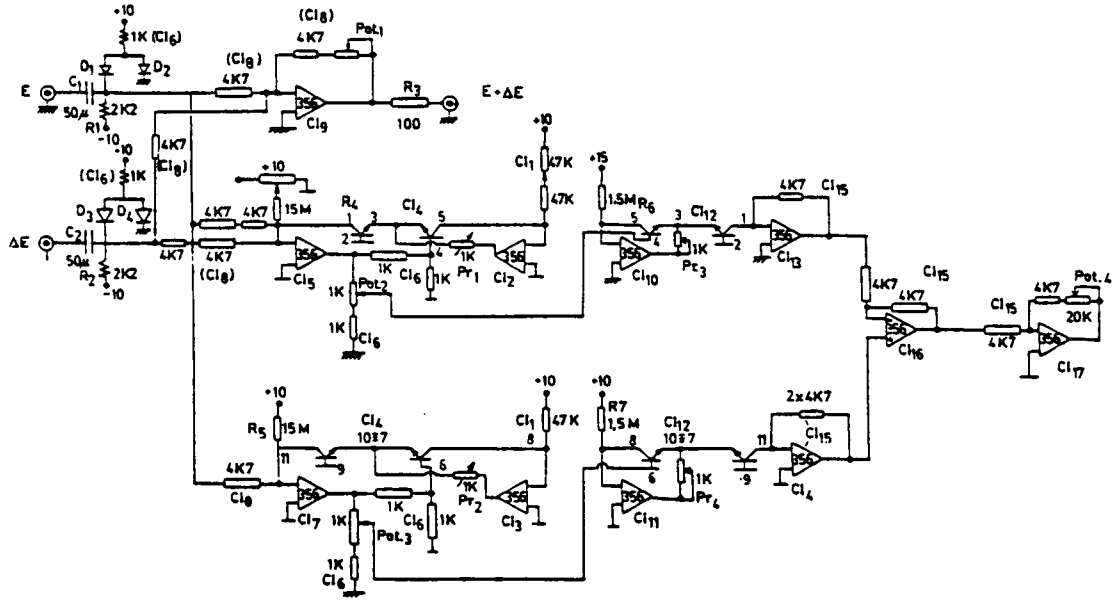

Fig. 1: Circuit diagram of the Particle Identifier

* Facultad de Ingeniería, Universidad de Buenos Aires

I.2.8 TEMPERATURE PROPORTIONAL CONTROLLER

D.V.Camin, B.Pinzón*, T.Schmukler

The solid state physics group makes measurements of electrical properties of crystals and their dependance with temperature. A special oven in which the sample is located must reach temperatures extending from 40°C up to 500°C. The temperature has to be linearly increased in sweeps which may range from minutes to several hours.

An electronic controller was built to permit the complete control of the oven temperature. To achieve high accuracy a derivative-proportional feedback loop was used. Power transistors adjust the output current to stabilize the programmed temperature. The reference ramp voltage is generated by a 12 bit DAC connected to a digital counter. Using a frequency divider and using a clock period of 15 msec, the ramp period can be selected from 2 min to 68 hours.

Different modes of operation are provided: The ramp can go up/down, stop at any point, reverse its direction and reset to a minimum temperature.

A Cr-Al thermocouple measures the oven temperature. Cold junction compesation is provided using a LM321 op-amp and a resistor network to match the op-amp drift to the cold junction voltage. A front panel connector provides a 10mV/°C external output to be used with a digital voltmeter. Also a pulse is generated to advance a digital recorder.

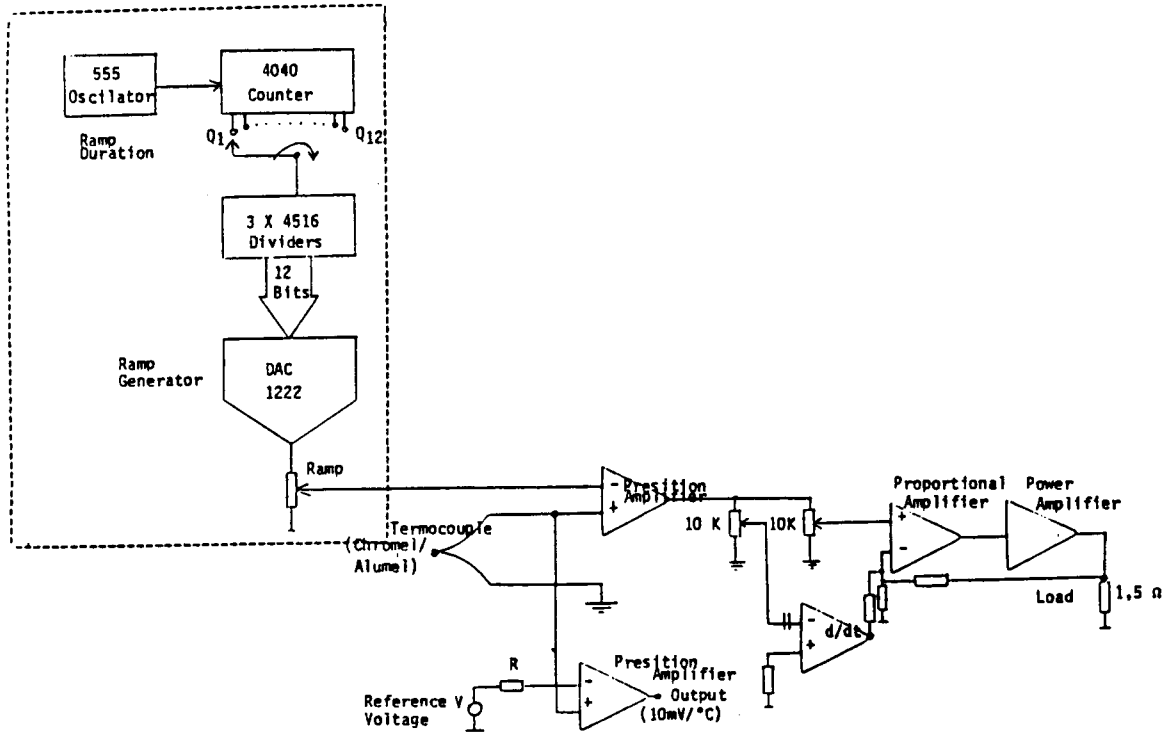

* Dirección General de Energía Nuclear, Guatemala

I.2.9 CAMAC AUTONOMOUS CRATE CONTROLLER

M.Satinosky, T.Schmukler

The Control System of the NAVE Project was implemented using CAMAC specifications. For this control system it was necessary to develop an Autonomuos Crate Controller based on a microcomputer.

This module, which uses an 8085, executes the most often used CAMAC functions in 5,4 microseconds. It is many times faster than similar commercial units. This was accomplished by using the address bus in a very efficient way.

The block diagram is similar to a conventional microcomputer. The principal blocks are: - microprocessor 8085
- EPROM memory
- RAM memory
- CAMAC interface

The Sub-address lines (A) and the Function lines (F) from the CAMAC Dataway, are transferred to the CAMAC interface via the microprocessor address bus. While this is done the data is sent to the CAMAC interface via the microprocessor data bus. (this explanation corresponds to a CAMAC Read)

The last single instruction of the dataway cycle, no data is transferred on the bus at this time, is used to obtain the value of the address of the Crate Number (N). This is accomplished by latching and decoding the above address (N).

A monostable is triggered at the same time the address corresponding to the Crate line (N) is latched. This pulse, of 1 microsecond duration, corresponds to the Busy (B) signal.

A counter and a decoder are used to generate the S1 and S2 signals using the clock-out signal from the microprocessor (time cycle = 200 nanoseconds).

The debug of the control system hardware and the maintenance of the whole system can be done using a conventional video terminal, through the RS 232 interface. A command interpreter program has been develop for this purpose. This program allows the user to execute CAMAC commands manually or preprogrammed.

The control program, actually in process of developing, is written in PLM 80 and 8085 assembler. 94 parameters can be controlled using only a pair of assignable shaft encoders, assignable meters and a light pen. The program is always sensing the actual values of the parameters and checks them with its maxima. When a parameter exceeds its maximum value the corresponding alarm becomes active.

See the Block Diagram in the following page.

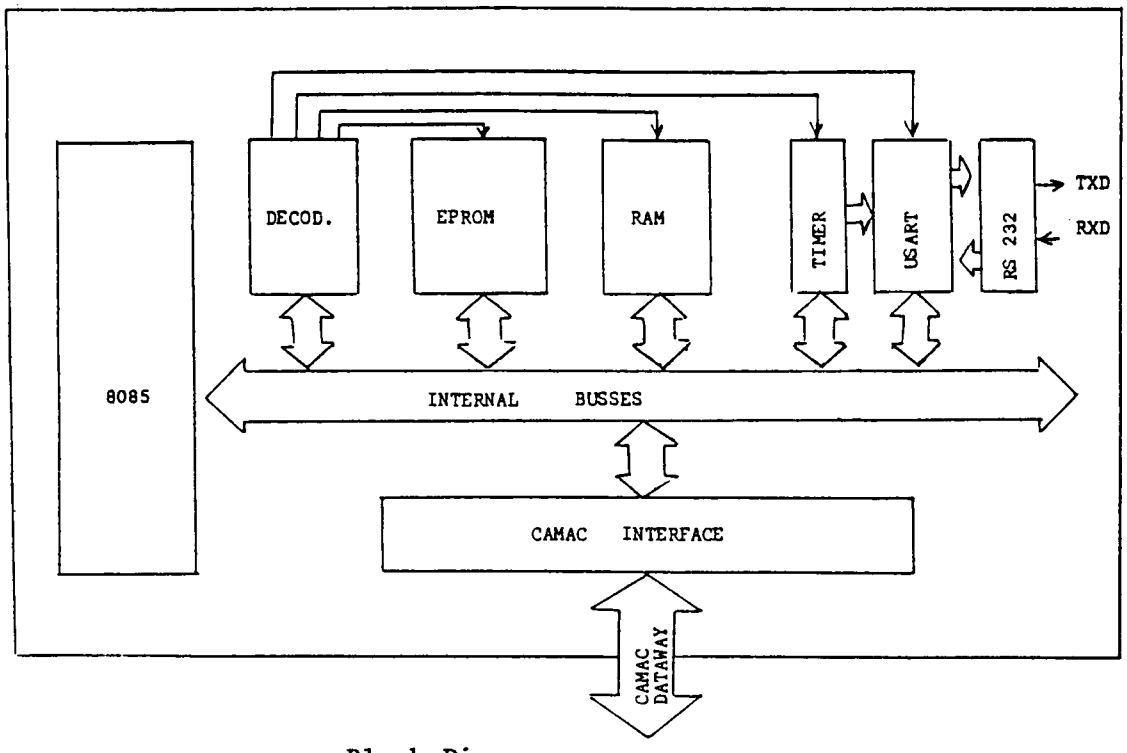

Block Diagram

I.2.10 CONTROL ELECTRONICS FOR THE ION SOURCE OF THE NAVE PROJECT

J.Mónico

The electronics needed to control and read out the devices specific to the ion source of this project (see Progress Report 1980/1981) were designed and built.

Voltage to frequency and Digital to Analog Converters with optical isolation were used to overcome such difficults as an off-ground potential Filament power supply, or an Arc power supply which must be controlled with isolated circuitry.

Figs. 1 and 2 show block diagrams of this electronics for the analog and digital parameters respectively.

Figs. 3 and 4 show block diagrams of the converters mentioned above.

All the input/output CAMAC lines are protected against sparks by suitable circuitry.

Typical schematics of these circuits, which differ depending on the CAMAC module, are shown in Fig. 5.

The devices described in Figs.1 to 5 are distributed in plug-in cards, allocated in a crate, where special care was put in the design of grounding and shielding, in particular the spark protection for the CAMAC modules.

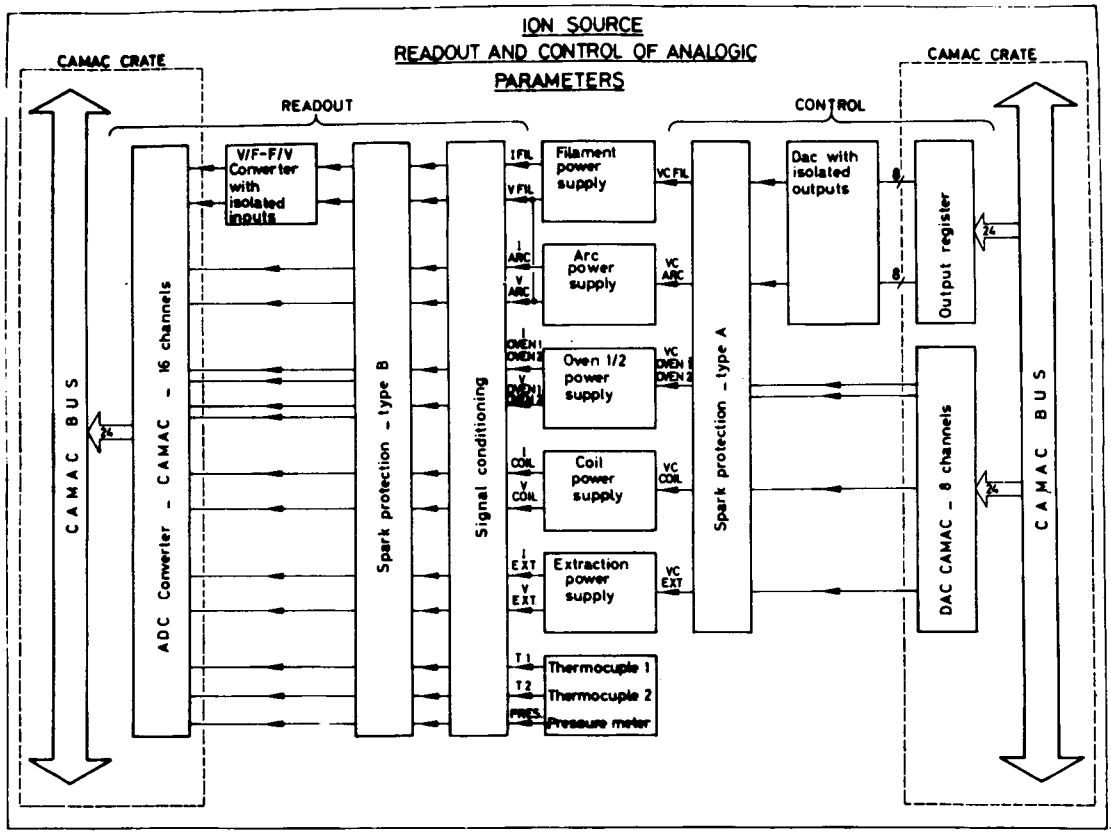

Figure 1

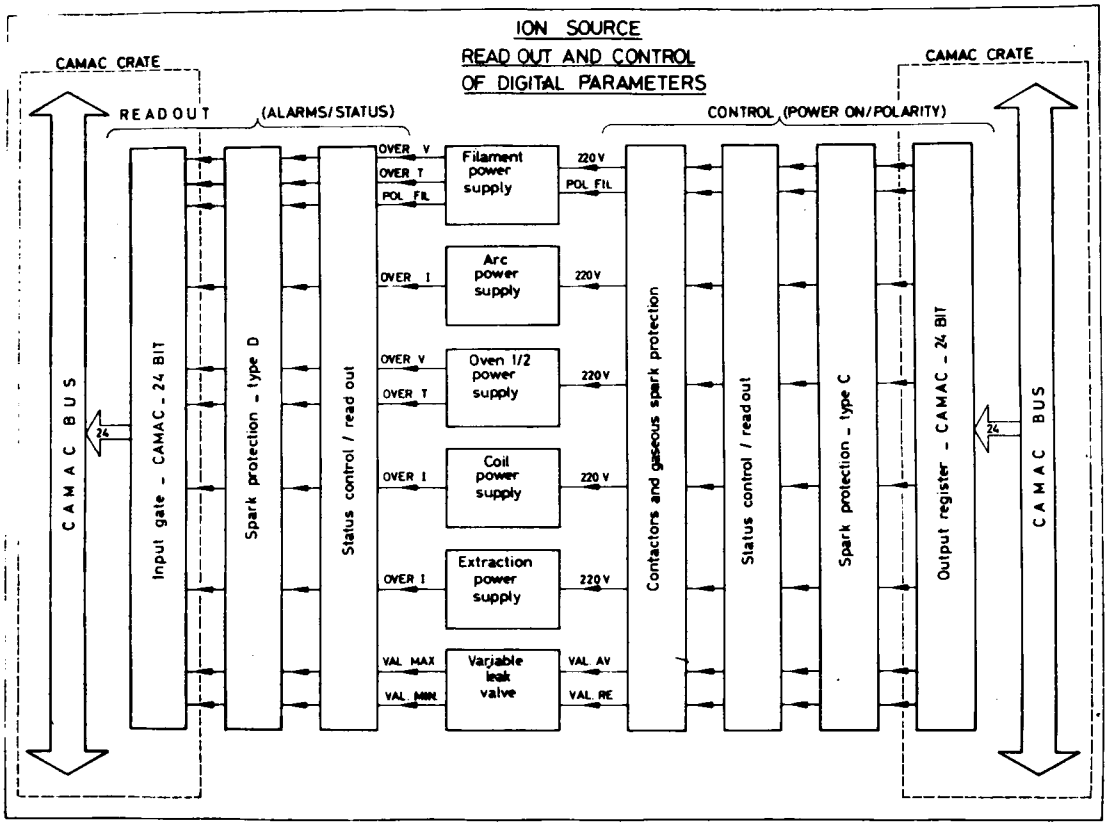

Figure 2

Fig.3

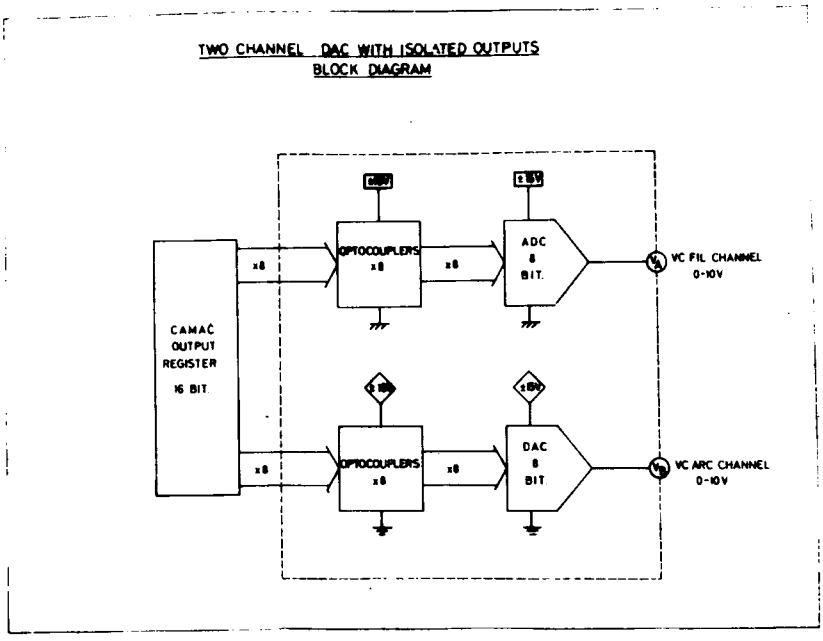

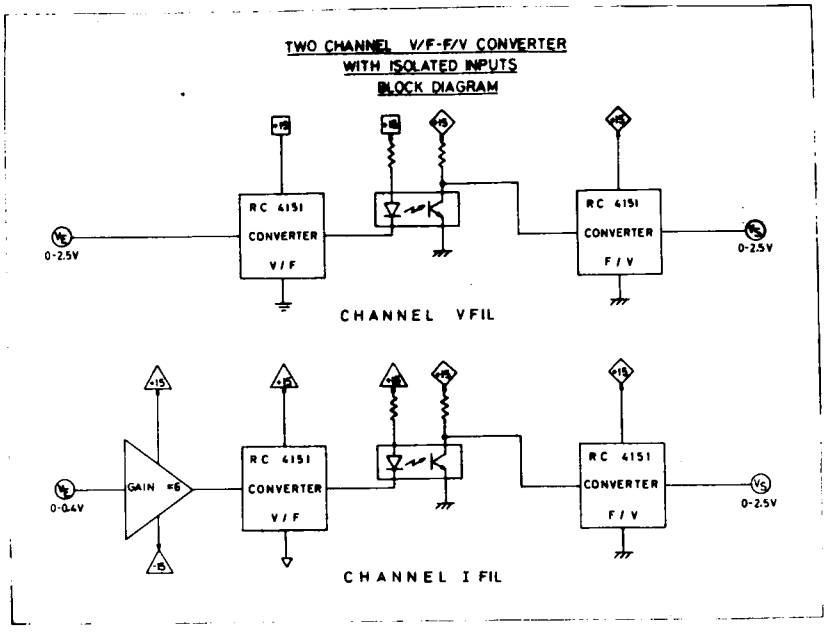

Fig.4

Fig.5

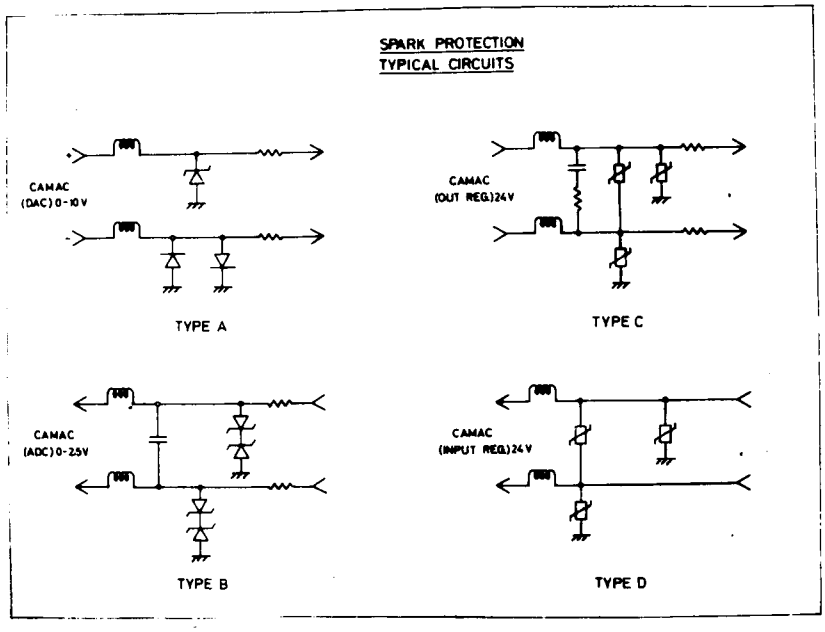

I.3 NUCLEAR FACILITIES

I.3.1 The magnetic spectrometer

C.Berisso, A.Etchegoyen and J.J.Rossi

Due to the different administrative difficulties that appeared for the acquisition of this instrument abroad, it was decided to undergo its construction entirely in our country.

Once the general characteristics of the instrument were defined, considering the requirements of the heavy ion physics to be performed with the 20 UD accelerator, an Argentinian company, INVAP SE (Bariloche) was selected for signing the construction contract.

The instrument will have a modest resolution and on the other hand a large solid angle as well as a broad range as far as heavy ions is concerned. The focal plane detection system will give the necessary information to be able to reconstruct the different trayectories and to correct for the remanent optical aberrations.

In order to obtain the detailed shape and working condition design of the polar pieces, several analyses have been performed with the use of a well known computing code which works out the tracking of the different trayectories and the estimation of the correspondent aberration coefficients. The code is at present working on the VAX 11/780 and its implementation demanded a very important effort.

The optical design is up to now close to completion, being the most favorable solution a QDDQ configuration. INVAP is well advanced in the execution of the mechanical drawings of the scattering chamber, rotating platform, focal plane detector, electronics and data acquisition system.

The actual building up will start in early 1984 and will require approximately twenty four months' work.

I.3.2 Experimental line for the all purpose scattering chamber

M.C.Berisso, A.Ceballos and J.Testoni

A general Ionex 2800 all purpose scattering chamber has been installed in target room B, together with the different elements for the experimental beam line.

The chamber centre is located at 11.94 mts from the deflecting magnet image slit. Between this point and the focusing quadrupole triplet of the line, the following elements have been placed: an NEC pneumatic valve, a diagnostic chamber and a beam steerer. From the quadrupole to the scattering chamber there are: a second diagnostic chamber, a remote control Faraday cup, a beam profile monitor and another pneumatic valve.

Two pairs of regulable tantalium collimators are located at the scattering chamber entrance. The chamber itself is 76.2 cm (30') in internal diameter and 25.4 (10') height and has two remote controled and digitally decoded rotating plates which can be positioned with .1° accuracy. Solid state detectors as well as gas fed detectors can be placed inside the chamber.

The target holder is a ladder with four different positions and can be removed from the chamber without opening to air. The body of the chamber has six circular windows of 10.16 cm (4") diameter. The chamber lid can be chosen among two different options, the flat one with its rotating plate and a simiespherical one with a 2π facility.

The diagnostic boxes in the experimental line are NUKLEAR TECHNIK designs, each one has six windows of different diameters and an electromechanical double actuator.

Three Air Products UHV 202-8B cryogenic pumps are connected to the line through the scattering chamber and the two diagnostic chambers.

The five pneumatic valves are operated from a remote control console; they are interlocked to prevent eventual vacuum failures.

At present the vacuum system has been tested up to 10^{-6} Torr in the scattering chamber; preliminar rough vacuum in the line is of about 10^{-4} Torr.

I.3.3 Nuclei far away from the stability valley

NAVE Proyect.

During 1982 several experiments have been completed using our old ISOL facility before dismantling and installing the isotope separator in a experimental room at the TANDAR building. Angular γ-γ correlations from ^{134}Tl and ^{134}I decays were completed. γ-γ coincidences in mass 133 as well as independent yield measurements for fast neutron induced ^{238}U fission have been performed successfully. The independent yield measurements help to

estimate the possibilities for the NAVE system when used on line with the 20UD accelerator.

Finally, the isotope separator has been installed in the new place and upgraded within the limited possibilities of the budget.

At present, most of the task is completed and it is expected to be ready in March 1984.

I.3.4 The heavy-ion scattering chamber

D.Napoli, D.Otero, A.N.Proto

The experimental set-up was presented in a previous report[1]. First experiments will intent to produce the same nucleus (A,Z) at similar excitation energies departing from different combinations target-proyectile. The relation between the cross sections for fusion-fission (σ_F) and deep inelastic colissions (σ_{DIC}) will be studied separating both process kinematically. Evaporated particles in coincidence with them will also be studied to infer the nuclear temperature.

---

1) Progress Report 1980-1981, CNEA NT-5/82.

I.3.5 Facility for on line γ-ray and electron spectroscopy

G.García Bermúdez

Two independent beam lines are being set up for this facility. One of them includes an angular distribution table, the other a specially designed chamber for conversion electron measurements. Such facilities are build and will stay in fixed positions.

The angular distribution table allows precise rotation of two Germanium detectors around the target and has room for other detector in a fixed position.

All movements are electrically drive allowing digital control for future needs. Two reaction chambers are being installed, in this line, one is cylindrical for measurments of γ-ray distributions and other of plane shape for coincidence and single work.

The electron chamber contains a cooled Si(Li) detector installed in the focus of a small permanent magnet spectrometer. This facility allows on line measurements of electron and γ-rays. Presently about 90% of these facilities are completed.

II. Nuclear Physics

1. Nuclear Structure
2. Nuclear Reactions

II.1 NUCLEAR STRUCTURE

II.1.1 Multi-step shell-model description of the Sn Isotopes[#]

L.Rydström[+], J.Blomqvist[+], R.J.Liotta[+] and C.Pomar

A multi-step shell-model method[1] is applied to describe the spectra around the core ^{132}Sn. The three- and four-particle spectra have been calculated. We found that the low lying levels of ^{129}Sn are grouped into multiplets arising from the coupling of the low lying two-particle states (^{130}Sn) to the first few single-particle states (^{131}Sn). This property reflects the weak influence of the Pauli principle in this region since the lowest single-particle are rather highly degenerate. The same feature is found in the four-particle nucleus (^{128}Sn) where all low-lying states λ^{π}_{1} (λ = angular momentum, π = parity, 1 = yrast) are virtually proportional to the state $^{130}\mathrm{Sn(gs)}\otimes{}^{130}\mathrm{Sn}(\lambda^{\pi}_{1})$. Although in all cases the agreement between theory and experiment is good, many states are predicted which have not been experimentally found so far.

[#]Physica Scripta T5(1983)149

[+]Research Institute for Physics S-104 05 Stockholm, Sweden

[1]R.J.Liotta and C.Pomar, Nucl.Phys. A362(1981)137.

II.1.2 Multi-step shell-model calculation of even-even nuclei

R.J.Liotta[+] and C.Pomar

The multi-step shell-model method (MSM) provides a convenient framework to analyse a many-body system in terms of any partition of its subsystem[1]. In this work, we study an s-particle nucleus (identical particles) in terms of the 2- and n-particle nuclei (s=2+n). The graphical method introduced in ref.[1] allowed us to find a close form to calculate the MSM overlap matrix for any number of particles, very schematically, one proceeds as follows. Just the "diamond" vertex is introduced as

where the vertices in 1(b) and 1(c) are defined in ref.[1] (for these and the vertices of fig.2 see ref.[1]). From fig.17 of ref.[1] and after some trivial graphical algebra one obtain

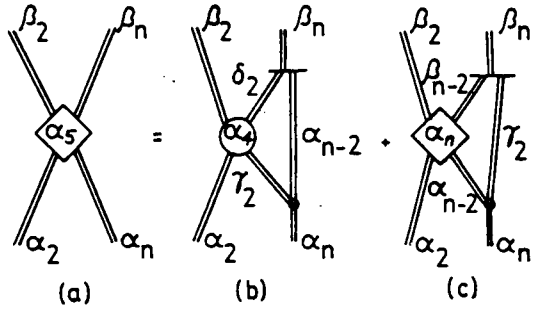

Figure 1

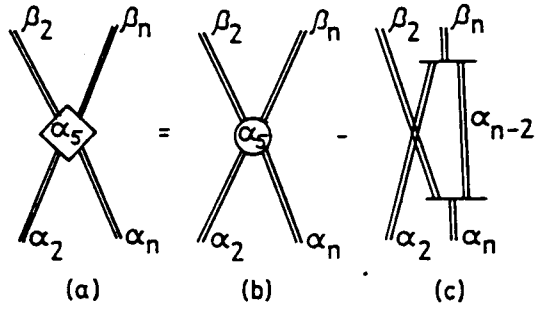

Figure 2

The vertices of fig.2(b) and 2(c) are calculated in previous step of the MSM, given a close form which is very well suited to construct a computer code. We did this computer code (which we called MSM1) and applied it to the N=50 nuclei. We took $^{88}_{38}Sr$ as a core and the single-particle states and interaction matrix elements as in ref.[2]. We calculated the spectra of all even-even nuclei up to the ground state of ^{100}Sn. For the nucleus ^{98}Cd we obtained the spectrum shown in fig.3 . Applications in the lead region are being carried out.

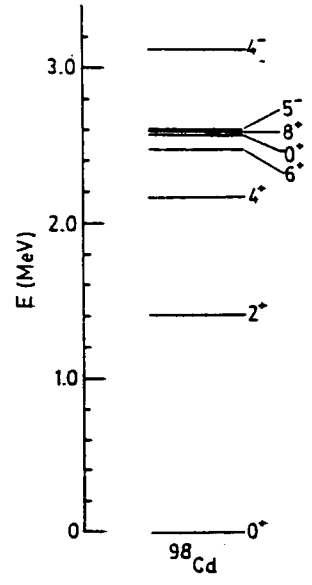

Figure 3: ^{98}Cd energy spectra calculated as ten particles on top of the ^{88}Sr core

+Research Institute for Physics S-104 05 Stockholm, Sweden
1) R.J.Liotta and C.Pomar, Nucl.Phys. A382(1982)1.
2) D.Gloeckner and F.Serduke, Nucl.Phys. A220(1974)477.

II.1.3 Multiplet Structure in ^{205}Pb and ^{203}Pb#

J.Blomqvist+, R.J.Liotta+, C.Pomar and L.Rydström+

We have applied the shell-model to analyse the three-hole spectrum of ^{205}Pb. The calculated spectrum agrees very well with experimental data. The particle-hole excitations do not play an important role at low excitation energy in this nucleus. The same nucleus has also been studied in terms of a correlated basis consisting of the tensor product of one- and two-hole excitations[1]. The two-hole spectrum (^{206}Pb) was taken from the calculation of Kuo and Herling[2] with suitable changes to get good agreement with available experimental data. We found that very few correlated states are needed to reproduce the shell-model calculation. The coupling of the single-hole to the two-hole states gives rise to some multiplets of states, as suggested by the weak coupling model. Yet the shell $p_{1/2}$ plays a very important role to block the occurrence of most of the expected multiplets.

We have also studied the five-hole nucleus (^{203}Pb) using the multistep shell-model method[3]. The MSM basis consisted of the coupling of one- and four-hole states. In this nucleus the Pauli principle affects strongly most of the low-lying basis states. As a results many of these states have negligible small norms. Moreover, many basis states with large norms are parallel to each other. Therefore, no complete multiplets of states of the form $| ^{207}\text{Pb} \otimes ^{204}\text{Pb} >$ are manifest. Yet, most physical states in ^{203}Pb (as was the case in ^{205}Pb) are well described within a basis consisting of very few MSM states. In particular, our calculated levels agree with the corresponding experimental data, when available, within a few (up to 50) keV.

#Phys.Rev.C (in press)

+Research Institute for Physics S-104 05 Stockholm, Sweden

1) R.J.Liotta and C.Pomar, Nucl.Phys. A382(1982)1.
2) T.T.S.Kuo and G.H.Herling, Naval Research Laboratory Report 2258 (Washington DC, 1971);
G.Herling and T.T.S.Kuo, Nucl.Phys. A181(1972)113
3) R.J.Liotta and C.Pomar, Phys.Lett. 105B(1981)92.

II.1.4 Multi-step shell-model method in light nuclei

R.J.Liotta, M.T.A.de Mehr y C.Pomar

The multi-step shell-model method was adapted to situation where isospin may be considered a good quantum number. The formalism is a generalization of the even-even case (see II.1.2 in this Progress Report) and a computer code called ISOS was built for the partition of the s-particle system into 2- and n-particle subsystems. The formalism is being applied to nuclei around ^{16}O with the aim of obtaining the ^{24}Mg spectrum which shows rotational-like features. The two-body interaction matrix elements were taken from previous standard shell-model calculation by Mc.Grory. Already the four-particle nucleus ^{20}Ne (corresponding to T=0) shows a rotational-like spectrum, as seen inf fig.1. It is interesting to analyse the structure of the states of fig.1 in terms of the MSM representation.

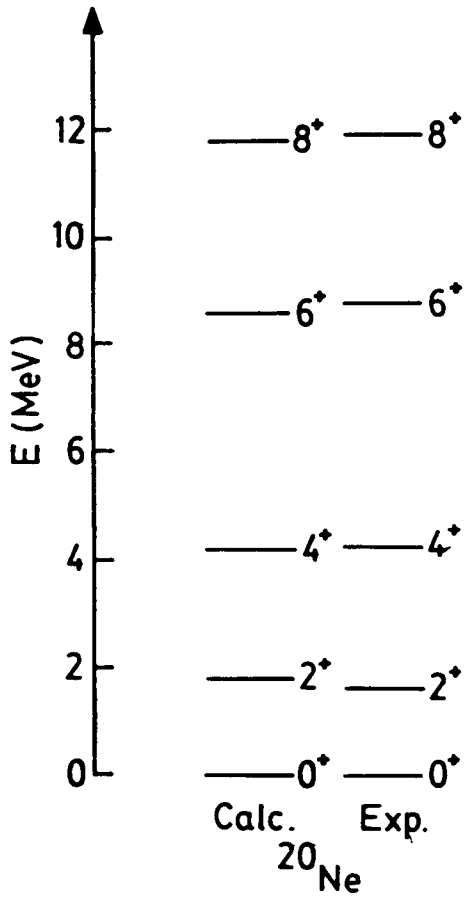

Figure 1

In table 1 we give the projection $F(\alpha_2\beta_2;\alpha_4) = \langle\alpha_4 \; (P^+(\alpha_2)\; P^+(\beta_2))\,\alpha_4 |0\rangle$ in terms of basic states $(P^+(\alpha_2)P^+(\beta_2))_{\alpha_4} \mid 0\rangle$. Only the largest values of F are given.

Table 1

α_4 (T=0)	α_2	β_2	$F(\alpha_2\beta_2;\alpha_4)$
0^+	$(\lambda T)_n$	$(\lambda T)_n$	
	$(1^+1)_1$	$(1^+1)_1$	1.01
	$(3^+0)_1$	$(3^+0)_1$	0.93
	$(0^+1)_1$	$(0^+1)_1$	1.09
	$(2^+1)_1$	$(2^+1)_1$	0.06
2^+	$(1^+0)_1$	$(3^+0)_1$	0.67
	$(0^+1)_1$	$(2^+1)_1$	0.83
4^+	$(1^+0)_1$	$(5^+0)_1$	0.66
	$(0^+1)_1$	$(4^+1)_1$	0.69
	$(2^+1)_1$	$(2^+1)_1$	0.82
6^+	$(5^+0)_1$	$(5^+0)_1$	0.95
	$(2^+1)_2$	$(4^+1)_1$	0.61
	$(2^+1)_1$	$(4^+1)_2$	0.76
8^+	$(5^+0)_1$	$(5^+0)_1$	1.18
	$(4^+1)_2$	$(4^+1)_1$	1.68

One clearly sees the influence of neutron-proton two-particle states to induce rotation-like spectra. While in the identical four-particle case (spherical nuclei) one would obtain very pure $|\alpha_4\rangle$ states (generally only one basis state is nearly parallel to the physical vector). In the case of ^{20}Ne there is a strong capture of T=1 and T=0 two-particle states.

At present the six-particle nuclei are being calculated.

II.1.5 Perturbation treatment of the interaction between correlated many-particle states

R.J.Liotta[+] and C.Pomar

Green's function techniques were recently used to describe a many-body system in terms of two of its subsystems[1]. We are using these techniques to study the time evolution of a many-particle propagator. This treatment allow us to introduce the concept of coupling constant among propagators (blocks) containing an arbitrary number of particles.

The s-particle Green function (s=m+n) is defined as ref.[1]

$$G(\beta_m\beta_n,\alpha_m\alpha_n;t) = i<0|T[P(\beta_n;t)P(\beta_m;t)P^+(\alpha_m)P^+(\alpha_n)]|0> \quad (1)$$

where $P^+(\gamma_n)$ creates the n-particle correlated state $|\gamma_n>$.

Equation (1) allows one to write a Bethe-Salpeter like equation with the interaction between the blocks given by a kernel K such that [1],

$$[[H,P^+(\alpha_m)],P^+(\alpha_n)] = \sum_{\beta_m\beta_n} K(\alpha_m\alpha_n;\beta_m\beta_n)P^+(\beta_m)P^+(\beta_n) \quad (2)$$

Using the kernel of eq.(2) one gets a series of TDA diagrams (hole excitations are not included) which can be summed up to all orders of perturbation.

The interaction induced by the kernel K gives rise to a series of Feynman diagrams where lines actually indicate many-particle blocks (which can be either fermions or bosons). A diagram of this type is given in fig.1. The value of this diagram is

$$C = G_0(\alpha_m;\tau-t_1)G_0(\alpha_n;-t_2)\sum_{\gamma_m\gamma_n} K(\alpha_m\alpha_n;\gamma_m\gamma_n)G(\beta_m\beta_n,\gamma_m\gamma_n;t-\tau) \quad (3)$$

where $G_0(\alpha_m,t)$ is the free propagator of the m-particle correlated state $|\alpha_m>$.

Expanding the Green function in the basis $\sum_{\alpha_s}|\alpha_s><\alpha_s|$ and with

$$\Lambda(\alpha_m\alpha_n;\alpha_s) = \sum_{\gamma_m\gamma_n} K(\alpha_m\alpha_n;\gamma_m\gamma_n)<\alpha_s|P^+(\gamma_m)P^+(\gamma_n)|0> \quad (4)$$

one gets

$$C = G_0(\alpha_m;\tau-t_1)G_0(\alpha_n;\tau-t_2)\sum_{\alpha_s} G_0(\alpha_s;t-\tau)\Lambda(\alpha_m\alpha_n;\alpha_s)\langle 0|P(\beta_n)P(\beta_m)|\alpha_s\rangle .$$

This equation shows that the quantity Λ has the meaning of a coupling constant. $\Lambda(\alpha_m\alpha_n;\alpha_s)$ couples the states $|\alpha_m\rangle$ and $|\alpha_n\rangle$ to the s-particle state $|\alpha_s\rangle$. This coupling takes place at a given time $\tau-t_1(t_2)$, while all states propagate freely, as shown in fig. 2.

These results include only TDA vertices. We have generalize the theory including other vertices. For the derivation corresponding to "scattering vertices" we have used the multistep shell-model method (MSM)[2]. For the one-particle state the commutator $[H,C_k^+]$ gives the usual Hartree-Fock contribution plus the scattering vertex shown in fig.(3.a). This particle-hole scattering vertex is given by

$$\Lambda(k\,k';\nu) = \tfrac{1}{2}\sum_{k''i}\langle k''k'|V|ik\rangle\langle\nu|C_{k''}^+C_i|\,0\rangle$$

in general one has the diagram of fig.(3b) i.e.

$$\Lambda(\alpha_s\alpha_{s'};\nu) = \sum_{\alpha_m\alpha_n\alpha_{n'}} Y(\alpha_m\alpha_n;\alpha_s)\,[\Lambda(\alpha_n\alpha_{n'};\nu)F(\alpha_m\alpha_{n'};\alpha_s) + (\;_{m'\,n'};\;)\,F(\;_{n\,n';\,s'})] \tag{5}$$

obtained from the MSM[2]. The wavefunction amplitude Y is defined by

$$|\alpha_s\rangle = (1+\delta(n,m))^{-1}\sum_{\alpha_m\alpha_n} Y(\alpha_m\alpha_n;\alpha_s)\,P^+(\alpha_m)P^+(\alpha_n)|\,0\rangle$$

and $F(\alpha_m\alpha_n;\alpha_s) = \langle\alpha_s|P^+(\alpha_m)P^+(\alpha_n)|\,0\rangle$ (see eqs. (2) and (5) of ref.2)). The coupling constants in the right hand side of eq.(5) are supposed to have been calculated in previous steps of the MSM.

As an example, we show in fig.(3c) one of the lowest order diagrams corresponding to "core polarization" effects upon two many-particle blocks. From this figure one gets

$$C = G_o(\alpha_m;\,\tau-t_1)G_o(\alpha_n;\,\tau-t_2)\sum_{\alpha_s} G_o(\alpha_s;\,t-\tau)\Lambda(\alpha_m\alpha_n;\,\alpha_s)$$

$$\times\,\langle o|P(\beta_n)P(\beta_m)|\alpha_s\rangle .$$

The choice of the energy $W(\alpha_s)$ depends upon whether one uses the Brillouin-Wigner or the Rayleigh-Schrödinger perturbation theory.

The present treatment generalise the nuclear field theory[3] where only couplings among two-particle (or particle-hole) and single-particle degrees of freedom are considered.

+) Research Institute for Physics, S-104 05 Stockholm 50, Sweden.

1) G.G.Dussel and R.J.Liotta, preprint for publication.

2) R.J.Liotta and C.Pomar, Nucl.Phys. A382(1982)1.

3) D.R.Bes et al., Nucl.Phys. A260(1975)77.

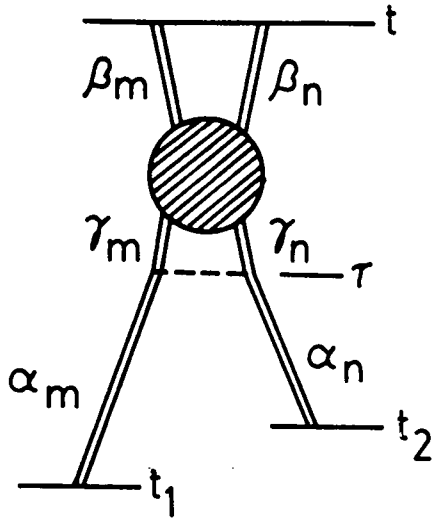

Fig.1:
The propagators α_m and α_n (with m and n particles, respectively) propagates freely up to the time τ when the interaction K (eq.(4)) takes place. From τ to t the full Green function (1) is propagated. The contribution of this diagram is called C in eq.(3).

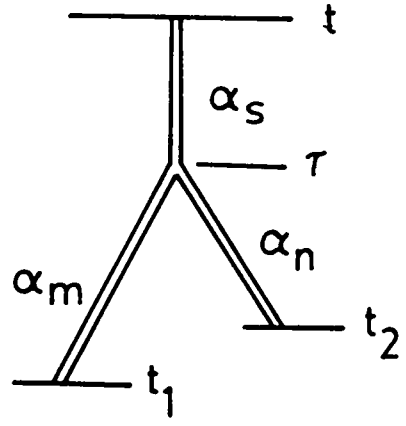

Fig.2:
Coupling of the propagator α_m and α_n to α_s (s=m+n). The value of the corresponding coupling constant is given in eq.(4).

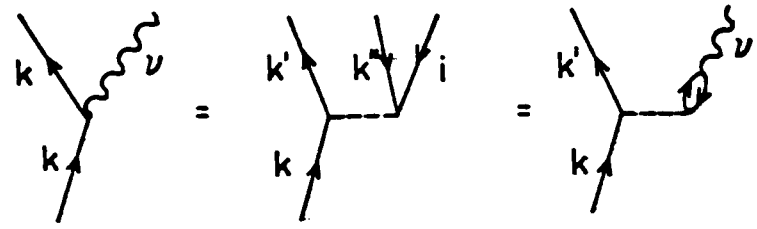

(a) Coupling corresponding to the scattering of a particle with a particle-hole phonon. The coupling constant is the one obtained in the nuclear field theory[3].

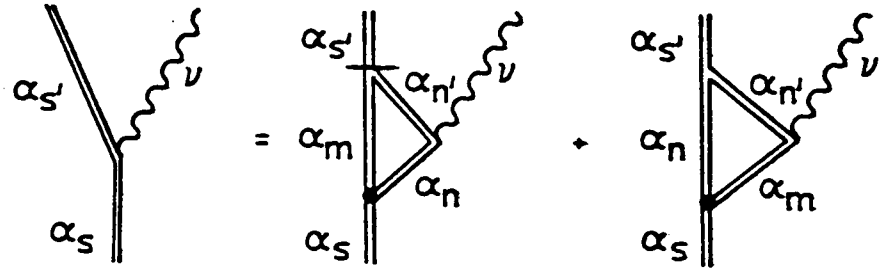

(b) Coupling corresponding to the scattering of a many-particle block with a particle-hole phonon.

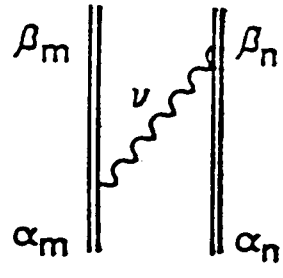

(c) "Core polarization" contribution to the effective interaction between two many-particle states.

Fig.3:

II.1.6 On the microscopic description of the discontinuity in Mallmann's plot

A.J.Kreiner and C.Pomar

In 1959 Mallmann[1] showed that for a very large class of nuclei, their ground state bands-energies, when plotted in the form of energy ratios $R_J=(E_J-E_0)/(E_2-E_0)$ (J=6,8) vs R_4 arrauge themselves on smooth curves suggesting the existence of a common mode of motion for them all. As more experimental data became available Mariscotti[2] based on the fenomenological model VMI[2], described these curves analytically. This work revealed the existence of a discontinuity in Mallmann's plot implying that two, instead of one, sets of curves were needed. Thus almost all nuclei seem to lie approximately on two disjunct families of curves in Mallmann's plot separated by a sharp break which may reflect two fundamentally different types of motion of the nucleus. These certainly is at the present time a lack of deep understanding of this striking behaviour. The purpose of the present work is to understand the microscopic structure (in the framework of the shell-model) underlying the observed sistematic behaviour as well as the sharp discontinuity in Mallmann's plot. Updating the experimental information we have found that in spite of some exception the rule [2] is still valid that doubly and singly closed-shell nuclei lie on the lower curve while those with both neutron and protons, shells open arrange themselves on the upper curve.

We concentrate around the different shell-closures. Fig.1 illustrates

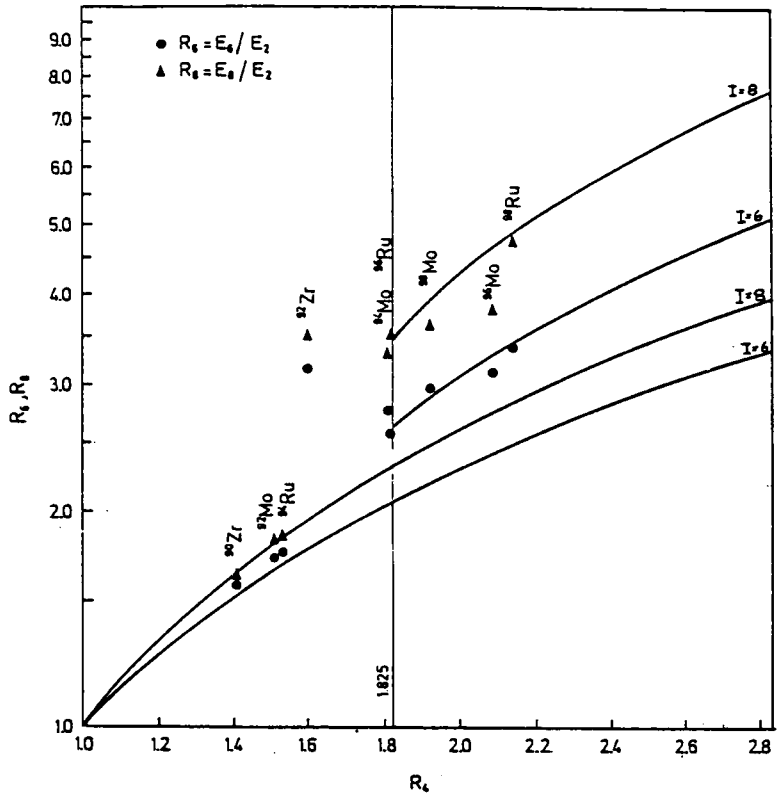

Fig.1

the regions of ^{90}Zr , which can be considered a doubly closed-shell nucleus with N=50 and Z=40. The nucleus ^{92}Zr (single-closed) is an exception and may be understood as reflecting the different microscopic structure of the sets of states $(0^+,2^+,4^+)$ and $(6^+,8^+)$. The first set is mainly described by the $(\nu d_{5/2})^2_J$ (J=0,2,4) configuration while the second one requires quite different degrees of freedom. In fact the singly closed-shell nuclei ^{92}Mo and ^{94}Ru in which the states $0^+,2^+,4^+,6^+$ and 8^+ have a common main configuration, i.e. $(\pi g_{9/2})^2_J$, lie as expected. On the other hand when a pair of neutron is added to these nuclei ^{94}Mo and ^{96}Ru are produced "jumping" into the upper curve just at the discontinuily point ($R\gtrsim 1.8$). The proton-neutron (p-n) interaction switched-on when the neutron-shell is opened should not be too strong according to the criterion introduced by the Shalit and Goldhaber[3] because $n_\nu \neq n_\pi$ and $l_\nu \neq l_\pi$ ($n_{\nu(\pi)}$= radial quantum number, $l_{\nu(\pi)}$ orbital quantum number). It should be pointed out that in other shell-closures were the condition $n_\nu \simeq n_\pi$, $l_\nu \simeq l_\pi$ (good overlap between the proton and neutron orbitals) is better fullfiled (like in the ^{16}O or ^{40}Ca region) a much more drastic "jump" is observed when both shells are opened. These facts strongly suggest the conection between the proton-neutron interaction and the existence of two families of curves with a sharp discontinuity in the Mallmann plot.

Using effective matrix elements in various shell-closures we have reinforced the previous conclusions about the relevance of the proton-neutron interaction for the existence of an upper curve in Mallmann's plot.

---

1) C.A.Mallmann, Phys.Rev.Lett. 2(1959)507.

2) M.A.J.Mariscotti, Phys.Rev.Lett. 24(1970)1242.

3) A. de Shalit and M.Goldhaber, Phys.Rev. 92(1953)1211.

II.1.7 Quantal description of the discontinuity in Mallmann's plot

A.J.Kreiner

A quantal description of one side of the discontinuity in the energy ratio (Mallmann)-plot E(I)/E(2) vs E(4)/E(2) for ground state bands of even-even nuclei is obtained by solving exactly a centrifugal stretching-like Hamiltonian. Its relation to the Bohr Hamiltonian is discussed.

II.1.8 Calculation of matrix elements from the time dependent variational principle

M.C.Cambiaggio, G.G.Dussel and M.Saraceno

A general prescription is given for the calculation of matrix elements as Fourier components of the time-dependent expectation value of the operator, evaluated with a periodic solution of the variational equations. It is applied to the time-dependent Hartree-Fock solution of the Lipkin model. As a second example we apply the time-dependent Hartree-Fock-Bogoliubov method to a two-level system with a pairing interaction. In both cases we campare the matrix elements and the excitation energies obtained within this approach, with the exact values and a very good agreement is observed for large degeneracies.

II.1.9 Configuration mixing calculations in soluble models[#]

M.C.Cambiaggio, A.Plastino, L.Szybisz and H.G.Miller

Configuration mixing calculations have been performed in two quasi-spin models using basis states which are solutions of a particular set of Hartree-Fock equations. Each of these solutions, even those which do not correspond to the global minimum, are found to contain interesting physical information. Relatively good agreement with the exact lowest lying states has been obtained. In particular, one obtains a better approximation to the ground state than that provided by Hartree-Fock.

[#] Nucl.Phys. A403(9183)381.

II.1.10 Maximum overlap and critical phenomena[#]

M.C.Cambiaggio and A.Plastino

Kümmel's maximum overlap treatment is reformulated and compared to a maximum overlap method based upon the generator coordinate method, with reference to two different quasi-spin models. The former theoretical approach is seen to be superior to the latter for the study of critical phenomena.

[#] Nucl.Phys. A403(1983)365.

II.1.11 On an iterative scheme for the solution of constrained variational equations

M.C.Cambiaggio and H.G.Miller

An iterative method for the solution of constrained variational equations proposed by Mang et al., has been investigated. Serious difficulties are found in the iterative scheme for satisfying the equation of constraint. A simple calculation in an exactly soluble model has been performed to illustrate the lack of convergence of the method.

II.1.12 Methods for describing the coexistence of competing degrees of freedom in a many body system

R.M.Quick, M.C.Cambiaggio and H.G.Miller

Methods for obtaining a description of a system of interacting particles in which competing degrees of freedom coexist have been presented and discussed. By mapping the problem onto a parametric subspace of the full Hilbert space, tractable means of handling such problems may be formulated and approximated.

A simple model calculation has been performed in an extended version of the Lipkin model which contains a quasi-spin pairing interaction as well as a monopole interaction. As the relative strengths of the respective interaction are varied, the system undergoes a phase transition which may be described by the present methods.

II.1.13 Pair correlations in boson systems

P.Curutchet, J.Dukelsky, H.M.Sofia

The purpose of this work is to approach the ground state of certain systems by a condensate of pairs of bosons. This means that we are looking at the possibility of obtaining boson-superfluidity in the same way that Cooper pairs simulate the ground state of superfluid nuclei.

We compare this approach with an SU3 exact result for well deformed nuclei and with the Cranked Hartree approximation[1] which assumes that the

ground state wave function is that of a condensate of only one kind of bosons.

We assume a quadrupole-quadrupole Hamiltonian

$$H = -KQQ$$

where

$$Q = (s^{+}\tilde{d} + d^{+}s) + \frac{X}{\sqrt{5}}(d^{+}\tilde{d})^{2}$$

The same form and parametrization of the boson quadrupole operator is used in both the Hamiltonian and in the E2 operator as suggested by Warner and Casten[2].

The problem was solved utilizing a variational method. We found the transformation coefficients

$$\Lambda^{+} = \sum c_{ij}\ \gamma_i^{+}\ \gamma_j^{+}$$

which minimize the ground state expectation value of H, where γ^{+} creates the state of one boson. Assuming that the ground state wave function is that of a condensate of Λ^{+}

$$|\phi_N\rangle = \frac{\Lambda^{+N}|0\rangle}{O(N)^{1/2}} \quad \text{with } O(N) = \langle 0|\Lambda^{N}\Lambda^{+N}|0\rangle$$

we solved the set of equations

$$\frac{\delta\langle 0|\Lambda^{N} H \Lambda^{+N}|0\rangle}{K\ O(N)} = 0$$

This transformation is equivalent to a number conserving Hartree-Bose-Bogoliubov calculation.

In the selfconsistent Q formalism the wave functions and the energies depend only on a single parameter X, which appears in the internal structure of the operator Q. The entire SU(3) - O(6) region, including both limiting symmetries was treated varying X between $-\sqrt{7}/2$ and 0, respectively.

Calculations were made including a total of 10 bosons with l=0,2. Results are shown in Fig.1 where we plot positive values of the ground state energies as a function of X for two cases:

a) axially symmetric wave functions

b) the correlated pairs of bosons are coupled to angular momentum zero (BCS calculation)

Preliminary results of this method compared to the ones coming from a diagonalization of the Hamiltonian (PHINT-CODE) show an improvement over the ones obtained with the Hartree-Bose approximation.

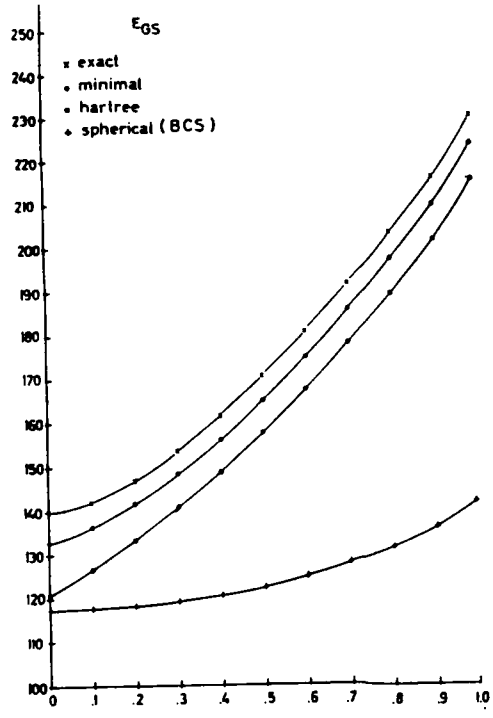

Fig.1

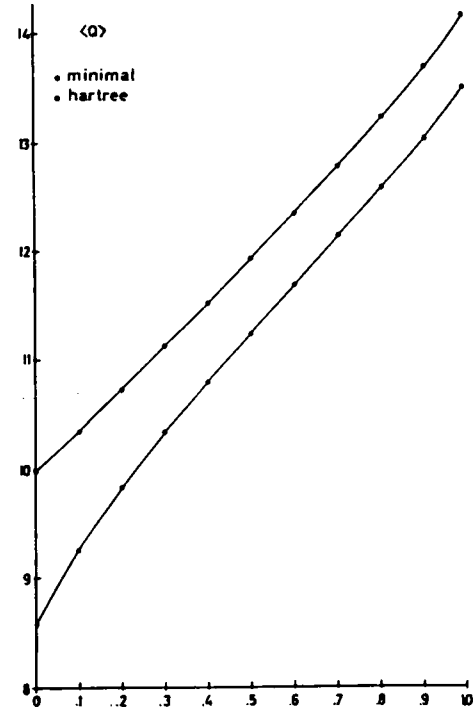

Fig.2

In Fig.2 we plot the mean value of the quadrupole operator (static quadrupole moment) against the parameter X and we find that it is smaller than the one obtained with the Hartree-Bose approximation but it does not vanish as the exact O(6) solution predicts. This is a result of using intrinsic states which do not have seniority as a good quantum number.

---

1) J.Dukelsky, G.G.Dussel, R.P.J.Perazzo, H.M.Sofia, Phys.Lett. 130B(1983)123

2) D.D.Warner and R.F.Casten, Phys.Rev. C25(1982)2019

II.1.14 An interacting quartet-boson model[#]

J.Dukelsky, P.Ferderman, R.P.J.Perazzo and H.M.Sofia

A new boson model is proposed, in which the bosons represent quartets of two neutrons and two protons rather than pairs of identical nucleons. The model is applied to calculate the energy spectra of ^{168}Er and other even-even rare earth nuclei containing equal number of valence neutrons and protons, with very satisfactory results.

[#] Phys.Lett. 115B(1982)359.

II.1.15 The nucleus as a condensate of monopole and quadrupole pairing vibrations[#]

R.A.Broglia, E.Maglione, H.M.Sofía and A.Vitturi

It has been shown that the aligned wave function, and the wave function obtained by restricting pairs of particles to be coupled to angular momentum zero and two, as assumed by the quadrupole phonon model (QPM) and by the interacting boson model (IBM) are, for strongly deformed systems, rather different. They become similar in the vibrational limit and display different degrees of similarity for intermediate (anharmonic) situations. To what extent this difference reveals itself in the predicted properties of the low-energy nuclear spectrum is an open question. In an attempt to clarify this point we have calculated the spectrum and the electromagnetic and two-nucleon transfer probabilities for some strongly anharmonic and transitional nuclei, in the framework of the nuclear field theory (NFT) version of the pair aligned model. These calculations, which are microscopic, depend on the strength of the pairing and particle-hole interactions. We find that for standard values of these parameters, the moment of inertia of both the beta- and the gamma-bands are too small.

While the main pattern of the phase transition observed in the Sm isotopes is displayed by the model, major deviations are observed concerning the properties of the beta-vibrations, and in connection with the two-nucleon transfer strength associated with the 2^+ member of the ground-state rotational band.

[#] Nuci.Phys. A375(1983)217.

II.1.16 Search for two-octupole-phonon states in ^{208}Pb[#]

M.A.J.Mariscotti, D.R.Bes, S.L.Reich, H.M.Sofía, P.Hungerford, S.A.Kerr, K.Schreckenbach, D.D.Warner, W.F.Davidson, W.Gelletly

A search for two-phonon octupole vibrational states in ^{208}Pb was carried out using the $^{207}Pb(n_{th},\gamma)$ reaction at the High Flux Reactor of the Institut Laue-Langevin.

The conversion electron spectrum was scanned with the spectrometer BILL with a sensitivity of 20 μb in the 4-6 MeV interval. Coincidence and singles gamma-ray measurements were performed at the end of the thermal neutron beam guide H22-F reaching a sensitivity of 80 μb for energies above 0.511 MeV. In addition the singles spectrum was investigated with the pair spectrometer at the tangential beam facility.

Levels have been observed at (energies in keV and parenthesis for tentative level identification and spin-parity assignments): $2614.4,3^-$; $3997(3^-)$;$4084.7,2^+$;$4253,(2^-,3^-)$;$4704,(2^-,3^-)$;$(4882.0),(0^+)$;$(4904.9),(0^+)$; $4935,2^+$;$(6343),(2^+)$ and the $0^-,1^-$ capture state at 7367.9 keV. The 4882.0 keV level probably corresponds to the known two-neutron pairing vibration. Possible candidates for two-phonon octupole excitations are the (0^+)(4904.9) and 2^+ 4935 keV states. The nuclear field theory formalism is used to calculate branching ratios and energies for states in ^{208}Pb under several assumption. The most important result of the comparison of theory and experiment is that the experimental properties of the 2^+ 4935 keV state favour the interpretation of this state as a two-phonon octupole vibration rather than as a one-phonon non-collective quadrupole state.

[#] Nucl.Phys. A407(1983)98.

II.1.17 Two correlated quasiparticles states in the Principal Series Approximation[#]

J.Dukelsky, G.G.Dussel and H.M.Sofía

The Principal Series Approximation is extended to the description of two correlated quasiparticles states, enabling a treatment of these states that takes into account the coupling among the two particle Green function and the particle-hole one. This description is related to a RPA treatment of collective states in open shell nuclei that includes simultaneously the particle-particle and particle-hole versions of the nuclear residual

hamiltonian. Using separables interactions it is found that the inclusion of the particle-particle part of the hamiltonians change greatly the properties of the 2^+ states in the Sn isotopes.

Phys.Rev. C27(1983)2954.

II.1.18 Separable interactions and excited states in open-shell nuclei#

J.Dukelsky, G.G.Dussel and H.M.Sofía

The relevant matrix elements of the Hamiltonian for a RPA description of collective states in open-shell nuclei are determined. For separable interactions it is found necessary to include the particle-particle and particle-hole interactions simultaneously. The energy-weighted sum rule for the electromagnetic operator (with angular momentum I) is greatly reduced by the use of the pairing interaction with the same angular momentum.

J.Phys.G: Nucl.Phys. 8(1982)L191

II.1.19 The RPA calculation of bandhead energies in many-boson systems#

J.Dukelsky, G.G.Dussel, R.P.J.Perazzo and H.M.Sofía

The RPA is used to correct the Hartree-self consistent single boson energies. The spurious states that appear as a consequence of broken symmetries are set at zero energy and can therefore be eliminated. The method is exemplified with an SU_3 Hamiltonian with only s and d bosons.

Phys.Lett. 129B(1983)1.

II.1.20 Connection between one-body operators in fermion and boson spaces#

B.R.Barrett, H.M.Sofía and J.P.Vary

One-body operators in fermion space are rewritten as pseudo-two-body operators in fermion space. Arbitrary two-body, unitary transformations permit transcription of the result to a basis of collective two-body modes. This latter results provides a useful link to the Interacting Boson Model

(IBM), since its form is similar to the IBM assumption for one-body operators in the boson space.

Submitted to Phys.Rev.C, Rapid Communication.

II.1.21 The moments of strength functions[#]

G.G.Dussel, R.P.J.Perazzo, S.L.Reich and H.M.Sofía

In this paper we show that a moment of order n of the strength function is determined by the same order of the Brillouin-Wigner perturbative expansion. This fact is used to study the second moment of single-particle and collective excitations in the framework of nuclear field theory. We discuss the relationship of the second moment with the spreading width of the giant isovector M1 resonances in ^{208}Pb.

Nucl.Phys. A401(1983)1.

II.1.22 Cranked Hartree approximation for systems with many interacting bosons[#]

J.Dukelsky, G.G.Dussel, R.P.J.Perazzo and H.M.Sofía

An extension to bosons of a cranked Hartree variational method is developed. This method is not limited to s and d bosons and can be extended to more complex boson spaces. An application to well deformed systems including g (ℓ=4) bosons is compared with the exact solution of the hamiltonian $H=- KQ_2.Q_2$.

Phys.Lett. 130B(1983)123.

II.1.23 On the assignment of high-spin cascades in ^{98}Rh and ^{98}Pd isotopes[#]

M.Behar, A.M.J.Ferrero, A.Filevich and A.O.Macchiavelli

Isotopic assignment of high-spin cascades in ^{98}Rh and ^{98}Pd have unambigously been obtained by a suitable combination of the ^{96}Ru(α,xn yp) and the ^{99}Ru(d,xn yp) reactions. As a result the band headed by the 841.3 keV

line was assigned to ^{98}Rh and the one headed by the 862.6 keV gamma-ray has been found to belong to ^{98}Pd. In the case of ^{98}Rh the band is based on the (2^+) ground state.

Z.für Physik (in press).

II.1.24 Equation of motion approach to the neutron-proton pairing problem#

F.Andreozzi, A.Covello, A.Gargano, E.E.Maqueda and R.P.J.Perazzo

The J=0, T=1 charge-independent pairing Hamiltonian is treated by means of the equations of motion for pair creation operators. Exact equations for the seniority-zero states of N nucleons are derived. It is shown that these equations can be solved by a step-by-step procedure which consists of progressively adding pairs of nucleons to a core. A method is given which removes the spurious effects arising from the redundancy of the set of basis vectors. The theory can be applied at several levels of approximation depending on the number of core states which are chosen to build up the basis vectors. Of special interest are the lowest orders of approximation, which are very simple in application. To assess the practical value of the present work, a three-level model calculation is performed using the first-order theory, wherein the core states are restricted to the lowest energy state for each value of the total isospin. Comparison shows that the energies, occupation probabilities, and two-nucleon transfer amplitudes for the lowest states of natural isospin are in very good agreement with the exact results for all values of N.

Phys.Rev. C27(1983)370.

II.1.25 The structure of the ^{100}Rh high spin states#

M.A.J.Mariscotti, A.J.Kreiner, G.García Bermudez and P.Thieberger+

In the last progess report we presented a level scheme[1] for the high spin states of ^{100}Rh. Calculations based on the two quasi-particle plus rotor model[2] with the purpose of understanding the underlying structure of these levels have been carried out. The main results achieved with this model,

modified by the addition of a p-n interaction acting on the valence nucleons and of a variable core moment of inertia are the following: a) in spite of the fact that ^{100}Rh lies in a nearly spherical region of the Periodic Table, this rotational model, in its simplest version, is appropiate to reproduce the main features of the lowest states; b) the p-n interaction has little influence but helps to improve the agreement, especially as regards the first 7^+ state; c) the assumption of a variable moment of inertia is essential to obtain agreement with the states above the lowest multiplet. In particular, by applying the VMI model with the θ'_o and C parameters extracted from the energies of the ^{98}Rn core, a remarkable agreement is achieved. Since ^{98}Rn is reproduced with the "anomalous" VMI root (that corresponding to $\theta_o < 0$) the present results constitute the first case in which such a root is applied to the description of a doubly odd nucleus.

#Submitted to Nuclear Physics

+Brookhaven National Lab., Upton, N.Y., USA.

1)M.Behar, A.Ferrero, G.García Bermúdez, A.J.Kreiner, A.O.Macchiavelli, M.A.J.Mariscotti and C.Baktash, Progress Report 1980-81, Dept. of Physics, CNEA NT-5/82 (1982) pag.b.20 .

2)A.J.Kreiner, Z.Phys. A288(1978)373.

II.1.26 New data for the controversial ^{100m}Rh scheme

H.Huck, A.Jech, M.A.J.Mariscotti, A.Filevich and P.Thieberger+

In the previous Report[1], the scheme shown in fig. 1 was proposed as a solution for the standing controversy on the ^{100m}Rh 4,5 min decay[2,3,4].

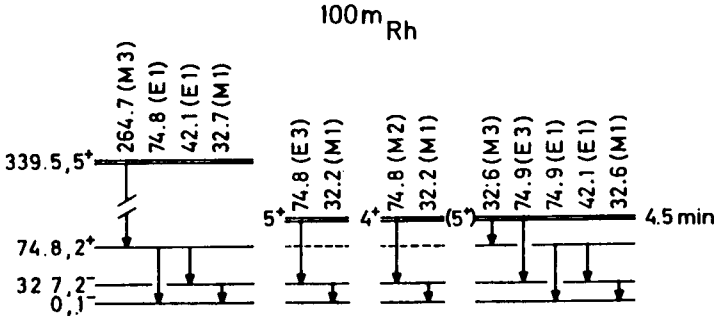

Fig.1

To test the validity of this scheme, which implies the existence of two unresolved doublets, a new measurements were performed with the purpose of determining the intensities of the 32.6, 42.1 and 74.9 keV lines.

The ^{100m}Rh isomer was produced via the ^{100}Ru(d,2n) reaction at 20 MeV with the BNL Tandem Van der Graff. Singles and coincidences spectra were accumulated during beam off periods of 3 min following 3 min irradiations with a beam current of 5 μA, using two high resolution Ge(Li) detectors of large efficiency for very low energy photons. The gamma intensities obtained from the single spectrum allowed us to calculate the "effective" conversion coefficients for the 32.6 and 74.9 keV lines. That corresponding to the later energy, results 80% larger than the measured value given by Babenko[4]. However, if with the coefficients so deduced one calculated the expected X-ray intensities, one obtain complete agreement with the measured intensity (see Table I).

Owing to the presence of two lifetimes: 219 and 100 ns[5] for the 2^+ and 2^- states respectively, the coincidence measurements only yielded positive results as regards the X-radiation with itself and the X-radiation with the 32.6 keV line. This lends further support for the proposed scheme.

It should be mention that the present analysis is based on the assumption that the isomer has $I^{\pi}=5^+$ as previously proposed[2,3], but the posibility $I^{\pi}= 5^-$ cannot be ruled out a priori. In this case however, the deduced X-ray intensity shown in Table I becomes $(3.6\pm0.4)\times10^{-4}$, which is not in agreement with the experimental value.

Table I

Energy	Multipole	Measured γ intensity	Deduced γ intensity	Deduced total intensity	Effective conv.coeff. deduced	Effective conv.coeff. measured	X-ray intensity deduced	X-ray intensity meas.
32.6	M_3	100	$<2\times10^{-2}$	90	10,4±1	8.1±3		
	M_1		100	1038				
42.1	E_1	9.6±1	9.6±1	27				
74.9	E_3	46±5	20±2	1013	21,8±2	12±3	$(4.7\pm.4)10^{-4}$	$(4.6\pm.4)\times10^{-4}$
	E_1		26±3	36				

+Brookhaven National Lab., Upton, N.Y., USA.

1) Progres Report 1980-81, Dept. of Physics, CNEA NT-5/82 (1982) pag.b.20.
2) J.Sieniowski, Acta Phys. Polónica, B5(1974)549.
3) B.G.Kiselev et al., Izv. Akad, Nauk, Ser, Fizika 42(1965)823.
4) V.V.Babenko et al., Izv. Akad, Nauk, Ser, Fizika 44(1980)1056.
5) A.M.Bizzeti-Sona et al., Z.Phys. A311(1983).

II.1.27 High-spin states in ^{218}Ra

J.Fernández Niello, H.Puchta[+], F.Riess[+] and W.Trautmann[+]

Yrast states in ^{218}Ra up to spin and parity $I^{\pi}=17^{-}$ were identified by means of the ^{208}Pb(^{13}C,3n) reaction and standard gamma-ray spectroscopic techniques. The level scheme is characterized by two bands of opposite parity with nearly constant level spacing. A cascade of strong E1 interband transitions connects both bands.

The negative-parity band which is observed from the $I^{\pi}=5^{-}$ to the $I^{\pi}=17^{-}$ state, is interpreted as an octupole vibrational band. The level scheme can be well reproduced in the vibrational limit of the interacting boson approximation (IBA1) which fails, however, to explain the strong E1 feeding of the negative-parity band from the ground-state band.

[+]Sektion Physik, Universität München, D-8046 Garching, FR Germany.

II.1.28 Evidence of g-bosons in the ^{218}Ra spectrum

J.Dukelsky, J.Fernández Niello, H.M.Sofía and R.P.J.Perazzo

The energy spectrum and deexcitation pattern of ^{218}Ra cannot be explained within the IBA unless g-bosons are included. This is done restricting the basis to fully aligned states. The framework developed is applicable to any situation in which prevails a vibrational pattern.

II.1.29 High spin states study in ^{217}Ra

C.Mittag[+], F.Riess[+], H.Puchta[+] and J.Fernandez Niello

The isotope ^{217}Ra was spectroscopied and its level scheme was established up to the spin 47/2. Levels below an isomeric state at 2.4 MeV were grouped in 3 bands, one of them with negative parity. These bands can be understood with the help of the shell model as 3 neutrons configuration wave functions. However, strong E1 transitions between the negative parity band and one band with positive parity suggest the existence of octupole deformations.

[+]Sektion Physik, Universität München, D-8046 Garching, FR Germany.

II.1.30 Deformation of the ^{75}Kr nucleus

G.García Bermúdez, C.Baktash[+] and C.J.Lister[++]

Recently Piercey et al.[1] studying the levels of $^{74-76}$Kr observed that the energies of the first 2^+ states deviate, when compared with the extrapolated value of the energies of the higher spin levels. This deviation was interpreted as a consequence of the perturbation between the ground and first 0^+ states with two different deformations. The concluded that the 0^+ ground state has a remarkably large deformation ($\beta \approx 0.4$) and the first excited 0^+ state is nearly spherical. Therefore it is interesting to study the odd-neutron ^{75}Kr nucleus, which lies between the ^{74}Kr and ^{76}Kr nuclei, and could show the effect of the defomations.

The decay of high spin states in ^{75}Kr was determined using the reaction ^{40}Ca(^{39}K,3pn) produced with a ^{39}K beam from the BNL Tandem accelerator at 120 MeV energy. The isotopic identification of the numerous gamma-rays observed in the single spectra was obtained measuring the coincidence between the gamma-rays and the particles emited by the compound nucleus. For this experiment a Ge(Li) detector together with a E-ΔE telescope, for charged particles detection and a liquid scintillator for neutron detection were used.

Using conventional techniques as gamma-gamma coincidences and angular distribution measurements the decay scheme shown in fig.1 was obtained.

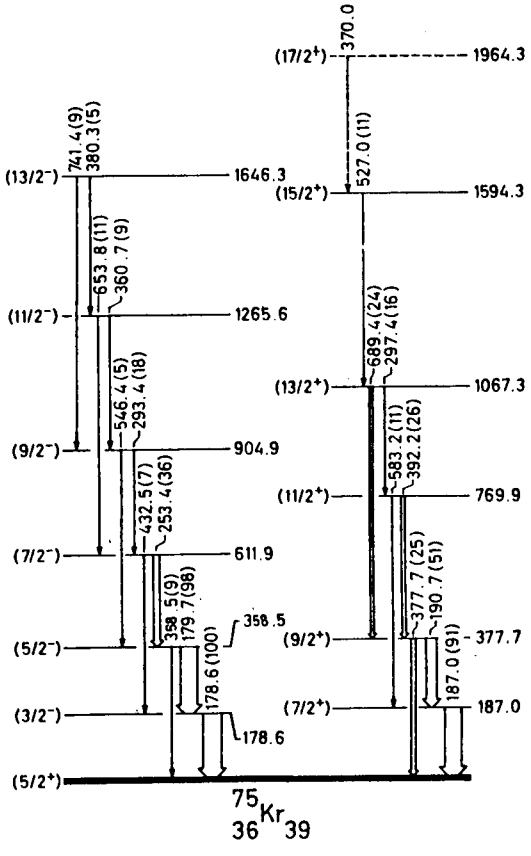

Fig.1

The decay to levels of ^{75}Br measurements suggest that the ground state is $I^{\pi}=(5/2^{+})$. Fig. 2 shows the present result compared with the ^{77}Kr nucleus, the similar decay pattern for both nucleus is apparent. This observation supported the proposed spin assignment for the excited level in the ^{75}Kr nucleus.

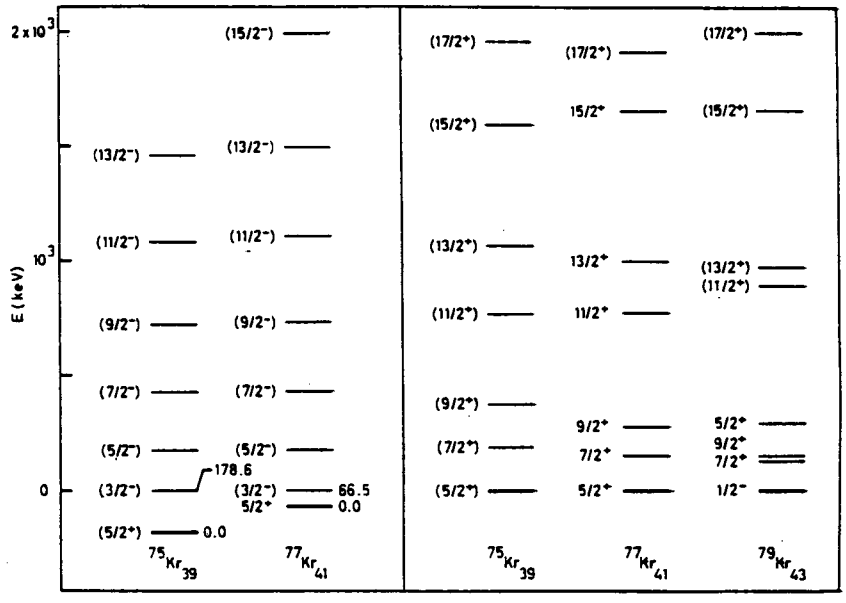

Fig. 2

The negative parity band built on the $(3/2^{-})$ at 178.6 keV energy can be fitted rather well with a rotational parameter of $A=\hbar^2/2\Theta=36(1)$ keV. Similar values for this parameter are obtained from $(3/2^{-})$ bands in the neighbouring odd-neutron nuclei which are 35(1) keV and 34 keV for ^{73}Se and ^{77}Kr respectively.

For this mass region the neutron Fermi level (for $\beta \approx 0.3$) lies approximately in the middle of the $g_{9/2}$ shell and is the origen of the positive parity band. The systematic of the positive parity band for the Kr isotopes is shown in Fig.2. The high spin study in ^{79}Kr (ref.3) determined three bands of $1/2^{-}[301]$, $5/2^{-}[303]$ and $5/2^{+}[422]$ parentage respectively. In ligher isotopes, bands of $5/2^{+}[422]$ and $3/2^{-}[301]$, are favored due to the decrease of the Fermi level. Theoretical calculations, in the framework of the Nilsson quasiparticle coupled to a rigid core model, describe the positive parity band for ^{79}Kr (ref.3) and ^{77}Kr (ref.4) rather well assuming a deformation of $\beta \simeq 0.3$. The decrease in the level staggering observed in the ^{75}Kr compared with ^{77}Kr positive parity band, could be described assuming a

small increase in the deformation (ϵ=0.32) that reduces the Coriolis perturbation.

Concluding, the interpretation of the experimental data suggest that the proposed high deformation for ^{74,76}Kr isotopes is not present in the odd-neutron ^{75}Kr nucleus.

+) Present address Oak Ridge National Laboratory, Oak Ridge, Tennessee, 37830 USA.

++) Present address Schuster Laboratory, Univ. of Manchester, Manchester, M139 PL, England.

1) R.B.Piercey et al., Phys.Rev.Lett. 47(1981)1514.

2) E.Nolte and P.Vogt, Z.Physik A275(1975)33.

3) M.Behar et al., Phys.Rev. C26(1982)1417.

4) A.J.Kreiner and M.A.J.Mariscotti, Phys.Rev.Lett. 43(1979)1150.

II.1.31 Band structure in ^{76}Rb

G.García Bermúdez, C.Baktash and C.J.Liester

The systematic study of doubly-odd nuclei at high angular momentum, in the A=70-80 region, revealed the predominant role played by the $g_{9/2}$ orbit in the structure of high spin states. Several collective bands built on an isomeric state of $I^{\pi}=4^{+}$, and structure $\pi g_{9/2} \otimes \nu g_{9/2}$, have been determined. The evolution of these bands towards lighter Br isotopes (Ref.1,2) for instance, suggests and increase in the deformation. The high spin study of ^{78}Rb (Ref.3) determined a band structure built on a isomeric state of I=4 (Ref.4) which shows a remarkable parallelism compared with the positive parity band of ^{76}Br and ^{77}Kr isotones (Fig.2). This observation supports the hypothesis of the existence of common mechanisms that describe

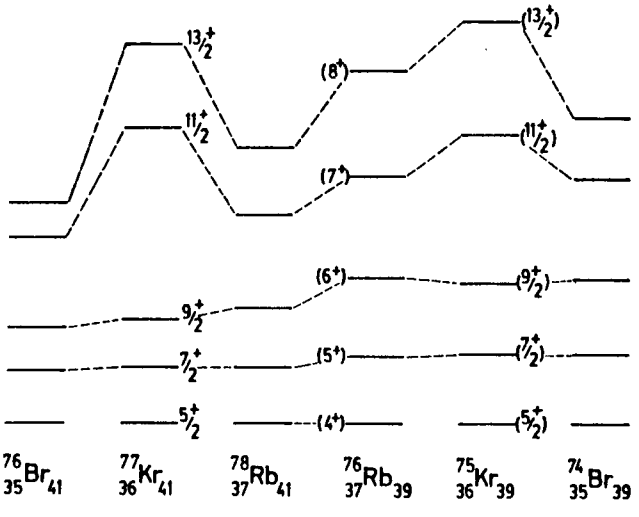

Fig.2

the low excitation energies of these nuclei. Latter theoretical calculations, using a Nilsson model of two quasiparticles coupled to a rigid core, confirmed rather well these ideas (Ref.5). The study of the evolution of the collective feature observed in the ^{78}Rb nucleus to lighter isotopes was the purpose of the present work. To populate high spin states in the very neutron deficient ^{76}Rb nucleus the ^{40}Ca(^{39}K,2pn) reaction was used. The experiments were carried out at the Brookhaven National Laboratory Tandem accelerator facility. To identify the gamma transitions belonging to the decay of ^{76}Rb the particle-gamma coincidence technique was used. The decay scheme obtained from the gamma-gamma coincidence and angular distributions measurements is shown in Fig.1. Two well developed collective bands built on the 1^- ground state and (4^+) isomeric state were found. The structure of the 1^- ground state of ^{76}Rb could be interpreted as a coupling of the g.s. of ^{77}Rb (Ref.4) $\pi 3/2^-[312]$ and the g.s. of ^{75}Kr (Ref.6) $\nu 5/2^+[422]$. The positive parity band is compared with the isotones ^{74}Br and ^{75}Kr in Fig.2.

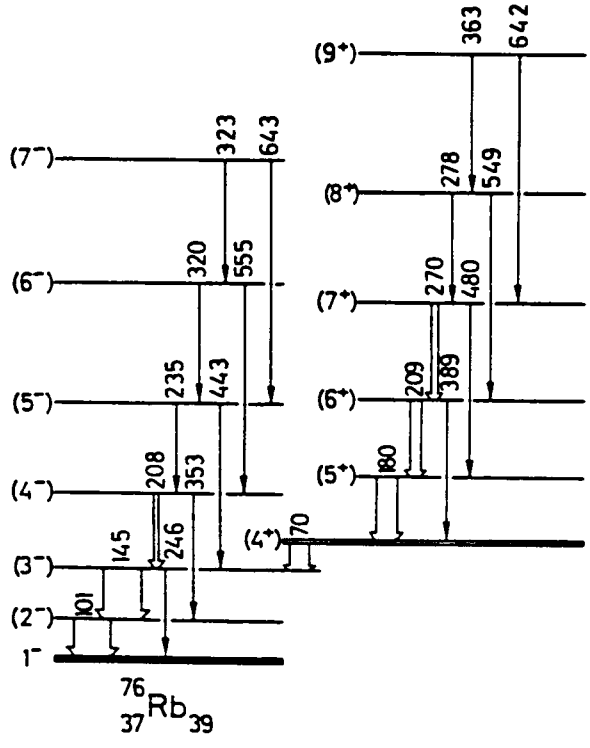

Fig.1

The parallelism observed for the ^{76}Br - ^{77}Kr - ^{78}Rb isotones is also extended to the ^{74}Br - ^{75}Kr - ^{76}Rb isotones. This result suggests that the odd-neutron plays an important role in the description of the low lying positive parity states. Fig.3 is a plot of the quantity $(E_I - E_{I-1})/2I$ for the proposed positive parity bands in ^{76}Rb and ^{78}Rb nuclei. For a rigid rotor this quantity assumes a constant value of $\hbar^2/2\mathcal{I}$. The decrease in the levels stag-

gering observed in Fig.3 for ^{76}Rb could be interpreted as an indication of an increase in the deformation. Recent theoretical studies which calculate the

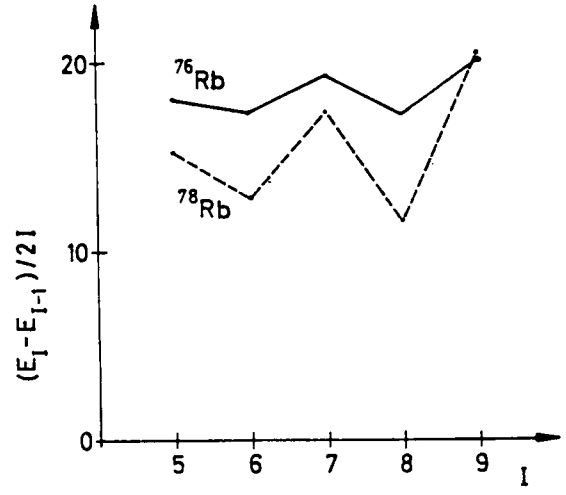

FIG. 3

nuclear shapes, throughout the chart of the nuclides, predict an island of high deformation ($\beta \simeq 0.4$) around N$\approx$40 and Z$\approx$40 (ref.7). The study of the $^{77-80}$Sr isotopes (ref.8) suggest that this region contains some of the most deformed nuclei known. The proximity of the ^{76}Rb to this region made it more interesting to further explore the properties of this nucleus.

---

1) G.García Bermúdez, A.Filevich, A.J.Kreiner, M.A.J.Mariscotti, C.Baktash, E.der Mateosian and P.Thieberger, Phys.Rev. C23(1981)2024.
2) G.García Bemúdez, C.Baktash, A.J.Kreiner, M.A.J.Mariscotti, Phys.Rev. C25(9182)1396.
3) M.A.J.Mariscotti, G.García Bermúdez, J.C.Acquadro, A.Lepine, M.N.Rao, W.Seale, E.der Mateosian and P.Thieberger, Phys.Rev. C19(1979)1301.
4) C.Ekström, S.Imgelman, G.Wannberg and M.Skarestad, Nucl.Phys. A311(1978)269.
5) A.J.Kreiner, M.A.J.Mariscotti, Phys.Rev.Lett. 43(1979)1150.
6) In this Report, II.1.30.
7) R.Bengtsson, P.Möller, J.R.Nix, Jing-ye Zhang, submitted to Physica Scripta.
8) C.J.Lister, B.J.Varley, H.G.Price and J.W.Olness, Phys.Rev. Lett C49(1982)308.

II.1.32 New method to interpret decoupled rotational bands

A.J.Kreiner

A new method is proposed to represent cuatitatively the excitation energy of decoupled rotational bands utilizing the collective angular

momentum R instead of the total angular momentum I. Decoupled bands are characterized by an yrast sequence of the $\Delta I=2$ type which is far from being reproduced by the I(I+1) law. It is generally accepted that the excitation energy of these bands follows the spectrum of neighboring even-even cores. However this rule is not very precise. It is shown here that it is possible to exhibit the parentage between decoupled bands and ground state bands of even-even neighbors (and reproduce cuantitatively the excitation energy of these decoupled bands) just by admitting a non-zero expectation value of R in the decoupled band heads and that from there on R increases in step of two units.

II.1.33 Double decoupling in doubly odd deformed nuclei: structure of $^{186}_{\ }Ir$

A.J.Kreiner, D.E.Di Gregorio, A.J.Fendrik, J.Davidson and M.Davidson

Stimulated by the finding of a decoupled rotational band (i.e. a $\Delta I=2$ sequence where the normal $\Delta I=1$ level ordering is reversed), while studying the high spin structure of ^{186}Ir (see fig.1), an analytical characterization of the conditions for doubly decoupling[1] was achieved for doubly odd deformed nuclei within the framework of the rotational model.

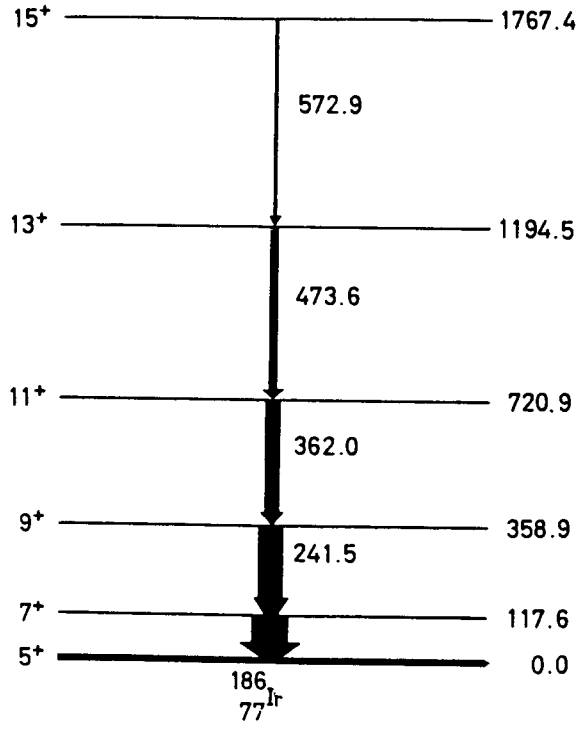

Fig.1

As it is well known the decoupling is related, in odd nuclei, to a single diagonal signature-dependent matrix element present only in K=1/2 bands[2]. In doubly odd nuclei there is no equivalente diagonal signature-dependent matrix element. In this case, an investigation of the rotational Hamiltonian shows that the equivalent role is played by a non-diagonal matrix element of the Coriolis operator connecting K=0 and K=1 states of special kind, namely $K=\Omega_n+\Omega_p=1/2+1/2=1$ and $K=\Omega_n-\Omega_p=1/2-1/2=0$. This matrix element reads: $-A(a_p+(-1)^{I+1}a_n)(I(I+1))^{1/2}$, where A is the rotational constant and $a_{n(p)}$ is the neutron (proton) decoupling parameter. In order to have decoupling, it is necessary that both decoupling parameters satisfy $|a_n|, |a_p| \gtrsim 1$. This is shown in figure 2 where excitation energies of several states are ploted against the ratio $x=a_n/a_p$ for the simplest two-band K=0 and K=1 system. The values $a_p=4.3$ is appropriate in magnitude for the participating $\pi h_{9/2}$ excitation known to give rise in odd Ir nuclei to decoupled bands. In fact, a more realistic calculation including all five Nilsson orbitals of $\pi h_{9/2}$ parentage, while leaving the decoupling conditions unaffected, brings the I=5 state down in energy to almost become the ground state.

Fig.2

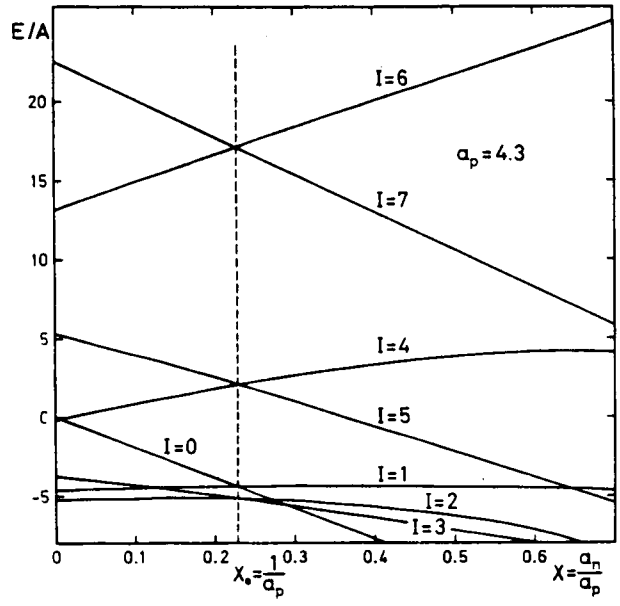

For the neutron there is a $\Omega_n=1/2$ orbital among the low lying negative parity states known in neighboring Os nuclei, which has $a_n \simeq 1$ bringing the situation very near to the crossing point $x_0=1/a_p$ (Fig.2). In conclusion, the ground state band of ^{186}Ir represents a very likely first candidate for the actual realization of the coupling scheme proposed here.

---

1) A.J.Kreiner, Z.Physik A288(1978)373 and references therein.

2) A.Bohr and B.R.Mottelson, Nucl.Structure, Vol. 2 (New York: Benjamin 1975).

II.1.34 Excited states of ^{188}Ir populated by the (α,3n) reaction

A.J.Kreiner, C.Alonso Arias, J.Davidson, M.Davidson, M.Debray, D.E.Di Gregorio and A.Pacheco

Enriched targets of ^{187}Re were bombarded with alpha-particles of energies in the 30-55 MeV range. Deexcitation of states in ^{188}Ir was studied using in-beam and off-beam gamma and electron spectroscopy techniques. A new level scheme (shown in Fig.1), exhibiting a rather high level density, is presented and an interpretation of the structure of these states is attempted using information on one-quasiparticle intrinsic states from neighboring odd-proton and -neutron nuclei.

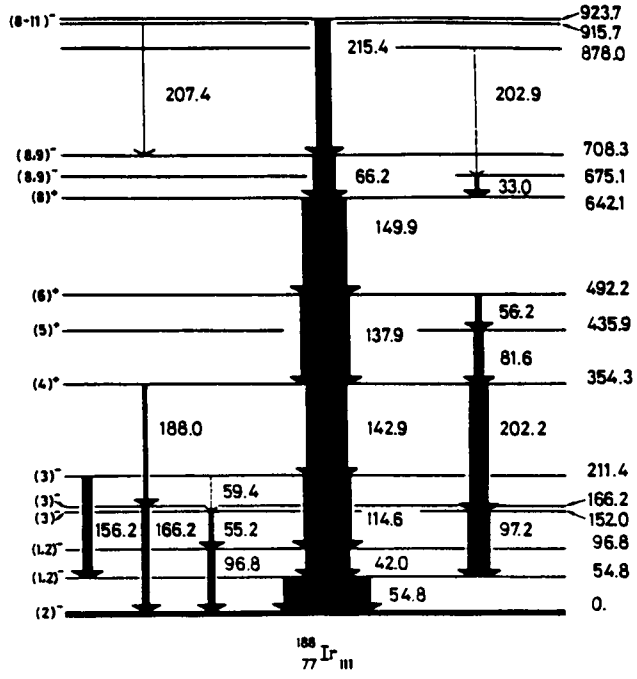

Fig.1

II.1.35 Isovector collective state with $K^{\pi}=1^{+}$ in deformed nuclei

D.R.Bes and R.A.Broglia

Isovector collective states with $K^{\pi}=1^{+}$ can be expected in deformed nuclei at relatively low energies[1-3]. The properties of these states are discussed within the RPA in a schematic model. We have successively studied the factors that influence the properties of these states (the energy and the reduced transition probability B(M1) to the ground state. They are:

i) the shell structure (we have assumed a pure harmonic oscillator as central potential);

ii) the correlations due to the residual quadrupole force;

iii) the polarization effects due to the shells with $\Delta N = \pm 2$;

iv) the pairing correlations;

v) the neutron excess.

Table 1 is obtained by successively including all these effects.

The B(M1) finally predicted is about 2 or 3 times larger than the presently available experimental numbers[4]. A calculation using Nilsson realistic single-particle levels is strongly reccommended.

Table 1

	$\omega/\delta\, A^{-1/3}$	$B(MI)/\delta A^{4/3}$ e/2Mc
i)	41	0.034
ii)	88	0.073
iii)	52	0.043
iv)	66	0.027
v)	65	0.025

1) N.Lo Indice and F.Palumbo, Phys.Rev.Lett. 41(1978)1532

2) E.Lipparini and S.Stringari, Phys.Lett. (to be published)

3) F.Iachello, Proc. of the Inter.Conf. on Nucl.Phys., Florence, Italy 1983.

4) A.Richter, Proc. of the Inter.Conf. on Nucl.Phys., Florence, Italy 1983.

II.1.36 Perturbative treatment of rotational motion

D.R.Bes, O.Civitarese and M.T.Acosta de Mehr

The perturbation treatment of deformed systems has been previously developed in ref.1 and applied to schematic models in ref.2. In the present work, this treatment is used to calculate the moments of inertia of a rotating system in a completely general quantum mechanical case.

The original hamiltonian H is replaced by the constrained hamiltonian H'

$$H' = \lim \left[H + \frac{1}{2D} \sum_{\nu}' (I_\nu - J_\nu)^2 + \frac{1}{2A} \sum_{\nu} \theta_\nu^2 \right]$$

where I_ν and J_ν are the components of the angular momentum operator acting on the collective and intrinsic subspaces, respectively. The angles θ_ν are conjugate variables to the J_ν. The properties of the RPA roots of H remain unaffected by the presence of the constraints but for the zero frequency modes which adquire an energy $(DA)^{-\frac{1}{2}}$. Within the RPA one obtains also an expression for the angles θ_ν and for the moments of inertia $\mathcal{J}_\nu$ through the known equations

$$[H, \theta_\nu] = -iJ_\nu / \mathcal{J}_\nu$$
$$[\theta_\nu, J_\nu] = i$$

The unitary transformation e^{IT} with $T = -\sum_\nu I_\nu \theta_\nu$ is used to eliminate the rotational and Coriolis terms in H'. This transformation yields smaller coupling terms, from which we return those which are linear and quadratic in the collective operators I_ν, and which are used to correct to the RPA moments of inertia. The limit $D \to 0$ has to be taken in the final expression, which should then be independent of the parameter Λ. Application to the calculation of the rotational properties in Mg^{24} is in progress.

---

1) V.Alessandrini, D.R.Bes and V.Machet, Nucl.Phys. B142(1978)489.

2) V.Alessandrini, D.R.Bes and V.Machet, Phys.Lett. 80B(1978)9.
D.R.Bes, G.G.Dussel and R.P.J.Perazzo, Nucl.Phys. A340(1980)157.
D.R.Bes, O.Civitarese and H.M.Sofía, Nucl.Phys. A370(1981)99.

II.1.37 Validity of the NFT lower orders

D.R.Bes and N.N.Scoccola

The validity of the lower orders of the NFT[1] has been previously studied in two different cases:

a) neutrons in realistic shells in the Pb region with a monopole pairing force between them[2].

b) 4 particles in a j-shell interacting through a general multipole force[3]

Although excellent results were obtain in the first case with the Rayleigh-Schrödinger perturbation theory, the convergence of the first order was very poor in the second case.

In this work we propose the use of a folded-diagram diagonalization method to treat the problem of 4-particles in a j-shell with a residual multipole interaction.

We obtain the addition pairing phonons in the TDA and construct the interaction effective hamiltonian including diagrams which correspond to the first and second order in the parameter Ω^{-1} (Ω representing the shell degeneracy). This diagrams are shown in fig.1.

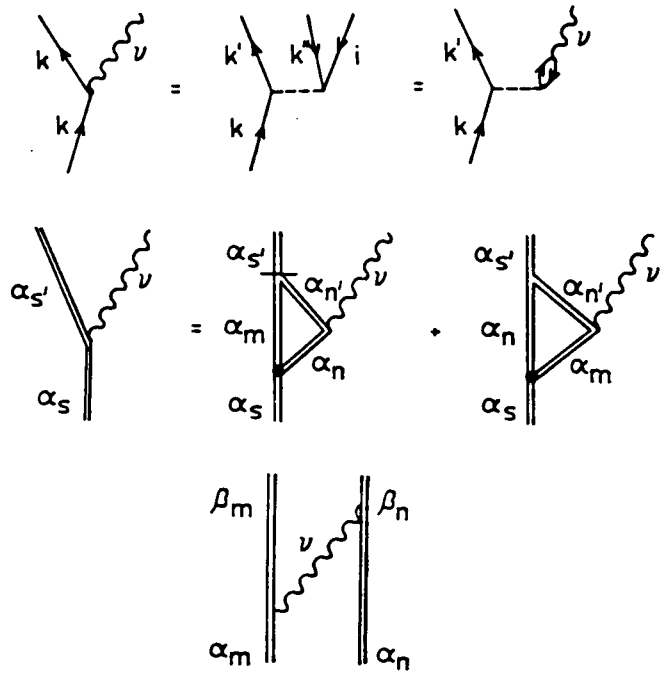

Fig.1

We calculate both energies and two-body transfer amplitudes with three different forces:

a) Almost pure monopole force

b) Almost λ-independent force

c) A monopole plus quadrupole force.

and for two different angular momentum of the shell: j=7/2;j=11/2.

Our main conclusions are that the R-S perturbation method gives very good results when no degeneracy exists between the NFT proper states. On the other hand when these degeneracies exist a diagonalization method is necessary and yield in general very good results. However the diagonalization method has problems when degeneracy exist between proper and improper states.

In the successful cases the first order is enough to reproduce the energies while the second order is necessary to reproduce the two-body transfer amplitudes, and to solve to a large extend the difficulties inherent to the degeneracy between proper and improper states.

---

1) D.R.Bes, G.G.Dussel, R.A.Broglia and B.R.Mottelson, Phys.Lett. 52B(1974)253.
2) P.F.Bortignon, R.A.Broglia and D.R.Bes, Phys.Lett. 76B(1978)153.
3) D.L.Wu and D.H.Feng, Phys.Rev. C24(1981)727.

II.1.38 The structure of the S and D pairs of the interacting boson model from the Hartree-Fock-Bogolyubov approximation[#]

S.Pittel and J.Dukelsky

The Hartree-Fock-Bogolyubov approximation is used to determine the optimum choice for the S and D pairs of the microscopic Interacting Boson Model. Results are presented for the even Sm isotopes.

[#] Phys.Lett. 128B(1983)9.

II.1.39 The quenching of $2p_{1/2}$ - $2p_{3/2}$ proton spin-orbit splitting in the Sr-Zr region

P.Federman, S.Pittel and A.Etchegoyen

The constancy in excitation energy of the lowest 2^+ state in the Sr isotopes across the N=56 subshell closure is shown to result from a reduction in the $2p_{1/2}$ - $2p_{3/2}$ proton spin-orbit splitting as the $2d_{5/2}$ neutron orbital is filled. Research is being carried out to see if the neutron-proton interaction also triggers collective-state wave functions in Sr isotopes.

II.1.40 OXBASH: The Oxford-Buenos Aires shell model Code

W.D.M.Rae, A.Etchegoyen, M.S.Goldwin and B.A.Brown

A new shell model code has been written for VAX11 computers. It works in the occupation number representation, where the occupancy (vacancy) of a bit in any given position of the computer (longword) symbolises the presence (absence) of a particle in a specific single particle state (i.e. in a given n,l,j,m_j,t_z state). As there might be in this representation, a maximum limit to the number of single particle states allowed in each calculation given by the number of bits per longword (32 for VAX11 systems), the programs generate and work with an m-scheme basis set in which any given basis state is a vector of 1,2,...longwords (for 32,64,... single-particle states). The great advantage of the occupation number representation technique is that it does not require large table of coefficients of fractional parentage.

The codes use an m-scheme Slater determinant basis, which is generated for a particular number of particle and a particular total J_z and T_z by the program 'BASIS'. The program 'PROJ' will construct basis states with good spin (J greater or equal J_z) and isospin (T greater or equal T_z). This is done by a projection technique. In this document the name 'PROJ' is used undistinguishably to replace either 'POSTPROJ' or 'PRIORPROJ' which are the actual program names. Therefore although there is not a computer code named 'PROJ', this name is used for either of two mentioned codes. Given this projected basis, the program 'MATRIX' constructed the Hamiltonian matrix for the case under consideration. Once the matrix has been produced, it has to be diagonalised, thereby giving the shell-model wavefunctions and for this purpose a LANCZOS algorithm is used. Finally, the wavefunctions can be used to calculated the following quantities by running the program 'TRAMP':

i) 1- and 2- particle parentage amplitudes,

ii) 1- and 2- body transition densities (to generate 1- and 2- body operator matrix elements),

iii) Overlaps of differents wavefunctions (this can be used to give SU(3) parentage amplitudes).

Many of the operations performed in this code do not promote particle from one J-orbit into another. This symmetry is referred as a partition symmetry and is intensively used throughout the coding. The partition of a basis pattern is stored as an integer, each byte of which is set to the number of particles in an specific J-orbit. Thus, the partition of an m-scheme basis vector tells how the total number of particles is split in the different J-orbits. Matrix elements will be non zero only when the sum of the partition number of the vector to which the operator is applied plus the partition number of the operator itself equals the partition number of the remaining vector (obviously, for direct overlaps of two m-scheme vectors, both vectors have to belong to the same partition). The partition symmetry greatly reduces both the CPU time and the core needed for the calculations.

II.1.41 Giant resonances in ^{208}Pb

D.R.Bes, P.Curutchet, S.L.Reich, N.N.Scoccola and H.M.Sofía

Recently new experimental information about the decay of giant multipole resonances in ^{208}Pb region has been available[1]. The empirical knowledge of

the detailed structure of these resonances motivated this work where we discuss the microscopic properties of the giant resonances in the framework of the NFT.

We propose that the resonance width is due to the mixing of the one phonon state with two phonons (2p-2h) and study the decay of these states through electromagnetic transitions.

The set of single particle states is calculated utilizing a harmonic oscillator potential with the parametrization given in ref.[2]. The one phonon states are generated through the RPA including both isoscalar and isovector residual interactions[3].

The calculations are carried out with the aid of the diagramatic expansion of the NFT. The diagram which contribute in first order to the decay of the giant resonance into the ground state are pictured in Fig.1 and those contributing to the one phonon state in Fig.2.

Other diagrams of the same order which include renormalization effects are taken into account through effective changes.

Figure 1

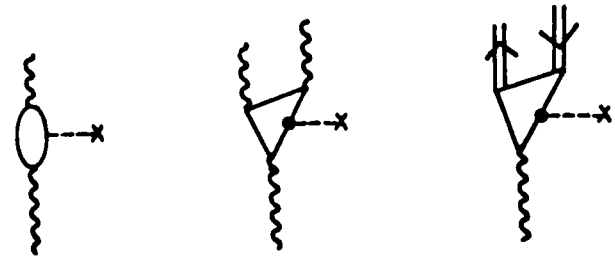

Figure 2

---

1) F.Bernard, private communication
2) S.G.Nilsson, C.F.Tang, A.Sobiczewski, Z.Szymanski, S.Wycech, G.Gustafson, I.Lamm, P.Möller and B.Nilsson, Nucl.Phys. A131(1969)1.
3) D.R.Bes, R.A.Broglia and B.S.Nilsson, Phys.Rep. Vol. 16C, N.1 (1975).

II.2 NUCLEAR REACTIONS

II.2.1 Cross sections calculations based on the intrinsic coordinates dependent collision matrix

M.Bernath, O.Dragún, J.Testoni and H.Massmann

The excitation of rotational and vibrational modes in deformed nuclei by heavy ion bombardment was calculated on the basis of the intrinsic coordinates dependent collision matrix (ICDCM) formalism.

The code VIBAND (VIbrational BANds) generates the intrinsic coordinates dependent collision matrix through standard nuclear optical model calculations.

This matrix was subsequently transformed in a collision matrix that depends on the final states quantum numbers. The code gives differential as well as integral cross sections and estimates the fusion cross section. Differential cross sections are calculated for each orientation of the residual nucleus intrinsic spin.

A remarkable feature of the method is that it can be use as an alternative to huge coupled channel calculations when the sudden approximations are valid.

In this way drastic improvements in memory and computing time have been obtained.

The treatment was succesfully tested in the cases $\alpha + {}^{154}Sm$ at E_α =50 MeV for the excited states 0^+, 2^+, 4^+, 6^+ and 1^-, 3^- and ${}^{12}C + {}^{150}Nd$ at $E_{^{12}C}$=70.4 MeV for the states 0^+, 2^+, 4^+ and 3^-.

II.2.2 An investigation of nuclear reactions leading to charge exchange between heavy ions

A.Etchegoyen, D.Sinclair, P.S.Fisher, S.Liu and M.C.Etchegoyen

A study of the ${}^{26}Mg({}^{12}C,{}^{12}B){}^{26}Al(5^+,3^+)$ and ${}^{7}Li({}^{10}B,{}^{10}Be){}^{7}Be(3/2^-,g.s.)$ charge exchange reactions and the ${}^{7}Li({}^{10}B,{}^{8}Li(2^+,1^+)){}^{9}B$ two proton transfer reaction was performed. The measurement and analysis of the reactions in terms of direct processes was described. Special emphasis was laid on the competition between one and two step (sequential) mechanisms for the reactions. The sequential process appears to make an important contribution

to all five of the above mentioned reactions while for two of them (^{7}Be(3/2^{-},g.s.) and ^{8}Li(2^{+},g.s.)) the one step mode is apparently also important.

Several analyses of one particle transfer reactions were also performed. These analyses are considered a necessary preliminary to the study of the much more complicated processes involved in charge exchange and two proton transfer. From the analysis of single particle transfer reactions it was possible to test (and fix when necessary) the optical model potentials needed for the reaction calculations and to test the parameters used in the description of the bound state wave functions.

Relevant parentage amplitudes and one body transition densities have been calculated from the shell model. The distorted wave Born approximation and the coupled reaction channel models were used as the basis for calculating the cross sections for particle transfer reactions. A microscopic direct model was reviewed, coded in FORTRAN and used to predict the contribution of the one step mode to the charge exchange reactions.

II.2.3 Spin determination via α-d angular correlations and α-transfer DWBA analysis in ^{18}F high energy states[#]

M.C.Etchegoyen, D.Sinclair, A.Etchegoyen and E.Belmont Moreno

Particle-particle angular correlations for reactions in non-zero degree geometry and with non-zero spin nuclei were investigated and found to be a valuable tool for spin determination. (d-α) angular correlations for ^{14}N(^{6}Li,d)^{18}F$^{*}\rightarrow$ (α) ^{14}N were measured for three strongly excited states in ^{18}F (9.58 MeV, 11.2 MeV and 14.1 MeV), at 36 MeV of bombarding energy. Spins and parities for two of the observed states were determined, and, in agreement with theoretical predictions, these states are suggested as members of the $K^{\pi}=1^{+}$ -rotational band. The three analyzed states are found to undergo a predominant α-particle decay to the ground state of ^{14}N. Angular distributions for all the observed states are measured and analyzed under Hauser Feshbach and exact finite range DWBA formalism with Gamow unbound wave functions. Spectroscopic factors are extracted and compared to the shell model predictions showing a reasonable agreement.

[#] Nucl.Phys. A402(1983)87-113.

II.2.4 Three particle transfer on ^{14}N

M.C.Etchegoyen, A.Etchegoyen and E.Belmont Moreno

(^{3}He-α) and (t-α) angular correlations for the reaction processes $^{14}N(^6Li,^3He)^{17}O^* \rightarrow (\alpha)\ ^{13}C$ and $^{14}N(^6Li,t)^{17}F^* \rightarrow (\alpha)\ ^{13}N$ respectively are measured at 36 MeV of ^{6}Li beam. High selectivity is observed for the three particle transfer processes. Structureless angular correlations hinder definite spin and parity assignments, but the displacement of the preferred direction observed in the decay patterns gives information on the range of plansible angular momenta. Shell model calculations are performed for comparison with the experimental data, and this allows tentative spin identification. EFR-DWBA coalculations are carried out, providing more confirmation on the spin suggestions. Useful nuclear structure information is obtained for the mass 17 nuclear states. Our data show a weak t+^{3}He clustering in ^{6}Li ground state.

II.2.5 A study of the $^{26}Mg(^{12}C,^{12}B)^{26}Al$ charge-exchange reaction[#]

A.Etchegoyen, D.Sinclair, S.Liu, M.C.Etchegoyen, D.K.Scott and D.L.Hendrie

The reaction $^{26}Mg(^{12}C,^{12}B)^{26}Al$ (5^+,3^+) has been studied using a beam of 102 MeV of ^{12}C. Shell-model, microscopic direct model and finite-range coupled reaction channel (CRC) calculations including a recoil effects, have been performed, for comparison with the experimental data. DWBA calculations were performed for the intermediate states of interest in the $^{11}B+^{27}Al$ and in the $^{13}C+^{25}Mg$ channels and these results were also compared with the experimental ones. The dominant reaction mechanism for the $^{26}Mg(^{12}C,^{12}B)^{26}Al$ (5^+,3^+) appears to be the sequential mode.

[#] Nucl.Phys. A397(1983)343.

II.2.6 $^{10}B+^{17}O$ fusion cross sections[#]

Y-D.Chan, D.E.Di Gregorio, J.L.C.Ford,Jr., J.Gomez del Campo, M.E.Ortiz and D.Shapira

The fusion cross section for $^{10}B+^{17}O$ has been measured at four excitation energies in ^{27}Al of E^*=48.4, 55.1, 66.9 and 74.4 MeV in order to study possible compound nucleus limitation effects on fusion for light heavy-ion systems at intermediate excitation energies. Comparing this data with other measurements for different entrance channels populating the same compound nucleus it is found that for $E^* \leq 60$ MeV all fusion bands in the E^*-J plane of ^{27}Al appear to be parallel and displaced by the corresponding differences in separation energies, and that for $E^* > 60$ MeV the bands tend to converge indicating a possible compound nucleus limitation effect. The data are compared with existing model for entrance channel and statistical yrast line limitations.

[#] Phys.Rev. C25(1982)1410.

II.2.7 Fusion, direct, and total reaction cross sections of the $^{10}B+^{14}N$ system up to $E_{^{14}N}$ =180 MeV[#]

M.E.Ortiz, J.Gomez del Campo, Y-D.Chan, D.E.Di Gregorio, J.L.C.Ford, D.Shapira, R.G.Stokstad, J.P.F.Sellschop, R.L.Parks and D.Weiser

The fusion cross section of the $^{10}B+^{14}N$ system has been measured at five energies covering the range $E_{^{14}N}$ =86-180 MeV. Angular distributions of fusion and direct reaction components for products from Z=3 to Z-11 have been determined. Hauser-Feshbach calculations of the Z distributions, energies and angular distributions of the evaporation residues are presented and compared to the data. The fusion cross section decreases slowly with increasing energy and reaches a maximum angular momentum of about $21\pm1\hbar$. The fusion cross section is discussed in terms of entrance channel models and compound nucleus formation and is compared to that of the $^{12}C+^{12}C$ system. The experimental total reaction cross sections are in good agreement with optical model calculations with parameters deduced from elastic scattering.

[#] Phys.Rev. C25(1982)1436.

II.2.8 $^{14}N+^{13}C$ fusion cross sections and compound nucleus limitation in ^{27}Al[#]

D.E.Di Gregorio, J.Gomez del Campo, Y-D.Chan, J.L.C.Ford, D.Shapira and M.E.Ortiz

Fusion cross sections for the $^{14}N+^{13}C$ system have been measured by detecting the evaporation residues at five bombarding energies which correspond to high excitation energies in the compound nucleus: $E^*(^{27}Al)$=64-110 MeV. The ^{27}Al nucleus can be populated by four different heavy-ion entrance channels ($^{15}N+^{12}C$, $^{16}O+^{11}B$, $^{14}N+^{13}C$ and $^{17}O+^{10}B$) which are accessible to experimental measurements. Comparing the present data with those already existing for the above channels, it is found that for $E^* > 60$ MeV the curves E^* vs J_{cr} for each system converge, which may be indicative of a limitation imposed by the compound nucleus. The data are discussed in terms of existing models for entrance channel and statistical yrast line limitations. The highest energy point also suggests the existence of a maximum absolute angular momentum limit of $\sim 28\hbar$.

[#] Phys.Rev. C26(1982)1490.

II.2.9 Fusion cross sections for the $^{12}C+^{15}N$ system[#]

R.Novotny, D.Shapira, Y-D.Chan, D.E.Di Gregorio, J.L.C.Ford,Jr., J.Gomez del Campo, M.E.Ortiz and F.Pougheon

Fusion cross sections were measured for the $^{12}C+^{15}N$ system at two ^{12}C bombarding energies, 98 and 117 MeV. The extracted fusion cross sections are 946 ± 74 mb for $E(^{12}C)$=98 MeV and 889 ± 89 mb for $E(^{12}C)$=117 MeV. The critical angular momenta for fusion deduced from the cross section measurements equal, within $1\hbar$, the values deduced from $^{14}N+^{13}C$ and $^{10}B+^{17}O$ at the same excitation energies, thus indicating a compound nucleus limitations for fusion.

[#] Phys.Rev. C26(1982)2664.

II.2.10 Fusion and peripheral processes in the collisions of $^{20}Ne+^{20}Ne$ and $^{20}Ne+^{16}O$[#]

D.Shapira, D.E.Di Gregorio, J.Gomez del Campo, R.A.Dayras, J.L.C.Ford,Jr., A.H.Snell, P.H.Stelson, R.G.Stokstad and F.Pougheon

Reaction products from the bombardment of ^{20}Ne and ^{16}O gas targets with ^{20}Ne beams have been measured at five laboratory energies between 70 and 160 MeV. Fusion, deep inelastic, and quasielastic processes were studied. Large deep inelastic yields ($\sigma_{DI} \gtrsim 600$ mb) with average Q values of -50 MeV are present at the highest energy. Analysis of the fusion cross sections for $^{20}Ne+^{16}O$ suggests that the maximum angular momentum in ^{36}Ar populated via this entrance channel may be as low as $29\pm2\hbar$.

[#] Phys.Rev. C28(1983)1148.

II.2.11 Charge distribution and pairing effects in cold fission processes

D.Napoli, D.Otero, A.Plastino and A.N.Proto

The fine structure of the fission yield for mass distributions is studied by the "surprisal" method[1-3]. Pairing effects in the scission point allow us to explain the fine structure, using the maximal entropy formalism. Our proposed empirical charge distribution which satisfy the maximum entropy principle is compared with previous hipothesis[4]. Even-even nuclei seem to be more abundant. This result points out that charge-equilibration demands more time than was previously supposed.

---

1) Y.Alhassid and R.D.Levine, J.Chem.Phys. 67(1977)4321

2) Y.Alhassid and R.D.Levine, Phys.Rev. A18(1978)89.

3) D.Otero, A.N.Proto and A.Plastino, Phys.Lett. 98B(1981)225.

4) R.Vandebosch and J.R.Huizenga, Nuclear Fission (Academic Press, New York, 1973).

II.2.12 Prediction of anomalous large angle scattering of heavy ions[#]

G.G.Dussel, A.O.Gattone and E.E.Maqueda

Simple total energy considerations allow an explanation for the nuclear surface transparency in heavy-ion elastic scattering and hence a prediction of the reactions that present a strong backward rise in the angular distributions.

[#] Phys.Rev.Lett. (in press).

II.2.13 Pair-exchange or double-charge-exchange reactions[#]

D.R.Bes, O.Dragún and E.E.Maqueda

Pair-exchange or double-charge-exchange reactions are studied from the point of view of one step processes. Two possible mechanisms are analyzed, involving either the simultaneous exchange of a dineutron and a diproton between the target and the projectile or the simultaneous transformation of the charge of the dinucleon in each system. Although the formalism is explicity developed for the (^{14}C,^{14}O) reaction, its extension to other projectiles is straighforward. The possibility of populating collective states which otherwise are very difficult to attain is stressed. Application is made to the cases of the $^{208}Po(^{14}C,^{14}O)^{208}Pb$ and $^{40}Ca(^{14}C,^{14}O)^{40}Ar$ reactions.

[#] Nucl.Phys A405(1983)313.

II.2.14 Form factors for many nucleon transfers

S.M.Lenzi and E.E.Maqueda

Some methods have been developed in order to check approximations used to calculate the form factors for many nucleon transfers. They find self consistently the potential that binds the transferred cluster. In a first approach a single potential for all the different number of nodes is adjusted to render the correct binding energy. A more satisfactory method is subsequently used, in which the potential is adjusted to give the asymptotic behaviour. Cross sections obtained with these methods are compared with the results of the usual approximations and experimetal data.

II.2.15 The (p,d) reaction: a good test to elucidate the strength of large energy loss one-step processes[#]

O.Dragûn, A.M.J.Ferrero and A.O.Gattone

The absolute contributions of the one-step neutron pick-up cross sections to the inclusive (p,d) cross sections in Fe, Sn and Bi are calculated within the framework ot the DWBA. The estimated cross sections of (p,p')(p',d) process is also given in the case of ^{54}Fe. Our results indicate that the one-step mechanism accounts for the total experimental yield only in the residual excitation energy range of 0 to 8-10 MeV.

[#] Phys.Lett. 119B(1982)25.

II.2.16 The contribution of one and two-step processes to inclusive (p,d) reactions[#]

A.O.Gattone, A.M.J.Ferrero and O.Dragûn

Absolute one and two-step angular cross sections are calculated for (p,d) inclusive reactions up to very large ejectile energy loss. Several targets and incident energies are considered in the applications. The (p,p',d) and (p,d',d) routes chosen for the two-step mechanism show a very different behaviour as a function of the excitation energy. As a main result we observe that the one-step process exhausts the total experimental yield only in the energy loss range of 0 to 7-10 MeV. For excitation energies greater than 25 MeV more than two-step processes must be include in order to account for the experimental result.

[#] Submitted to Nucl.Phys. A.

II.2.17 Alpha-particle emission from the reaction 1354 MeV ^{165}Ho+^{181}Ta[#]

L.G.Sobotka, R.J.McDonald, G.J.Wozniak, D.J.Morrissey, A.J.Pacheco and L.G.Moretto

The emission of α particles from the deep-inelastic reaction 1354 MeV ^{165}Ho+^{181}Ta has been studied. Alpha particles were detected in coincidence with a projectilelike fragment, both in and out of the reaction plane. Average velocity diagrams, α -particle energy spectra as a function of angle,

and α -particle angular distributions are presented. The in-plane data show that the bulk of the α particles in coincidence with the deep-inelastic exit channel can be explained by evaporation from the fully accelerated fragments. The out-of-plane α -particle angular distribution data together with gamma-ray multiplicity data from previous work give a consistent picture of the transfer and partitioning of angular momentum between the two fragments.

Phys.Rev. C28(1983)219.

II.2.18 Angular momentum, statistical equilibrium and sequential fission in very asymmetric systems#

D.J.Morrissey, G.J.Wozniak, L.G.Sobotka, A.J.Pacheco, C.C.Hsu, R.J.McDonald adn L.G.Moretto

The in- and out-of-plane angular distributions for fission fragements in coincidence with projectile-like products from the reaction of 252 MeV ^{20}Ne with ^{197}Au and ^{238}U have been measured. The results are compared to a statistical model which has successfully explained γ -ray anisotropies from a heavy symmetric system. The agreement is rather good after proper consideration of the direction of the line-of-centers at contact.

Z.Phys A305(1982)131.

II.2.19 The effect of statistical fluctuations on the measurement of the total energy and multiplicity of γ rays following deep-inelastic reactions#

A.J.Pacheco and L.G.Moretto

We discuss the effect of statistical fluctuations on the first and second moments of both the intrinsic rotational energy and the sum of spin magnitudes in deep-inelastic fragments, as extracted from measurements of the total γ -ray energy and the γ -ray multiplicity, respectively. The calculations were done in the framework of a model that considers the thermal excitation of rotational modes in the intermediate dinuclear complex, accounting exactly for the correlations between the angular momenta generated in both nuclei.

Z.Phys. A306(1982)259.

II.2.20 Intrinsic fragment spins generated in the reactions of ^{20}Ne with ^{197}Au and ^{238}U at 12.6 MeV/nucleon[#]

D.J.Morrissey, G.J.Wozniak, L.G.Sobotka, A.J.Pacheco, R.J.McDonald, C.C.Hsu and L.G.Moretto

The average magnitude and alignment of the intrinsic spin of the heavy partner from the reaction of 252 MeV ^{20}Ne with ^{197}Au and ^{238}U were determined as a function of Q-value. These spin values were extracted from sequential fission angular distributions obtained in coincidence with projectile-like products. For all Q-values a large out-of-plane anisotropy was observed, while for large negative Q-values an in-plane anisotropy was observed. A very large entrance-channel mass-asymmetry was chosen to provide a stringent test of equilibrium statistical model predictions for the spin alignment. The importance of determining the direction of the line-of-centers of the dinuclear system at scission is discussed. Large values of P_{zz} were deduced for all Q-values. P_{xy} was observed to be positive in the quasielastic region and negative in the deep-inelastic region. The extracted alignment data are compared to equilibrium statistical model calculations.

[#] Nucl.Phys. A389(1982)120.

II.2.21 Equilibrium treatment of spin-depolarizing modes in mass asymmetric heavy-ion systems

R.P.Schmitt and A.J.Pacheco

A two-sphere model is developed for the thermal excitation of spin-depolarizing modes in mass asymmetric heavy-ion systems. The effect of these modes on the spin distributions and the spin alignment of the fragments is investigated.

[#] Nucl.Phys. A379(1982)313.

II.2.22 Evidence for spin fluctuations in the deep-inelastic reaction $^{165}Ho+^{165}Ho$ at 8.5 MeV/amu[#]

R.J.McDonald, A.J.Pacheco, G.J.Wozniak, H.H.Bolotin, L.G.Moretto, C.Schück, S.Shih, R.M.Diamond and F.S.Stephens

Both the magnitude and alignment of the transferred angular momentum in the reaction $^{165}Ho+^{165}Ho$ have been measured as a function of Q-value via continuum γ -ray multiplicity and anisotropy techniques. The spin transfer and the continuum γ -ray anisotropy increase throughout the quasi-elastic region. The spin transfer as a function of Q-value saturates at $\sim 35\hbar$/fragment, the anisotropy peaks at a value of ~ 2 and then decreases to near unity for the largest Q-values. The observed anisotropies are in good agreement with predictions from an equilibrium statistical model in which thermal excitation of angular-momentum-bearing collective modes and neutron evaporation give rise to in-plane components of the angular momentum.

[#] Nucl.Phys. A373(1982)54.

II.2.23 Angular-momentum transfer and alignment in deep-inelastic reactions for nearly symmetric heavy-ion systems[#]

A.J.Pacheco, G.J.Wozniak, R.J.McDonald, R.M.Diamond, C.C.Hsu, L.G.Moretto, D.J.Morrissey, L.G.Sobotka and F.Stephens

The magnitude and alignment of the spin transferred to the fragments in the deep-inelastic reactions of 8.5 MeV/nucleon ^{165}Ho on ^{176}Yb, ^{148}Sm and ^{nat}Ag were investigated using continuum gamma-ray multiplicity and anisotropy techniques. The detection system consisted of a highly redundant arrangement of particle and gamma-ray detectors and a gamma-ray multiplicity filter. By using suitable reduced quantites we show that for the most negative Q-values the multiplicity data are consistent with rigid-rotation of the intermediate dinuclear complex. The anisotropy data are compared to an equilibrium statistical model calculation. The sensitivity of the calculation to different assumptions concerning the composition of the gamma-ray spectra is investigated. The magnitude and alignment of the spin imparted to the individual fragments as a function of Q-value are extracted for the three reactions.

[#] Nucl.Phys. A397(1983)313.

II.2.24 The characteristics of electric dipole strength built on highly-excited continuum states[#]

A.M.Sandorfi, J.Barrette, M.T.Collins, D.H.Hoffmann, A.J.Kreiner, D.Branford, S.G.Steadman and J.Wiggins

High-energy gamma-ray spectra from heavy-ion fusion reactions have been measured with low background and high resolution over a broad mass range. The data have been fitted with statistical-evaporation calculations in which the gamma-ray strength associated with each level follows a lorentzian. The extracted resonance widths are generally much larger than the width of the giant dipole resonance built on the ground state of the compound system (gs-GDR). The centroids of these excited-state resonances are shifted from those of the gs-GDRs, but no simple $A^{-1/3}$ dependence is evident. The most surprising result is that the extracted sum rule strengths of these resonances track those of the gs-GDRs observed in photoabsorption.

[#]Phys.Let. 130B(1983)19.

II.2.25 Time-Dependent Variational Description of alpha-alpha scattering[#]

M.Saraceno, P.Kramer and F.Fernandez

The time-dependent variational principle is applied to the simple but quite realistic situation of alpha-alpha scattering. The effects of antisymmetrization are included and we show that they lead to a change in the structure of the phase space of relative motion. The main new feature is the appearance of forbidden regions in the phase space which have, in the quantum treatment, a close connection with states excluded by the Pauli principle. The elastic phase shifts are evaluated semiclassically in the distorted phase space and compared to a quantum calculation by the resonating group method.

[#]Nucl.Phys. A405(1983)88

II.2.26 Study of the alpha-^{16}O reaction

M.Saraceno, L.F.Canto and R.Donangelo

We extend the method applied to alpha-alpha scattering in ref.[1] to the more complex case of alpha-^{16}O. Besides the treatment of the Pauli principle we include in classical phase space the effects of parity proyection. In addition we show that bound states and rotational bands are reproduced by the time dependent variational calculation with the same accuracy as phase shifts. The results encourage the application to heavier systems.

---

[1] M.Saraceno, P.Kramer, F.Fernandez, Nucl.Phys. A405(1983)88.

II.2.27 Some physical quantities of interest in nuclear reactions and their dependence upon the projectile-target system: Characteristic curves for the TANDAR accelerator.

J.O.Fernández Niello and A.J.Pacheco

The design and analysis of experiments involving heavy-ion reactions usually require the knowledge of a number of characteristic parameters (grazing angular momentum, center-of-mass, energy above the Coulomb barrier, etc.), and their dependence upon the entrance-channel reaction system. Under same reasonable assumptions, all these physical quantites may be expressed as very simple functions of the mass and atomic numbers of the projectile and target nuclei (Z_p, Z_t, A_p, A_t), and of the bombarding energy (E_p). However, if are attempts to apply these formulae to the case of reactions induced by particles provided by a specific accelerator, the above simple picture is often obscured by the characteristic dependence of the projectile energy upon its mass or charge. In this work, we present graphs corresponding to different physical quantities for reactions induced with an electrostatic accelerator operating at terminal voltages, similar to those expected to be reached by TANDAR. The information is displayed in the form of contour plots in two equivalent two-dimensional coordinate systems $(Z_p,Z_t)_x$ and $(A_p+A_t, (A_t-A_p)(A_t-A_p))$, corresponding to alternative representations of all the possible projectile-target combinations.

III. Solid State Physics

1. Vibrational Spectroscopy
2. Crystal Structure and Phase Transformations
3. Crystal Growth
4. Mössbauer Spectroscopy
5. Theoretical Solid State Physics
6. Geological Applied

III.1 VIBRATIONAL SPECTROSCOPY

III.1.1 Polarized Raman spectra of a single crystal of Bromine

E.Halac and H.Bonadeo

The polarized Raman spectra of a single crystal of bromine have been obtained and the results lead to an unambiguous assignment of the corresponding fundamental bands. The resulting vibrational pattern is similar to that reported for solid iodine from inelastic neutron scattering experiments.

III.1.2 Lattice dynamics and crystal stability of bromine

Z.Gamba, E.Halac and H.Bonadeo

The lattice dynamics and crystal stability of bromine have been studied using an interaction potential which includes atom-atom and coulombic terms. It was found that in addition to high order electrostatic terms, a specific interaction of the form $-D/r^8$ between nearest neighbor atoms, which is identified as an induced dipole-induced quadrupole term, is needed to stabilize the observed orthothombic structure and to give a good fit with other static and dynamical observables.

III.1.3 A cryostatic cell for polarised Raman studies

E.Halac and N.Gutierrez

A low-temperature cell for polarised Raman spectroscopy is described with facilities for growing single crystals from the liquid, and for the orientation of the samples with the aid of X-ray diffraction.

III.2 CRYSTAL STRUCTURE AND PHASE TRANSFORMATIONS

III.2.1 The crystal structure of copper strontium formate hydrate ($CuSr_2(COOH)_6.8H_2O$)

R.F.Baggio, P.K.de Perazzo and G.Polla

The crystal structure of $CuSr_2(COOH)_6.8H_2O$, has been determined by three dimensional X-ray analysis. The crystals are triclinic, space group $P\bar{1}$, with a=6.61(1) Å, b=8.84 (2)Å, c=8.90(2) Å, α=104,5(1)°, γ=88,5(1)°, β=96.0(1)°; Z=1.

The structure was solved by the heavy atom method through a Patterson synthesis and refined by full matrix least squares to a final R=0.092 . The coordination around heavy atoms is normal. The copper atom, situated at a center of symmetry, is surrounded by a Janh-Teller deformed octahedron made up by six oxygen atoms from six different formate groups. The Sr atoms have a ninefold coordination polihedron of evenly distributed oxygen atoms, five of them from formate ions and the remaining four from water molecules. The different coordination polyhedra are strongly linked to each other, both by corner and edge sharing as well as by bridges through one of the formate groups. This results in a tightly woven two-dimensional network stretching parallel to (010). Interconections between layers is achieved by means of only one type of H boding, thus explaining the neat cleavage along (010).

III.2.2 Topotactic transformation in ($CuSr_2(CO_2H).8H_2O$)

R.Baggio, M.A.R.de Benyacar, P.K.de Perazzo and G.Polla

The topotactic transformation of Copper-Strontium formate hydrate, into Strontium formate was studied by single crystal and powder X-ray diffraction as well as high temperature optical microscopy.

Single crystal studies at room temperature gave a unique relationship between the orientation of parent (triclinic) and product (orthorrombic) phases.

$(hol)_T^*$ // $(HOL)_O^*$ $\qquad$ $\langle ool\rangle_T^*$ // $\langle OOL\rangle_O^*$

(in reciprocal space)

$\langle oko\rangle_T$ // $\langle OKO\rangle_O$ $\qquad$ $(hko)_T$ // $(HKO)_O$

(in real space)

These orientation relationship could not be explained by the conservation of any structural motives, as is usually the case in this type of transformations.

Oriented nucleation, however, can sometimes take place just because of a metric match between both lattices; the transformation being then a "recrystallization" process.

This seems to be the case in Copper-Strontium formate dehydration where cell dimensiones in (ool) planes are almost coincident for both phases:

a = 6.63 Å	b = 8.77 Å	γ = 88°35'
A = 6.79 Å	B = 8.76 Å	Γ = 90°

Besides, the hint of a recrystallization of the orthorrombic phase was observed on an optical microscopy heating stage where well developed single crystals of Sr $(HCOO)_2$ were found to grow at a very high rate in the core of copper Strontium hydrate formate single crystal, with temperatures ranging from 80 to 120°C.

A high correlation between their growth directions was found, being larger for lower transformation temperatures. X-ray diffraction as well as EDAX analysis of the transformed sample, showed a high concentration of unidentified crystalline material containg copper in the outermost part of the specimen.

Research on the subject is in progress.

III.2.3 Phase transitions in $8PbO.V_2O_5$

R.Baggio, L.Schmirgeld, M.A.R.de Benyacar

A new, first order, reversible phase transition is reported in $8PbO.V_2O_5$ (T_c = 250-270°C on heating; 170-190°C on cooling).

Together with the already known, ferroelastic transition at 153°C it gives rise to a fairly complex domain structure which is described as a function of temperature.

III.2.4 Phase transitions and physical properties of $Pb_8V_2O_{13}$ single crystals.

R. Baggio, M.A.R. de Benyacar, H. de Dussel, G. Polla and L. Schmirgeld.

$Pb_8V_2O_{13}$ undergoes two reversible phase transitions: a second order one at T_1= 153°C and a first order one at T_2= 250-270°C on heating and at 180-210°C on cooling [1-2]. In this a paper we report results from X-ray diffraction, optical microscopy, DSC and dielectric measurements in order to better characterize the three phases. We conclude that the material behaves as a semiconductor and that T_2 is strongly dependent on the strains present in the sample.

III.2.5 On the influence of different parameters on the phase transition temperatures and ferroelectric domain structure in $H(UO_2)(AsO_4).4H_2O$

R.Baggio, M.A.R.de Benyacar, H.L.de Dussel, P.K.de Perazzo and L.Schmirgeld.

Thermal hysteresis of the ferroelectric-ferroelastic transition has been observed in virgin and heat treated samples by means of differential scanming calorimetry, X-ray diffraction of oriented samples and electron microscopy observation of replicas of the cleavage surfaces . These replicas provided for the first time direct evidence of the ferroelectric domain structure. In the ferroelastic-paraelastic transition, transition temperature changes, under different atmospheric surrounding, have been observed.

III.2.6 Ferroelectricity in phase II of synthetic troegerite

H.L.de Dussel, L.Schmirgeld and M.A.R.de Benyacar

The ferroelastic character of phase II of $(AsO_4)_2\ H_2(UO_2)_2.8H_2O$ is reported. The Aizu species characterizing the transition as well as the corresponding lattice distortion are determined. The spontaneous strain tensors characterizing the different orientation states are calculated.

A comparison of the domain structure and the domain wall orientation with Aizu's and Sapriel's theories is presented.

III.2.7 Crystallochemical study of calcinosis from connective-tissue deseases

R.Matalon, M.A.R.de Benyacar, O.García Morteo[+], J.A.Maldonado-Cocco[+], J.C.Marcos[+] and A.S.Arturi[+]

Apatite crystal formation has been associated with connective tissue deseases, but it has not been always clearly identified and characterized. The aim of this work was to investigate the composition of the drystalline deposits involved in the calcinosis of two patients with dermatomyositis and two patients with the CREST syndrome. The samples were obtained as granular material and as a white creamy fluid obtained by spontaneous drainage of the calcified subcutaneous masses.

The following techniques were used: X-ray diffraction for the identification of the mineral phase; infrared (IR) spectrophotometry for the identification of the functional groups, particularly $CO_3^{=}$ ions, and Energy Dispersive X-ray Analysis (EDAX) for the confirmation of the cualitative chemical composition and the determination of the Ca/P ratio. In all the samples the only mineral phase detected was calcium carbonate-hydroxiapatite. IR spectra showed the presence of carbonate ions belonging the an A-B type carbonate-hydroxiapatite. From this work we conclude that the ratio of $CO_3^{=}$ ions replacing both HO^- and PO_4^{3-} groups is not constant for all the patients, in good agreement with the variable Ca/P ratio obtained from EDAX. Our results are strinkingly similar to those observed in dental enamels by K.Jonas. Although mucopolyssacharides are usually present in connective tissue, their close association with the calcium carbonate hydroxiapatites studied suggests that they play a role in the deposition mechanism of the mineral phase.

[+]Instituto Nacional de Rehabilitación, Buenos Aires, Argentina.

III.2.8 Crystallographic study of heterotypic calcifications present in connective tissues diseases

R.O.Toubes Spinelli, M.A.R.de Benyacar and O.Hübscher

The aim of this work was to investigate the composition of two samples of cutaneous calcifications from two patients with the CREST syndrome and two samples from a patient with dermatomyositis. The first two samples were obtained by removing surgically the calcified tissues, the other two samples were obtained by spontaneous drainage of calcified subcutaneous masses.

The following techniques were used: X-ray diffraction, infra-red spectroscopy, transmission and scanning electron microscopy and qualitative chemical analysis using Energy Dispersive X-ray Analysis (EDAX).

In all the samples studied, the only mineral phase found was calcium carbonate-hydroxy-apatite.

The two samples belonging to patients with the CREST syndrome and one of the samples belonging to the patient with dermatomyositis are B-type calcium-carbonate-hydroxyapatite while another sample from this last patient shows an A-B-type calcium-carbonate-hydroxyapatite.

III.2.9 Identification of radiactive minerals by X-rays

R.O.Toubes Spinelli

X ray spacing data of radiactive minerals published up to 1981 are collected in a single volume. They are alphabetically arranged, and include the most important bibliographic data. Physical and chemical properties, paragenetic relations, principal types of deposits, and general data which can be usefull for specimen identification are also included. The first part of the booklet includes a Search Manual which is helpful for a prompt identification of the specimen studied.

III.2.10 First mention of kirovite for the Argentine Republic

R.O.Toubes Spinelli

The kirovite species form Santa Elena mine, La Alcaparrosa creek, San Juan province, is described; their optical, chemical and roentgeno-

graphic data is presented. This is the first reported occurrence of the mineral in Argentina.

III.2.11 Zinciferous aluminocopiapite from Santa Elena Mine, La Alcaparrosa Gorge, San Juan province

R.O.Toubes Spinelli

A zinciferous aluminocopiapite from Santa Elena mine, La Alcaparrosa creek, San Juan province, is described; their optical, chemical and roentgenographic data is presented. This is the first reported occurrence of the mineral in Argentina.

III.3 CRYSTAL GROWTH

III.3.1 Hydrogen uranyl hydrate single crystals $H_2(UO_2)(AsO_4)_2 \cdot 8H_2O$, gel growth and characterization*

E.Manghi and G.Polla

Single crystals of hydrogen uranyl arsenate hydrate (HUAsH) were grown in tetramethoxisilane gels at different temperature, below and above the paraelastic-ferroelastic transition temperature T_c.

The crystals were characterized by X-Ray diffraction, chemical etching scanning, electron microscopy and optical microscopy.

The habit of the gel grown crystals allowed us the 3-dimensional features of the domain structure to be studied for the first time we have shown that there are three types of domains walls in the low temperature phase: one paralell to the tetragonal c axis and two symmetrically inclined to it.

Growth hystory has been inferred from chemical etching of defects and domain structure observations.

Etch pits developed in cleaved slices show that screw dislocations play an important role in the nucleation and growth of crystals.

---

*J.Cryst. Growth 61(1983)603.

III.3.2 Synthesis of bismuth oxalate single crystals using two different techniques

G.Polla, R.Baggio, E.Manghi and P.K.de Perazzo

To obtain bismuth oxalate single crystals, gel-growth and slow evaporation from solution were tried.
For both methods simultaneous growth of $Bi_2(C_2O_4)_3 \cdot 7H_2O$ and $Bi_2(C_2O_4)3\ H_2C_2O_4$ was observed.
This work includes a comprehensive characterization for both compounds performed on the much better gel grown specimens as well as single crystal and powder X-ray data and a thorough study of the thermal behaviour.

III.3.3 Nucleation of new orientations in water droplets frozen on an ice substrate

L.Levi[+] and O.Nasello[++]

The probability P for supercooled droplets to form new orientations when they freeze in contact with a basal or prism ice substrate is studied. In agreement with previous results, the nucleation theory is satisfactorily applied to correlate the supercooling ΔT^* where P=0.5 with the area $S=(\pi/A)d_e^2$ of the droplet-ice interface. The sharp variation of P for ΔT varying about ΔT^* is also shown to correspond to the theoretic behaviour of a nucleation process. For droplets slowly spreading on the substrate, the parameters relating ΔT^* with d_e are evaluated by using both the spherical cap and the two-dimensional nucleation models. The best adjustment is obtained with the latter. This gives, for the crystal-embryo interface free energies, on the basal and prism substrate, γ_{ce}=0.04 and γ_{ce}=0.02 erg/cm^2 respectively. The vanishing value of γ_{ce} in the first case is related to the stacking fault possibly generating the new crystals, with their c-axis at 70° to the substrate c-axis. The study of droplets frozen after colliding at 30m/s with the substrate shows that ΔT^* increases with the collision speed. This is related to the decreased thickness of the water layer formed by the droplets on the substrate and the consequent decrease of the time t during which nucleations may occur.

[+]CNEA and Consejo Nacional de Investigaciones Científicas y Técnicas (CONICET), Buenos Aires, Argentina
[++]IMAF, Buenos Aires, Argentina

III.3.4 Grain growth in ice

L.Levi[+] and E.A.Ceppi[++]

Grain growth is studied in polycrystalline ice, consisting of elongated grains, of $(200 \div 300)\ \mu m$ mean width $\bar{w}$ and $(2 \div 3)$ mm mean length $\bar{l}$. The samples are annealed at different temperatures, between 0°C and -10°C. It is found that $\bar{l}$ is not affected by annealing, while $\bar{w}$ increases with the annealing time. Below the melting point, $\bar{w}(t)$ tends to a limit value $\bar{w}_s$. This behaviour is related to the pinning action of air bubbles, which would be similar to that found for solid inclusions in metals. By assuming $\bar{w}_s = \bar{d}/f$, where $\bar{d}$ is the mean bubble diameter and f is the volume fraction of air dissolved in water, reasonable values are found for $\bar{d}$. The activation energy of the phenomenon is evaluated on the basis of the present and of Jellinek and Gouda's results. It is found Q=0.6 eV, which value approximately coincides with that for bulk self-diffusion as it occurs for metals, several degrees below the melting point. This coincidence suggests that, for ice, grain growth would be controlled by bulk impurity diffusion up to the very melting point.

[+] CNEA and CONICET, Buenos Aires,Argentina

[++] IMAF, Buenos Aires, Argentina

III.3.5 Effects of growth temperatures and surface roughness on crystal orientation in ice accreted in a dry regime

L.Levi[+] and F.Prodi[++]

The dependence of crystal orientation on air and deposit temperatures in the dry growth regime has been re-examined by producing accretions over a wide range of these temperatures and critically examining the structural aspects of the deposits, such as surface roughness. It is shown that the variation in the preferred c-axis orientation with the air and deposit temperatures during growth is an intrinsic effect of the freezing mode of ice, rather than an effect of surface roughness.

The $F(\varphi)$ distributions of the angle φ between the accretion radius and the crystal c-axis, and those of its component angles $F(\eta)$ and $F(\vartheta)$, have been obtained. It is shown that for cloud temperature $T_a > -18°C$, the $F(\varphi)$ distributions have a main maximum at small angles. For $-18°C \geq T_a \geq -23°C$ the location of the maximum depends strongly on the deposit temperature T_d, reaching values near 45° for $T_d < -10°C$. For $T_a < -23°C$ the distributions show a large disorder at $T_d \geq -5°C$, but a maximum about 45°C when T_d is below this value.

Sharp secondary peaks frequently appear at the side of, or superposed to, the main maxima. The application of the χ^2-test to the distributions shows that secondary maxima may not be used to establish a more precise definition of T_a and T_d. They may on the other hand be a consequence of the shape of the lobes, which may determine the splitting of the main maxima.

The application of the results to natural hailstone analysis is discussed.

+CNEA and CONICET, Buenos Aires, Argentina
++Istituto FISBAT, CNR, Bologna, Italia

III.3.6 Crystal size and orientation in ice grown by droplet accretion in wet and spongy regimes

F.Prodi+, L.Levi++, A.Franzini+ and C.Scarani

The size and orientation of crystal grains in wet and spongy ice formed by accretion of supercooled droplets has been determined in a wide range of air temperatures (-8 to -25°C). Particular care has been taken in reducing the spurious ice crystals in the icing wind tunnel which according to former investigators could affect the crystal characteristics in these growth regimes. The c-axis orientation analysis of the grains has been used to check that spurious ice crystals have not been incorporated in a significant number into the structure.

As for the orientation of the c-axis it has been observed that different deposits grown at $T_a \geq -22°C$ show a rather similar behaviour, especially in the $F(\Theta)$ and $F(\Psi)$ distributions; however, the probability that the distributions belong to the same populations is small. At $T_a = -25°C$

there is a larger disorder in the c-axis orientation. Therefore the analysis of the crystal orientation should be primarily used to determine the growth regime, dry or wet-spongy, and not to determine T_a, which does not seem to be responsible for the observed differences in orientation, which are more probably due to variations of sponginess or surface roughness.

As for crystal size parameters, the results show that the average surface area $\bar{\sigma}$ of the grains is lower in the wet-spongy accretions than in dry ones grown at the same air temperatures and at deposit temperatures just below 0°C. This observed difference could be correlated with the different freezing mechanism in the two regimes, which must be also responsible for the different behaviour in the c-axis orientation. The mean maximum length $\bar{l}$ has the same beahviour as the mean surface area $\bar{\sigma}$, while the mean maximum crystal width $\bar{w}$, unlike in the dry growth regime, is almost independent of the air temperature T_a.

Therefore, considering the application to the analysis of natural hailstones, the mean surface area $\bar{\sigma}$ and the mean maximum length $\bar{l}$ of the crystals seem to be the best parameters to follow in evaluating the air temperature T_a in wet and spongy regimes.

+Istituto FISBAT, CNR, Bologna, Italia
++CNEA and CONICET

III.4 MÖSSBAUER SPECTROSCOPY

III.4.1 Analysis of argentine biotites samples by Mössbauer Spectroscopy

C.Saragovi-Badler

During the weathering process of clays minerals, iron plays an important role and therefore information concerning the amount, valencia and site occupation of this element is essential. Taking into account this fact the oxidation process of natural argentine biotites was studied by Mössbauer spectroscopy. Samples were provided by Centro de Investigaciones en Recursos Geológicos.

Spectra of natural biotites samples from two locations and of the same mineral heated at 500 °C and 800 °C under O_2 atmosphere were recorded.

Experimental results show the existence of Fe^{2+} and Fe^{3+}, both of them in M_1 and M_2 sites; heating at 500 °C increases the percentage of Fe^{3+} reducing the Fe^{2+} percentage. The Fe^{2+} remains only in M_2 sites while all the Fe^{3+} occupy M_1 sites. Heating to 800 °C oxidises all the remaining Fe^{2+} to Fe^{3+} which occupy the M_1 sites. One of the series presents a magnetic component, which remains unaltered under the heat treatment, and whose parameters corresponds to hematite or paramagnetic geothites. The presence of hematite would indicate that this biotite was formed in an air environment at more than 1000 °C.

III.4.2 Mössbauer studies of the corrosion reactions in arc-furnace refractories. Part I.

C.Saragovi-Badler, C.Puglisi[+]

The aim of this paper is to show the kind of information that can be obtained from the use of Mössbauer spectroscopy when used as a complement of the conventional techniques, in the study of the reactions that take place between refractories and metallurgical enviroments. Mössbauer spectroscopy provides information concerning the local surroundings of iron ions in any solid material, and this can be useful in the study of the above mentioned reactions, considering the important rol of iron in them. Well known examples of corrosion reactions are used, namely the wear mechanism of arc-furnace refractories obtained from the roof and the slag line at the end of a campaign.

The analysis of the high alumina bricks indicate that the chemical reactions taking place in service produced mainly calcium ferrite, some cordierite and anortite. The iron oxide migrating into the brick was partially incorporated by thecorundum grains as solid solution and partially remained as impurified magnetite and hematite. The reaction with lime proceeded only to a first stage as no CA_6 has been found. The same can be said about iron oxide, which was incorporated to the Al_2O_3 without separation of hercynite.

In the case of the slag-line magnesio bricks, the main identified products are magnesio-ferrite and magnesio-wustite. The rest of the iron content is distributed in the silicate phase which was probably liquid at the service temperature, giving use on cooling to glassy and crystalline silicates. The experimentally founds phases an the expected one when the CaO/SiO_2 ratio is approximately 2.

From the peaks area of the Mössbauer spectra an estimation of the iron distribution among the different components has been done in the two bricks analyzed.

[+]Centro de Investigación para las Industrias Minerales. Instituto Nacional de Tecnología Industrial (INTI), San Martín, Buenos Aires, Argentina.

III.4.3 Mössbauer studies of the corrosion reactions in arc-furnace refractories. Part II.

C.Puglisi[+], F.Labenski, C.Saragovi-Badler

Mössbauer spectroscopy has been used, together with conventional techniques, in the study of corrosion reactions taking place in service in co-clinkered chrome-magnesite bricks from the hot spots of an electric-arc furnace. Co-clinkered bricks have hot-strength properties and an increased amount of spinel-bonding uniformly distributed to resist slag attack and liquid penetration.
Considering the iron uptake in service, the Mössbauer data show that only spinel compounds are formed by reaction between the brick and the iron components of the slag. The obtained Mössbauer spectra present high line with values indicating that the iron containing spinels are contaminated and higly substituted. This is expected in compounds where considerable amount of impuritis have been incorporated due to the complex environment in which they are formed. The complex spinels that are present in this case follow the magnetic behaviour of the similar pure chromite $FeCr_2O_4$ when iron is incorporated.
The experimental results confirm the relative stability of the spinel phase in the presence of the migrating components of the slag.

[+]Centro de Investigación para las Industrias Minerales, Instituto Nacional de Tecnología Industrial (INTI), San Martín, Buenos Aires, Argentina.

III.4.4 Quantitative studies of thalassemic red blood cells with Mössbauer Spectroscopy

F.Labenski de Kanter

As part of a joint project between the Hematology Department of the Children Hospital "Ricardo Gutierrez" and our laboratory, a research programme on the use of Mössbauer spectroscopy to make a quantitative study of thalassemic red blood cells from children suffering this kind of anemia is been started. As a first stage in this programme we measured three samples of adult normal red blood cells. The obtained Mössbauer parameters are in agreement with those found in the literature. We are now working in the measurements of red blood cells samples of normal children of different ages.

Next s measurements of thalassemic red blood cells from
patie age range as the normal ones.

---

tudy of clays minerals from Cordoba province, Argentina, with Mössbauer spectroscopy

C.Saragovi-Badler and F.Labenski

Our ory together with the Departamento de Geología Económica (C.N.I.E.)
ha ed a joint project "Arsenic and other oligoelements natural contamina
t: waters and sediments at the south eastern plain in Cordoba province".
T n of this part of the project is to use the Mössbauer Effect, which has
] an established method of clay research, to study all the iron containing
nents. We have started the Mossbauer study of some volcanic and altered
canic samples.

the first cases the experimental results are the expected one, that means
on containing amorphous silicates. Some samples show Fe^{+2} and Fe^{+3} in an
morphous environment and other samples show a mixtures of this sites. In the
case of the altered sample the Mössbauer parameters reveal the presence of
Wyoming type montmorillonite and hematite or highly substituted goethite.
From the area peaks an estimation of the iron concentration in the M_1, M_2 and
magnetic sites has been done.

III.5 THEORETICAL SOLID STATE PHYSICS

III.5.1 Cluster calculation on the interaction and discharge of ions on a silver surface

M.Weissmann and N.V.Cohan

The interaction of halogen and alkali ions with the (100) surface of silver was studied at very short distances. Calculations were performed by the iterative extended Hückel method (IEHT) for $(Ag_nX)^{\pm}$ clusters with n=9 and n=37 and X=F, Cl for the negative and X=Na, K for the positive clusters. A careful analysis of the parameters used in the IEHT was performed and the main results obtained are: Cl^- ions lose more of their negative charge than F^- ions on approaching the (100) silver surface, and the electronic charge thus transferred to the silver cluster is distributed as far as possible from the adsorbed species. Both halogens form localized bonds with the nearest Ag atoms, which are very similar to those for the neutral adsorbed species. The interaction of the alkali ions with silver is very small and it decreases as the size of the cluster increases, supporting the idea that the alkali ions interact only via a solvation shell.

III.5.2 Calculation of the density of states of NbN_x by the recursion method

A.M.Llois , N.V.Cohan and M.Weissmann

The density of states, n(E), of NbN_x has been calculated by means of the Recursion Method for $x \leq 1$. The results have been compared with experiment, obtaining that the most important trends of the density of sta-

tes are reproduced fairly well, even if the variation of the density of states at the Fermi level, as a function of the concentration of N-impurities cannot be predicted.

III.5.3 Electronic density of states of incommensurate-disordered systems

A.M.Llois, M.Weissmann, N.V.Cohan

We have calculated the electronic density of states of one-dimensional incommensurate systems within the tight-binding approximation with first neighbor interactions for several modulation functions for the self-energies. Among them, zig-zag, saw-tooth and soliton-like functions were used. We find that the density of states is strongly dependent on the type of modulation. Two different types of disorder were introduced simulating a melting process, becoming the systems practically indistinguishable from a totally disordered model even when partially disordered.

III.5.4 Vibrational density of states of rare-gas crystals doped with impurities

A.Frigerio, H.Bonadeo, M.Weissmann and N.V.Cohan

The vibrational density of states of disordered $Xe_{1-x}Cs_x$ and $Xe_{1-x}Kr_x$ crystals is studied for $x \lesssim 0.05$. It is obtained as an average of local densities of states, which are calculated by the continued-fraction

method. Two sets of asymptotic values for this expansion are used for a satisfactory approximation of both the main band and the minority peaks outside it. The use of a bond-stretching coordinate basis allows a physical interpretation of each local density of states and also gives simple kinetic and force constant matrices. The drawback of overcompleteness of this basis is easily overcome.

III.5.5 Phason and amplitudon-like vibrations of one-dimensional incommensurate systems

N.V.Cohan and M.Weissmann

In this paper we show that phason- and amplitudon-like vibrations can be obtained in one-dimensional incommensurate systems with harmonic interactions between first neighbours only. This is achieved provided a realistic modulation of the force constants is used. The incommensurate systems are approximated by commensurate ones with large unit cells. Several criteria are used to characterise the phason- and amplitudon-like vibrations and we find that these types of vibrations exist, for reasonable values of the amplitude of the modulation, if there is a sufficient number of atoms per modulation period.

III.5.6 Localization in different models for one dimensional incommensurate systems

A.M.Llois, N.V.Cohan and M.Weissmann

We have studied the localization properties of one-dimensional incommensurate systems within the tight-binding approximation with first-neighbor interactions for several modulation functions: sawtooth, zig-

zag and soliton-like functions. We show that the localization properties are strongly dependent on the type of modulation used. In the case of a soliton-like system we also studied the charge distribution, finding that electronic charge has the tendency to localize on dislocations.

III.5.7 Specific adsorption of halogen ions on silver surfaces

M.Jauregui, N.V.Cohan and M.Weissmann

In this work we study the interaction of halogen ions with some low index silver surfaces. We use the iterative extended Hückel theory for $(Ag_n X)^-$ clusters, with X = F, Cl, Br and n of the order of 10. Calculations are performed for three different silver clusters, that model the (111), (110) and (100) surfaces, as a function of the distance between the halogen and silver atoms. We find that the halogens are adsorbed very close to the silver surfaces, thus giving a mixed layer configuration. Chlorine and bromine adsorptions are very similar while fluorine has a much smaller adsorption energy. Chlorine and bromine become practically neutral on adsorption while fluorine remains negatively charged.

III.5.8 Analytical calculation of a class of integrals containing exponential and trigonometric functions

V.Massida

It is shown how to evaluate analytically integrals from 0 to 2π of functions of the type $f(\phi)g(\phi)\exp\{G(\phi)\}$, where $g(\phi)$ and $G(\phi)$ are linear combinations of powers of $\sin\phi$ and $\cos\phi$, and $f(\phi)$ is such that its Fourier coefficients can be evaluated analytically. The result is expressed in terms of Bessel functions.

III.5.9 Order-disorder transitions for a two-dimensional lattice of reorientable quadrupoles in the mean-field approximation

V.Massida and J.Hernando

We consider a two-dimensional lattice of reorientable point quadrupoles which interact electrostatically with each other. We introduce a set

of probability distribution functions $n_\ell(\varphi)$ describing the orientational behaviour of the quadrupoles. We write down the free energy in the mean-field approximation as a functional of the n_ℓ . By a variational procedure we find a set of transcendental equations whose solution gives the n_ℓ . This formalism is applied to three particular cases: A) square lattice, B) rectangular lattice, C) triangular lattice. In all cases an order-disorder phase transition is found. The transition is second-order in cases A and C; in case B it can be first- or second-order, depending on the kind of quadrupoles. A particular case of C) is that of a layer of N_2 molecules on graphite, for which our model predicts the right low-temperature structure and a transition temeperature in reasonable agreement with the experimental one.

III.5.10 A numerical method and general discussion of integral equations for the primitive model of the electric interface

L.Blum, J.Hernando and J.L.Lebowitz

We describe an efficient numerical algorithm for solving integral equations commonly used in the theory of the primitive electrode. The method is applied to an approximation obtained from the first BGY equation using a modified Croxton-McQuarrie local neutrality ansatz, with accurate bulk correlations. For 1M solutions of 1-1 electrolytes, and 0.5M solutions of 2-2, 2-1 and 1-2 electrolytes the agreement with computer experiments is good.

To apply the method to other integral equations we formulate them as approximation schemes for the closure of the first member of the BGY hierarchy. Many of them are then seen to satisfy the local electroneutrality condition. We also suggest a new approximation which might be accurate even at very high couplings.

III.5.11 A program for the evaluation of two-dimensional lattice sums

J.Hernando and V.Massida

A FORTRAN program was written for the calculation of the electric field and its derivatives up to third order created by a two-dimensional lattice of point charges at an arbitrary point of that plane. This pro-

gram makes use of the formulas given by R.D.Brown and B.W.N.Lo, J.Phys. C4(1971)263.

III.5.12 Nonuniversality in a model hamiltonian with four-spin interactions

S.D'Elía

We introduce a model Hamiltonian with six types of four-spin interaction terms (coupling constants $\{\Gamma_i\}$) that couple four Ising-like lattices in two dimensions.

The model reduces to asymmetric Ashkin-Teller or eight-vertex models by an appropriate choice of $\{\Gamma_i\}$.

The decoupling point is studied using Kadanoff's operator algebra.

The several operators that characterize physical magnitudes show dependence on the different linear combinations of $\{\Gamma_i\}$. We have a nonuniversal critical surface, rather than nonuniversal critical lines.

Also the model has three nonuniversal decoupling planes on which coupling only occurs between pairs of lattices. In each plane there are four multicritical lines with an additional marginal operator, responsible of nonuniversality when we move out of the plane. This follows from the equivalence between the eight-vertex and Ashkin-Teller models with the Gaussian model.

III.5.13 Dual transforms in a model Hamiltonian with four-spin interactions

S.D'Elía

A model Hamiltonian which includes Ashkin-Teller and eight vertex models is introduced. Its transfer matrix is formulated in terms of the bidirectional transfer matrix, following a previous work of C.Fan. We study two dual transforms and their related invariant surfaces in the coupling parameter space. One of these surfaces includes both eight vertex and the Ashkin-Teller critical lines, while the other surface contains the critical surface of the pure four-spin interaction part of our model Hamiltonian. In particular, we found that the Random Chesboard model, previously introduced, is critical for a value of its coupling constant equal to the Ising critical value.

III.5.14 Montecarlo determination of the phase diagram of a model Hamiltonian with four-spin interactions

S.D'Elía, H.Ceva

A model Hamiltonian introduced previously by the authors and related with the Ashkin-Teller and eight vertex models is studied with the Monte-Carlo technique in a two dimensional square lattice of NxN sites for N=12, 20 and 30.

The physics of the system is characterized by the ratio between the four-spin interaction (λ) and the two spin interaction (K_2), $X=\lambda/K_2$. We have determined the "polarization", the magnetization and several susceptibilities as a function of temperature for 17 different values of $X>0$.

In all cases the polarization is a valid order parameter. For N=20 we found that below $X\cong 35$ the system has an order similar to the Ising model, although it has first order transitions for $X\leq 1.67$. Metaestable states are found and discussed.

For $X\geq 35$ the system displays a very interesting finite size effect characterized by a network of vertical and horizontal walls.

Moreover the magnetization ceases to be a good order parameter. A phase diagram of the system is presented.

III.5.15 A new model Hamiltonian with four-spin interactions: phase diagrams and formation of domains and walls*

S.D'Elía and H.Ceva

A model Hamiltonian related with the Ashkin-Teller and eight vertex models is introduced and studied in a two dimensional square lattice of NxN sites. It is formulated in terms of a vector variable $\vec{S}$ with four states, and has two body (K_2) and four body (λ) interactions. If $K_2=0$ the ground state of this system is highly degenerate and almost all of these states have domains and walls.

We also study the region $x>>1$ of the phase diagram $K_2=(x)$, where $x=\lambda/K_2$, obtaining conditions for the existence of these walls. We find that for $\lambda \sim (x/N)>>1$ there is a crossover towards an Ising-like ordering, without walls.

---

*Phys.Rev. B28(1983)4001.

III.5.16 Magnetic susceptibility of a model for valence fluctuations between two magnetic configurations: renormalization group approach

R.Allub, H.Ceva and B.Alascio

Using Wilson's renormalization group technique we have calculated the temperature dependence of the magnetic susceptibility of an impurity model that describes valence fluctuations between two magnetic configurations. The model contains two parameters: Δ the energy difference btween the two configurations and Γ the level width. We find a doublet ground state leading to a divergent susceptibility at low temperatures. The temperature dependence of the effective magnetic moment can be understood on the basis of the regimes: a) an intermediate valence regime at high temperatures, b) an local moment regime at intermediate temperatures, and c) an strong coupling regimen at low temperatures. For $|\Delta| >> \Gamma$ and negative, the model shows a spin one Kondo behaviour and exhibits universality.

III.5.17 Crystal structure and lattice dynamics of chlorine. The role of electrostatic and anisotropic atom-atom potentials*

E.Burgos, C.S.Murthy and R.Righini

An extensive analysis of the intermolecular forces in the chlorine crystal has been performed. Different models of the intermolecular potential, including anisotropic terms and electrostatic contributions from multipoles higher than quadrupole have been taken into account and tested for their ability to reproduce static and dynamical properties of solid chlorine. The inclusion of anisotropic dispersion forces reproduces correctly the orthorhombic unit cell. Anisotropic terms are required also in the short range repulsive atom-atom interactions to obtain a good fit to lattice frequencies and stability of the C mca structure with respect to a hypothetical cubic phase. A tensor formalism particularly convenient for dynamical calculations is developed and used to describe angular dependent atom-atom interactions.

---

*Molecular Physics, 47 (1982) 1391.

III.5.18 The effects of anisotropic atom-atom interactions on the crystal structure and lattice dynamics of solid CS_2 *

E.Burgos and R.Righini

The intermolecular forces in CS_2 crystals are described by means of a potential consisting of an electrostatic part, represented by a distributed multipoles model, and of a repulsion-dispersion potential accounting for the anisotropic effects in the atom-atom interactions. A good agreement with the experimental crystal structure and with the observed lattice frequencies is obtained. The role of the anisotropic short range interactions in the static and dynamics of the crystal of CS_2 and other linear molecules is discussed.

---

*Chem.Phys.Lett. 96(1983)525.

III.6 GEOLOGICAL APPLIED

III.6.1 Geology of the Bertrab nunatak, Argentine Antartic sector*

R.Toubes Spinelli

The Bertrab nunatak (77°44' South - 34°48' West), Argentine Antartic Base General Bergrano II site, is a very small outcrop of a reddish gray to gray mottled white and reddish granite. Riolitic porphyry, granitic porphyry and spessartite veins, at least two occupying fault planes, intrude it. There are also barite with amethyst and milky quartz veinlets. The strong jointing gives to the outcrop a prominent fractured surface aspect. In comparsion with dated similar rocks of nearby nunatak (Moltke, Littlewood) it would be considered that the age of this granite is upper precambric.

---

*Contribution of the Instituto Antártico Argentino, in press.

III.6.2 Potassim-argon dating of some rocks from Sierra de Valle Fértil, San Juan Province*

R.Toubes Spinelli

The radiometric ages of ten pegmatites and six metamorphic rocks from the Valle Fertil sierra, San Juan Province, were measured. Some of these metamorphic rocks are wall rocks of the pegmatites. The pegmatites are grouped in three cycles: a) 600-650 m.y. (mentioned for the first time for the Sierras Pampeanas); b) about 500 m.y. and c) about 430 m.y. and maybe one more about 750 m.y. The metamorphic rocks are an anphibolite with 800 m.y., tonalitic gneises with minimum apparent ages of 620-630 m.y. and granodioritic gneises, aged nearly 490 m.y. We could not detect any relationship between ages and radioactive mineralization of these pegmatites.

---

*Rev.Asoc.Geol.Arg., in press.

III.6.3 ¿What is a mineral?

R.Toubes Spinelli

This is a detailed critical revision of the definition of a mineral species Analysis is based on examples relevant to every aspect of the definition most commonly used at present. The article concludes by offering a definition which is considered from data available as more adequate for most minerals.

IV. Solar Energy

IV. SOLAR ENERGY

IV.1 Experimental and theoretical studies on solar radiation concentrators

Solar Energy application group*

The general purpose of this program is to heat fluids up to temperatures from 150 to 350°C using solar radiation concentrators, in order to provide heat for industrial processes and to generate steam suitable for the production of mechanical and electric energy.

Parabolic trough concentrators have been chosen for the design and the construction of an industrial prototype of concentrators permitting the development of the adequate technology for production in series.

On the basis of the theoretical studies on linear focus concentrators carried out by the Group, a computer program permitting to optimize the parameters of said concentrators either with planar or cylindric receiver was developed.

As a first stage, the adequate parameters for the heating of a fluid in the range of 180 to 220°C in order to use the concentrators to provide heat for industrial processes were chosen. The system's basic engineering was carried out and its detailed engineering as well as the construction of some of the previously defined components were started. At the same time, operating tests with the laboratory prototypes of fixed- faceted-mirror solar-concentrators built by the Group were continued. For these tests, a new installation for the measurement of thermal parameters was designed, constructed and assembled, which will be used in the future as a concentrator testing bench. Additionally, a new logic unit was designed and constructed for controlling the froscking of the Sun's apparent movement, permitting to operate eight concentrator lines simultaneously.

Work on the elaboration of black chromium selective surfaces for high temperatures was started in cooperation with the Electrochemistry Section of CNEA's Chemical Processes Branch.

A theoretical study on the maximum concentration factor obtainable was made for concentrators with linear or point focus, for different models of radiation intensity distribution on the solar disc.

---

*The work was carried out by agreement between the Physics Department and the Department of Prospective and Special Studies in the frame of programs financed and controlled by the latter.

IV.2 Photovoltaic Conversion

Solar energy application group*

Work on the updating of the evaluation on the state of development of photovoltaic conversion of solar energy in the world was continued. Visits to photovoltaic module production plants and related laboratories in the US.A. and Europe were made, with the purpose of identifying technologies, processes, equipment and experts in order to permit the development of a project of an experimental installation for the demonstration of technologies of the fabrication of photovoltaic panels.

Theoretical studies on Solid State Physics oriented to semiconductors were continued, in order to provide suitable bases for future theoretical studies on photovoltaic conversion.

Appendix

Staff
Publications
Table of Conterts

PERSONNEL OF THE PHYSICS DEPARTMENT

Research Staff

Abriola D.	on leave at State Univ. of N.Y.at Stony Brook,USA
Achterberg E.	
Baggio R.	
Benyacar M.	Head Solid State Physics Division
Berisso M.C.	
Bes D.R.	*
Bonadeo H.	*
Burgos E.	*
Ceballos A.	
Ceva H.	
Dragún O.	
Debray M.	
Di Gregorio D.	
Dussel G.G.	*
Dussel H. Lanza de	
Dukelsky J.	
Etchegoyen A.	
Fernández Niello J.	
Ferrero A.	
Filevich A.	Head Experimental Nuclear Physics Division
Frigerio A.	
Gamba Z.	
García Bermúdez G.	*
Gattone A.	on leave at Indiana University, USA
Gil S.	on leave at University of Washington, USA
Halac B.	
Hernando J.	
Huck H.	
Jech A.	*
Kreiner A.	
Labensky F.	
Macchiavelli A.	on leave at Lawrence Berkeley Lab., USA
Manghi E.	
Maqueda E.E.	* Head Theoretical Nuclear Physics Division
Mariscotti M.	
Massidda, V.	
Mehr M.T.	
Moragues J.	* Head Solar Energy Group
Napoli D.	
Otero D.	
Pacheco A.	
Perazzo P. Koning de	
Perazzo R.P.J.	
Pérez M.L.	
Pérez Ferreira E.	Chairman Department of Physics
Pomar C.	
Proto A.	
Polla G.	
Reich S.L.	
Rossi J.J.	

Saraceno M.	
Saragovi-Badler C.	
Sccocola N.	
Scheuer W.	
Sofía H.M.	
Spina M.E.	on leave at Univ. of Heidelberg, W.Germany
Testoni J.	
Toubes R.	
Ventura E.	
Wainer L.	

*Under contract of Carrera del Investigador Científico, CONICET, Argentina

Research Staff Associated to the Physics Department

Cambiaggio M.C.	*
Cohan N.	*
Curutchet P.	+
Fendrik A.	+
Levy L.	*
Lenzi S.	**
Llois A.M.	**
Waissmann M.	*

*Under contract of Carrera del Investigador Científico, CONICET, Argentina
**Fellowship from the CONICET, Argentina
+ Fellowship from the Comisión de Investigaciones Científicas de la Prov. de Buenos Aires, Argentina

Engineering Staff

Camín D.V.	
Fazzini N.	
Giménez C.	
González H.	
Granata J.	
Martí G.	
Milberg J.	
Mónico J	
Nicolai J.	
Requejo R.	Head of Engineering Division
Ribarich R.	
Satinosky M.	
Simoncelli D.	
Navarro D.	
Tau S.	
Tersigni A.	
Vieiro J.	

Visiting Scientists

Abrahm E.	Harriot Watt University, U.K.
Axe J.	Oak Ridge Nat. Lab., USA *
Ball J.	Oak Ridge Nat. Lab., USA *
Barret B.	Tucson, Arizona, U.S.A.
Barretto J.L	UFRJ, Brazil * and **
Bayman B.	Univ. of Minnesota, USA
Bezerra Coutinho F.	USP, Brazil *
Blum L.	Puerto Rico University, Puerto Rico
Borello Lewin T.	USP, Brazil *
Butt N.	Pinstech, Pakistan
Brandan M.E.	Univ.Chile
Brieva F.	Univ.Chile *
Canto L.F.	UFRJ, Brazil *
Civitarese O.	UNLP, Argentina
Dias H.	USP, Brazil *
Dietzsch O.	USP, Brazil *
do Barros S.	UFRJ, Brazil * and **
Donangelo R.	UFRJ, Brazil *
Duval P.	Tucson, Arizona, USA
Drugowich F.	USP, Brazil *
Ferrareto M.	USP, Brazil *
Fulfaro R.	IPEeN, SP, Brazil *
Giambiaggi J.J.	CBPF, Rio de Janeiro, Brazil
Gomes L.C.	CBPF, Rio de Janeiro, Brazil
Huberman B.	Xerox, California, USA
Levine R.	Hebrew Univ. *
Lepine A.	USP, Brazil *
Liotta R.	Forskinstitutet, Sweden
Mang H.	Univ. of Münich *
Massmann H.	Univ.Chile *
Menchaca Rocha A.	Univ.Chile
Murgich J.	IVIC, Venezuela
Nunes L.	USP, Brazil *
Paciornik S.	USP, Brazil *
Pittel S.	Univ. Delaware, USA
Ramirez J.C.	Univ.Chile *
Ramos Parente C.B.	IPEeN, SP, Brazil *
Rasmussen J.	Lawrence Berkeley Lab., USA
Rao N.	USP, Brazil *
Rotberg V.	USP, Brazil **
Sala O.	USP, Brazil *
Seale W.	USP, Brazil *
Seltz R.	CIN of Strasbourg, France
Stokstad R.G.	Lawrence Berkeley Lab., USA
Szantos de Toledo A.	USP , Brazil *
Thieberger P.	Brookaven National Lab., USA
Tomanek	Universidad Libre de Berlin
Valdés Flores J.	UNAM *
Vary J.	Iowa Univ., USA

* **Assistant to the "Vth Nuclear Physics Workshop" Chapdamalal, Buenos Aires.
** Assistant to the "VIth. Nuclear Physics Workshop" Tandar, Buenos Aires.

Research Students

Aliaga J.
Bejer S
Bernath M.
Blum B.
Camin D.
Cardona M.A.
Carpintero E.
Figliola M.A.
Folcia C.
Gonzalez A.D.
Gonzalez Tamburri M.
Gravielle M.S.
Iaría P.
Jauregui M.
Levy Yeyati A.
Mota V. de la
Nievas G.
Pinzón B.
Rocco C.
Sainato C.
Salem L.
Simone L.
Tau R.

Technical Staff

Antonuccio F.
Bergaglio J.
Binda A.
Bolaños C.
Cabello B.
Coralo J.
Cordeyro S.
D'Agostino R.
Denari M.
Díaz Romero A.
Di Paolo H.
Garanzini J.
Garay Ramos E.
Grahmann H.
Gutierrez N.
Ietri B.
Ietri G.
Igarzábal M.
Kesque J.M.
Laffranchi J.
Lolago E.
Menéndez E.
Miguez C.
Morales A.
Montrasi C.
Montrasi C.
Nigro S.

Nuñez N.
Orecchia J.
Palacio C.
Petragalli I.
Professi M.
Professi J.
Ramírez M.
Rendina J.
Riso J.M.
Rodríguez J.C.
Rugilo A.
Schevenels L.
Schiavino R.
Vidallé J.

Administration

Blanco L.
Boretto J.
Cáceres A.
Carmuega M.T.
Escrivá G.
Galván de González L.
Ghiotti B.
Gismondi M.
Lires S.
Puyau A.
Prieto J.
Rodríguez L.
Soler H.

Others

Barzola G.
De Brasi O.
Dieguez R.
Gómez L.
Gutierrez E.
López F.
Manavella A.M.
Molina G.
Molina J.C.
Piccini G.

PUBLICATIONS OF THE PHYSICS DEPARTMENT

NUCLEAR PHYSICS

The ground state of deformed nuclei as a boson condensate.
J. Dukelsky, G.G. Dussel, H.M. Sofía.
Nucl. Phys. A 373 (1982) 267

High-spin states in ^{94}Te.
M. Behar, A. Ferrero, A. Filevich, G. García Bermudez, M.A.J. Mariscotti.
Nucl. Phys. A 373 (1982) 483

The nucleus as a condensate of monopole and quadrupole pairing vibrations.
R.A. Broglia, E. Maglione, H.M. Sofía, A. Vitturi.
Nucl. Phys. A 375 (1982) 217

In-beam study of ^{78}Br.
M. Behar, D. Abriola, A. Filevich, G. García Bermúdez, A.J. Kreiner, M.A. Mariscotti, J.A. Pinston, D. Barneoud.
Nucl. Phys. A 376 (1982) 131

Levels in ^{156}Gd studied in the (n, γ) reaction.
A. Backlin, G. Hedin, B. Fogelberg, M. Saraceno, R.C. Greenwood, C.W. Reich, H.R. Koch, H.A. Baader, H.D. Breitig, O.W.B. Schult, K. Schreckenbach, T. von Egidy, W. Mampe.
Nucl. Phys. A 380 (1982) 189

A graphical procedure to evaluate the many-body shell-model equations.
R.J. Liotta, C. Pomar.
Nucl. Phys. A 382 (1982) 1

Cluster of nucleons as elementary modes of excitation in nuclei.
G.G. Dussel, R.J. Liotta, R.P.J. Perazzo.
Nucl. Phys. A 388 (1982) 606

High spin states in ^{218}Ra.
J. Fernández Niello, H. Puchta, F. Riess, W. Trautmann.
Nucl. Phys. A 391 (1983) 221

Angular-momentum transfer and alignment in deep-inelastic reactions for nearly symmetric heavy-ion systems.
A.J. Pacheco, G.J. Wozniak, R.J. McDonald, R.M. Diamond, C.C. Hsu, L.G. Moretto, D.J. Morrissey, L.G. Sobotka, F.S. Stephens.
Nucl. Phys. A 397 (1983) 313

Spin determination via α-d angular correlations and α- transfer DWBA analysis in ^{18}F high-energy states.

M.C. Etchegoyen, D. Sinclair, A. Etchegoyen, E. Belmont Moreno.
Nucl. Phys. A 402 (1983) 87

Maximum overlap and critical phenomena.
M.C. Cambiaggio, A. Plastino.
Nucl. Phys. A 403 (1983) 365

Configuration mixing calculations in soluble models.
M.C. Cambiaggio, A. Plastino, L. Szybisz, H.G. Miller.
Nucl. Phys. A 403 (1983) 381

Thermal aspects of the pairing correlations in finite nuclei.
O. Civitarese, G.G. Dussel, R. P. J. Perazzo.
Nucl. Phys. A 404 (1983) 15

The (^{14}C,^{14}O) reaction considered as simultaneous pair-exchange or double charge-exchange processes.
D.R. Bes, O. Dragún, E.E. Maqueda.
Nucl. Phys. A 405 (1983) 313

Search for two-octupole-phonon states in ^{208}Pb.
M.A. Mariscotti, D.R. Bes, S.L. Reich, H.M. Sofía, P. Hungerford, S.A. Kerr, K. Schreckenbach, D.D. Warner, W.F. Davidson, W. Gelletly.
Nucl. Phys. A 407 (1983) 98

The high spin structure of ^{100}Rh.
M.A. Mariscotti, A.J. Kreiner, M. Behar, A.O. Machiavelli, G. García Bermúdez, A. Ferrero, C. Baktash, P. Thieberger.
Nucl. Phys. A (in press)

Time - dependent Hartree-Fock-Bogoliubov description of the pairing interaction.
M. C. Cambiaggio, G.G. Dussel, M. Saraceno.
Nucl. Phys. A 415 (1983) 70

High spin states in the doubly odd ^{72}Br nucleus.
G. García Bermúdez, C. Baktash, A.J. Kreiner.
Phys. Rev. C 25 , 3 (1982) 1396

^{10}B + ^{17}O fusion cross section.
Y-d. Chan, D.E. Di Gregorio, J.L.C. Ford, Jr., J. Gómez del Campo, M. E. Ortiz, D. Shapira.
Phys. Rev. C 25, 3 (1982) 1410

Fusion, direct, and total reaction cross sections of the ^{10}B + ^{14}N system up to E_{14} =180MeV.
M.E. Ortiz, J. Gomez del Campo, Y.D. Chan, D.E. Di Gregorio, R.G. Stokstad, J.P.F. Sellschop, R.L. Parks, D. Weiser.
Phys. Rev. C 25, 3 (1982) 1436

Graphical multistep shell-model calculation of the even tin and lead ground states.
C. Pomar, R.J. Liotta.
Phys. Rev. C 25, 3 (1982) 1656

^{129}Sn and ^{129}Sb beta decays.
H. Huck, M.L. Pérez, J. Rossi.
Phys. Rev. C 26, 2 (1982) 621

High-spin states in ^{79}Kr populated by the ^{78}Se(α,3n) reaction and interpreted in terms of a quasiparticle-plus-rotor model.
M. Behar, A. Filevich, A.O. Machiavelli, L. Szybisz, P. Thieberger.
Phys. Rev. C 26, 4 (1982) 1417

$^{14}N + ^{13}C$ fusion cross sections and compound nucleus limitation in ^{27}Al.
D. E. Di Gregorio, J. Gomez del Campo, Y.D. Chan, J.L.C. Ford, Jr., D. Shapira, M.E. Ortiz.
Phys. Rev. C 26, 4 (1982) 1490

Collective states in the doubly odd ^{72}Br Nucleus.
G. García Bermúdez , C. Baktash, O. Kistner.
Phys. Rev. C 26, 4 (1982) 1748

Fusion cross sections for the $^{12}C + ^{15}N$ system.
R. Novotny, D. Shapira, Y-d. Chan, D. E. Di Gregorio, J.L.C. Ford,Jr., J. Gómez del Campo.
Phy. Rev. C 26, 6 (1982) 2664

Equations-of-motion approach to the neutron-proton pairing problem.
F. Andreozzi, A. Covello, A. Gargano, E.E.Maqueda, R.P.J. Perazzo.
Phys. Rev. C 27, 1 (1983) 370

Comparison of upper and lower bound methods using a soluble many-fermion model.
M.C. Cambiaggio, A. Klar, F.J. Margetan, A. Plastino, J.P. Vary.
Phys. Rev. C 27, 6 (1983) 2340

Two correlated quasiparticles states in the principal series approximation.
J. Dukelsky, G.G. Dussel, H.M. Sofía.
Phys. Rev. C 27, 6 (1983) 2954

Fusion and peripheral processes in the collisions of $^{20}Ne + ^{20}Ne$ and $^{20}Ne + ^{16}O$.
D. Shapira, D.E. Di Gregorio, J. Gómez del Campo, R.A. Dayras, J.L.C. Ford, Jr., A.H. Snell, P.H. Stelson, R.G. Stokstad, F. Pougheon.
Phys. Rev. C 28, 3 (1983) 1148

Evidence of g-boson in the ^{218}Ra spectrum.
J. Dukelsky, J.Fernández Niello, H.Sofía,R.P.J. Perazzo.
Phys. Rev. C 28, 5 (1983) 2183

Eherenfest theorem and information theory.
D.Otero, A.Plastino, A.N.Proto and G.Zannolli.
Phys.Rev. A26(1982) 1208

Error sources for the analysis of doppler broadening in positron annihilation spectra.
D.Otero, AN.N.Proto, R.Romero and A.Somoza
App. Phys. A29 (1982) 213.

Multiplet structure in ^{205}Pb and ^{203}Pb.
J. Blomqvist, R.J. Liotta, C. Pomar, L. Rydström.
Phys. Rev C (in press)

Microscopic description of yrast states in spherical nuclei.
R.J. Liotta, C. Pomar.
Phys. Lett. B 112 (1982) 292

An interacting quartet-boson model.
J. Dukelsky, P. Federman, R.P.J. Perazzo, H.M. Sofía.
Phys. Lett. B 115 (1982) 359

The (p,d) reaction: a good test to elucidate the strenght of large energy loss one-step processes.
O. Dragún, A.M.J. Ferrero, A.O. Gattone.
Phys. Lett. B 119 (1982) 25

The structure of the S and D pairs of the interacting boson model from the Hartree-fock-bogolyubov approximation.
S. Pittel, J. Dukelsky.
Phys. Lett. B 128 (1983) 9

The RPA calculation of bandhead energies in many-boson systems.
J. Dukelsky, G.G. Dussel, R.P.J. Perazzo, H.M. Sofía.
Phys. Lett B 129 (1983) 1

The characteristics of electric dipole strength built on highly-excited continuum states.
A.M. Sandorfi, J. Barrette, M.T. Collins, D.H. Hoffmann, A.J. Kreiner, D. Bradford, S. Steadman, J. Wiggins.
Phys. Lett. B 130 (1983) 19

Some implications of a two-component reduction of Dirac phenomenology.
E.D. Cooper, A.O. Gattone, M.H. Macfarlane.
Phys. Lett. B 130 (1983) 359

Cranked Hartree approximation for systems with many interaction bosons.
J. Dukelsky, G.G. Dussel, R.P.J. Perazzo, H.M. Sofía
Phys. Lett B 130 (1983) 123

On the calculation of matrix elements from the time-dependent variational principle.
M.C. Cambiaggio, G.G. Dussel, M. Saraceno.
Phys. Lett. B (in press)

The Nilsson-Bogolubov and the IBM picture of deformed nuclei.
D.R. Bes, R.A. Broglia, C. Maglione, A. Vitturi.
Phys. Rev. Lett. 48 (1982) 1001

Structure of the single-particle states in spherical nuclei within the framework of the multistep shell-model method.
R.J. Liotta, C. Pomar.
Phys. Rev. Lett. 49 (1982) 1142

Prediction of enhanced large angle scattering in heavy ion elastic reactions.
G.G. Dussel, A.O. Gattone, E.E. Maqueda.
Phys. Rev. Lett. 51 (1983) 2366

Multi-step shell-model description of Sn isotopes.
L. Rydström, J. Blomqvist, R.J. Liotta, C. Pomar.
Phys. Scripta T5 (1983) 149

Self-consistent treatmente of the pairing plus quadrupole force in the Nilsson plus BCS model and in the interacting boson model.
D.R. Bes, R.A. Broglia, E. Maglione, A. Vitturi.
Phys. Scripta 28 (1983) 527

The nuclear field theory.
D.R. Bes.
Prog. Theor. Phys. Suppl. 74 (1983) 1

Hechos y personajes en la historia de la Asociación Física Argentina.
M.A.J. Mariscotti
Revista de la Asociación Física Argentina 1, (1983) 2

Band structure of the transitional nucleus ^{218}Ra.
J. Fernández Niello, H. Puchta, F. Ries, W. Trautmann.
Progress in particle and nuclear physics, 9. Pergamon Press, 1983. p. 567

Perturbation treatment of the interaction between correlated many-particle states.
R.J. Liotta, C. Pomar.
Zentrum für Interdisziplinäre Forsechung. Proyect n° 2, 1983-1984.
Universitet Bielefeld, W. Germany.

Perturbation theory for a system of fermions in a deformed basis.
D.R. Bes.
(Contemporary Research Topics in Nuclear Physics, D.H. Feng, M. Vallieres, M.W. Guidry, L.L. Riedinger, ed. New York : Plenum, 1982. p. 309)

SOLID STATE PHYSICS

Ferroelectricity in phase II synthetic troegerite
H.L. Dussel, Lelia Schmirgeld, M.A.R. Benyacar
Ferroelectrics 46, (1982) 25

Phase transitions in $8PbO.V_2O_5$.

R. Baggio, L. Schmirgeld de Wainer, M.A.R. de Benyacar
Ferroelectrics 47, (1983) 9

Phase transitions and physical properties of Pb_8V_2O13 single crystals

R. Baggio, M.A.R. de Benyacar, H. de Dussel, G. Polla, Lelia Schmirgeld.
Ferroelectrics (in press)

The crystal structure of copper strontiom formate, hydrate $(CuSr_2(COOH)_6.8H_2O)$

R. Baggio, P.K. de Perazzo, G. Polla
Acta Crystallographica (in press)

On the influence of different parameters on the phase transition temperatures and ferroelectric domain structure in $H(UO_2)$ (AsO_4). $4H_2O$.

R.F. Baggio, M.A.R. de Benyacar, H.L. de Dussel, P.K. de Perazzo, L. Schmiergeld.
Ferroelectrics (in press)

Lattice dynamics and phase transition of acetylene.
Z. Gamba , H. Bonadeo.
J. Chem. Phys. 76, (1982) 6215

Lattice dynamics and crystal stabiblity of bromine
Z. Gamba, E. Halac , H. Bonadeo
J. Chem. Phys. (in press)

Vibrational density of states of rare-fos crystals doped with impurities.
A. Frigerio, H. Bonadeo, M. Weissmann , N.V. Cohan.
J. Phys. C: Solid State Phys 16, (1982) 3435

A cryostatic cell for polarised Raman studies
E. Halac, N. Gutierrez
J. Phys. E: Scient. Instrum. 16, (1983) 471

Polarized Raman spectra of a single crystal of bromine
E. Halac, H. Bonadeo
J. Chem. 78, (1983) 643

The effects of anisotropic atom-atom interactions on the crystal structure and lattice dynamics of solid CS_2.
E. Burgos, R. Righini
Chem. Phys. Letters 96, (1983) 525

Crystal structure and lattice dynamics of chlorine. The role of electrostatic and anisotropic atom-atom potentials.
E. Burgos, C.S. Murtly, R. Righini.
Mol Phys. 47, (1982) 1391

Mösbauer studies of the corrosion reactions in arc furnace refractories. Part I.
C. Saragovi-Badler, C. Puglisi
Ceramic International (in press)

Mösbauer studies of the corrosion reactions in arc furnace refractories. Part. II.
C. Puglisi, F. Labenski, C.Saragovi-Badler
Ceramic International (in press)

Genesis of sandstone-type uranium deposits in the Sierra Pintada District. Mendoza, Argentina : A Mösbauer study.
F. Labenski, H. Nicolli, C. Saragovi-Badler.
Uranium 1, (1982) 1-18

Influence of a $CuSO_4$ treatment on atmospheric steel rust formation. A Mössbauer spectroscopy study.
C. Saragovi-Badler, I.A. Maier, F. Labenski.
Corrosion 38, (1982) 206

Effects pf growth temperatures and surface roughness on crystal orientation in ice accreted in a dry regime.
L. Levi . F.Prodi.
J. Atmos. Sci, 40. (1983) 1281

Crystal size orientation in ice grown by droplet accretion in wet and spongy regimes
F. Prodi, L.Levi, A.Franzini, C.Scarani.
J. Atmos. Sci. 39, (1982) 2301

Grain Growth in Ice.
L.Levi , E.A. Ceppi.
Il Nuovo Cimento, 5C, (1982) 445

Symmetry and size effects on the determination of critical indices.
Santiago D'Elía, Horacio Ceva.
Phys. Rev. B 26, (1982) 5207

New model hamiltonian with four-spin interactions: phase diagram and formation of domains and walls.
Santiago D'Elía, H. Ceva.
Phys. Rev. B 28, (1983) 4001

Magnetic susceptibility of a model for valence fluctuations between two magnetic configurations: renormalization group approach.
R. Allub, H. Ceva, B. Alascio.
Phys. Rev. B (in press)

Newton Everett interpolation of continuous functions
J.Hernando.
Comp. Phys. Comm. 27, (1982) 73

A modification to PLATTSUM, a program that evaluates electrostatic lattice sums by the planewise summation method
J. Hernando , V. Massida.
Comp. Phys. Comm. (in press)

Identity relations for a certain type of lattice sums
V. Massidda.
Physica 114B, (1982) 327

Numerical method and general discussion of integral equations for the primitive model of the electric interface
L. Blum, J. Hernando, J.L. Lebowitz.
J. Phys. Chem. (in press)

Analytical calculation of a class of integrals containing exponential and trigonometric function
V. Massidda.
Math. of Comput. (in press)

Order-disorder transitions for a two-dimensional lattice of reorientable quadrupoles in the mean-field approximation.
V. Massida, J. H.Hernando.
Physica A (in press)

Charge transfer in structurally disordered alloys.
M Weissmann, N. V. Cohan.
Phys. Stat. Solidi 113 , 6 (1982) 395

Charge distribution in structurally disordered systems.
N.V. Cohan, M. Weissmann.
Solid State Comm. 45, (1983) 427

Calculation of the density of states pd Nb Nx by the recursion method.
A. M. Llois, M. Weissmann , N.V. Cohan.
Solid State Comm. 44, (1982) 681

Cluster calculation on the interaction and discharge of ions on a silver surface.
M. Weissmann, N.V. Cohan.
Journal of electroanal. chem. 146, (1983) 171

Electronic density of states of incommensurate disordered systems.
A.M. Llois, M. Weissmann, N.V. Cohan.
Phys. Rev. B 27, (1983) 7379

Vibrational density of states of rare gas crystals doped with impurities
A. Frigerio, H. Bonadeo, M. Weissmann, N.V. Cohan.
Journal of Physics C 16, (1983) 3435

Phason and amplitudon-like vibrations of one dimensional inconmensurate systems.
N.V. Cohan , M. Weissmann.
Jour. of Phys. C 16, (1983) 5581

Localization in different models for one dimensional in different models for one dimensional inconmensurate systems.
A.M. Llois, N.V. Cohan, M. Waissmann.
Phys. Rev. B (in press)

Specific adsorption of halogen ions on silver surfaces
M. Jauregui, N.V. Cohan, M. Weissmann.
Journal of Electroanal. Chem. (in press)

Comparison between gel grown and solution grown crystals: case of ADP and KDP.
F. Lefaucheux, M.C. Robert, E. Manghi.
J. Cryst. Growth 56, (1982) 141

Hydrogen uranyl arsenate hydrate single crystals: $H_2(UO_2)_2(AsO_4)_2.8H_2O$ gel growth and characterization.
E.Manghi, G.Polla.
J.Cryst. Growth 61, 3 (1983) 606

Geología del nunatak Bertrab, Sector Antártico Argentino.
R.O. Toubes Spinelli.
Contribución del Instituto Antártico Argentino, (in press)

¿Qué es un mineral?
R.O. Toubes Spinelli.
Ciencia divulgada, año 3, noviembre-enero, 91 (1982/83)

Aluminocopiapita zincífera de la mina Santa Elena, quebrada de la Alcaparrosa, provincia de San Juan.
R.O. Toubes Spinelli.
Rev. Asoc.Arg. Miner., Petrol. y Sedim. 13, 1-2 (1982) 25

Edades potasio-argón de algunas rocas de la Sierra de Valle Fértil, provincia de San Juan.
R.O. Toubes Spinelli.
Rev. Asoc. Geolo. Arg. (in press)

Primera mención de kirovita para la República Argentina.
R.O. Toubes Spinelli.
Rev.Asoc. Arg. Miner., Petrol. y Sedim.(in press)

PAPERS PRESENTED AT MEETINGS AND CONFERENCES

Reunión Nacional de Física (1982 : La Plata, Argentina)

Fluctuaciones de valencia entre dos configuraciones magnéticas: grupo de renormalización.
R. Allub, H. Ceva, B. Alascio.

Transiciones orden-desorden en una red bidimensional de cuadrupolos.
V. Massida , J. Hernando.

Densidad de estados electrónicos de sistemas inconmensurados con desorden.
A.M. Llois, M. Weissmann, N.V. Cohan.

Fasones , amplitudones en sistemas inconmensurados unidimensionales.
N.V. Cohan, M. Weissmann.

Construcciones de las configuraciones no equivalentes de "Clusters" finitos con desorden celular usando teoría de grupos.
H. Bonadeo.

Mezcla de configuraciones en modelos con solución exacta.
M.C. Cambiaggio, A. Plastino , L. Szybisz.

Comparación entre dos métodos de máxima superposición.
M. Cambiaggio , A. Plastino.

Dinámica de redes , transición de fase del cristal de acetileno (CrH_2).
Z. Gamba , H. Bonadeo.

Nueva regla para el cálculo de denominadores en diagramas de la NFT.
D.R. Bes , N. Scoccola.

Estados de cuasi-partículas en nucleos esféricos.
R.L. Liotta , C. Pomar.

Ancho de la función excitación de decaimiento .
G.G. Dussel, R.P.J. Perazzo, S.L. Reich , H.M. Sofía.

Hacia una descripción microscópica de la discontinuidad en el gráfico de Mallman.
A.J. Kreiner , C. Pomar.

Hartree-Fock-Bogoliubov en un espacio restringido.
J. Dukelsky, G.G.Dussel , H.M. Sofía.

Estructura del ^{186}Ir , condiciones generales para el desacoplamiento en nucleos doblemente impares.
D. Di Gregorio, A.J. Fendrik, A.J. Kreiner, J. Davidson, M. Davidson.

Búsqueda de estados vibracionales de dos fonones octupolares en el ^{207}Pb.
D.R. Bes,M.A.J. Mariscotti, S.L. Reich,H.M. Sofía.

Estados de alto momento angular en el ^{100}Rh.
M. Behar, A.M.J. Ferrero, G.García Bermúdez, M.A.J. Mariscotti, C. Baktash.

Bandas rotacionales en ^{75}Kr.
G.García Bermúdez, C.Baktash, C. Lister

Obtención autoconsistente del factor de forma para la transferencia de varios nucleones.
S.M. Lenzi, E. Maqueda.

Estructuras simplécticas asociadas a la interacción de fragmentos nucleares.
M. Saraceno.

Efectos de apareamiento de nucleones en procesos de fisión.
D.Napoli, D. Otero, A. Plastino, A. N. Proto.

Teorema de Ehrenfest , teoría de la información en la aproximación termodinámica.
D. Otero, A. Plastino, A.N. Proto.

Tensor no local de tensiones.
E. Duering, D. Otero, A. Plastino, A. Proto, M.A. Figliola

Generalización de la respuesta lineal.
E. Duering, D.Otero, A. Plastino, A. Proto.

Invariantes dinámicos.
E. Duering,D. Otero, A. Plastino, A.N. Proto., G. Zannoli.

Cálculo de la densidad de estados de NbN_x por el método de recurrencia.
A.M. Llois, N.V. Cohan, M Weissmann.

Crecimiento en el gel , caracterización de monocristales de arseniato de uranilo e hidrogeno hidratado (HUAsH).
E. Manghi , G. Polla.

Hamiltonianos no lineales , teoría de la información.
G. Zannoli, D. Otero, A. Plastino, A. Proto.

Anomalías en algunas propiedades físicas del $8PbO.V_2O_5$
Ricardo Baggio, María A. R. de Benyacar, Hilda L. de Dussel , Lelia Schmirgeld, Diana Zadunaisky

Transiciones de fase en HUAsH: histeresis térmica de la transición fase III-Fase II .
M.A. Rodríguez de Benyacar, H. Lanza de Dussel, P. Köning de Perazzo, Lelia Schmirgeld.

Interacción y descarga de iones sobre una superficie de plata.
M. Weissmann , N.V. Cohan.

Cálculo de anarmonicidades de estados colectivos en nucleos esféricos.
P. Curutchet, H.M. Sofía.

Densidad de estados vibracionales de cristales de fases nobles impurificados.
A. Frigerio, H. Bonadeo, M. Weissmann , N.V. Cohan.

Espectros Raman polarizados de monocristal de bromo.
E. Halac, H. Bonadeo.

Caracterización parcial de la evolución estructural del sistema amorfo $La_{70}\ Cu_{30}$.
P.Esquinazi, B.Guillet, H.L.de Dussel.

Síntesis y caracterización de monocristales de $H_2(UO_2)_2(AsO_4)_2\ 8H_2O$.
E. Manghi, G. Polla.

INS International Symposium on Dynamics of Nuclear Collective Motion (1982 : Mt. Fuji, Tokyo)
Proceedings.

Summary talk.
D.R. Bes.

Simposio Latinoamericano de Física de Superficies (2 : 1982 : Puebla, México)

Ecuaciones integrales y reglas de suma para el modelo primitivo de una interfase electrodo-electrolito.
L. Blum, J. Hernando.

American Physical Society. Meeting (1982 : Washington, D.C.)

Fusion of $^{14}N + {}^{13}C$ and compound nucleus limitations in ^{27}Al.
D. E. Di Gregorio, J. Gomez del Campo, Y-d. Chan, J.L.C.Ford, Jr., D. Shapira, M.E. Ortiz.
Bull. Am. Phys. Soc. 27 (1982) 478

Reuniao de Trabalho sobre Física Nuclear no Brasil (5.: 1982 : Itatiaia, Brasil) Revista brasileira de fisica, sept. 1982.

Actividades del grupo de física nuclear teórica de la Comisión Nacional de Energía Atómica.
Silvia L. Reich.

Actividades del grupo de física experimental de la CNEA.
A.J. Kreiner.

The time dependent variational description of the scattering on nuclear fragments.
M. Saraceno.

Nuclear Physics Workshop (5 : 1982 : Chapadmalal, Prov. de Buenos Aires)
Comisión Nacional de Energía Atómica. CNEA-NT 20/58

One and two step processes contribution to the cross section in the preequilibrium regime.
A.O. Gattone, O. Dragún, A.M.J. Ferrero. p. 366

Excitation of the octupole vibration in ^{154}Sm.
O. Dragún, H. Massmann, G. Ramírez. p. 368

Wigner versus Heisenberg processes in pair-exchange reactions.
D.R. Bes, O. Dragún, E. Maqueda. p. 370

Quantal description of the discontinuity in Mallmann's plot.
A.J. Kreiner. p. 379

Structure of ^{186}Ir and general conditions for decoupling in doubly odd nuclei.
D. Di Gregorio, A.J. Fendrik, A.J. Kreiner. p. 382

An interacting quartet-boson model.
J. Dukelsky, P. Federman, R.P.J. Perazzo, H. Sofia. p. 384

Cluster of nucleons as elementary modes of excitation in nuclei.
G.G. Dussel, R.J. Liotta, R.P.J. Perazzo. p. 387

A description of the TANDAR facilities.
E. Pérez Ferreira. p. 145

Some ideas of external users.
M.A.J. Mariscotti. p. 155

Concluding remarks.
D.R. Bes. p. 141

Asociación Física Alemana . Jornadas (1982 : Karlsruhe. Alemania)

Strukture der Yrastzustände in ^{218}Ra.
J. Fernández Niello, H. Puchta, F. Riess, W. Trautmann.

Nordic Meeting on Nuclear Physics (1982 : Djurland, Denmark)

Multi-step shell-model description of Sn Isotopes.
L. Rydström, J. Blomqvist, R.J. Liotta, C. Pomar.

IAEA. Advisory Group Meeting on Data Acquisition Systems (1982 : Viena, Austria)

Preventive maintenance, service and repair of data acquision systems.
D. Camín.

Nordic Meeting on Nuclear Physics (1982 : Djurland, Denmark)

Multi-step shell-model description of Sn Isotopes.
L. Rydström, J. Blomqvist, R.J. Liotta, C. Pomar.

Reunión Nacional de Física (1983 : Tucumán, Argentina)

Síntesis y carácterización de monocristales de oxalatos de Bismuto.
G.Polla, R. Baggio, E. Manghi, P.K. de Perazzo.

Teoría de transiciones de fase: un nuevo paradigma. Informe.
H. Ceva.

Modelos colectivos nucleares. Informe.
R.P.J. Perazzo.

Análisis de la interacción dispersora de 3 cuerpos en sólidos.
E. Burgos.

Transformación topotáctica en $CuSr_2(COOH)_6.8H_2O$.
P.K. de Perazzo, R. Baggio, M.A.R. de Benyacar, G. Polla

Dinámica de redes y estabilidad del cristal de Bromo.
Z. Gamba, E. Halac , H. Bonadeo

Estructuras colectivas en ^{189}Tl.
A.J. Kreiner, H.O. Mosca, L. Riedinger

Bandas rotacionales en ^{180}Re.
D.Abriola, J.Davidson, M. Davidson, A.J.Kreiner, C.Pomar, P.Thieberger.

Estados a alto momento angular en el ^{76}Rb.
G.García Bermúdez, C. Baktash,C. Lister.

Estructura del nucleo transicional ^{218}Ra.
C. Mittag, F. Riess, J. Fernández Niello, H. Sofía, G.G. Dussel, R.P.J. Perazzo.

Estudio de estados de alto espin en ^{217}Ra.
C. Mittag, F. Riess, H. Puchta, J. Fernandez Niello.

Asignación de cascadas de alto espin en isotopos de ^{98}Rh y ^{98}Pd.
M. Behar, A.M.J. Ferrero, A. Filevich, A.O. Machiavelli.

Excitación de dos partículas y dos agujeros.
G.G. Dussel, R.J. Liotta, C.Pomar, S. Reich.

Análisis microscópico de los estados exitados de baja energía en el ^{205}Pb y ^{203}Pb.
J. Blomqvist, R.J. Liotta, C. Pomar.

Nuevo método para interpretar bandas rotacionales desacopladas.
A.J. Kreiner.

Factores de forma para transferencia de varios nucleones.
S.M. Lenzi, E.E. Maqueda.

Cálculo de secciones eficaces de dispersión inelástica de ^{12}C de 70.4 MeV por isotopos de Nd utilizando el método de la matriz S dependiente de coordenadas intrínsecas.
O. Dragún, J. Testoni, M. Bernath, H. Massmann.

Tratamiento perturbativo DWBA modificado, aplicado a la transferencia de partículas alfa entre nucleos deformados.
M. Bernath, O. Dragún, J. Testoni, H. Massmann.

Localización en diferentes modelos inconmensurados unidimensionales.
Ana María Llois, Norah V. Cohan, Mariana Weissmann.

Crecimiento en el gel y caracterización de monocristales de oxalatos de bismuto.
G. Polla, R. Baggio, E. Manghi, P.K. de Perazzo.

Transformaciones de dualidad en un modelo con interacciones de cuatro spins.
Santiago D'Elía.

El algebra de operadores en un modelo con interacciones de cuatro spins.
Santiago D'Elía.

Formación de paredes en un nuevo Hamiltoniano (RCHB) con interacciones de cuatro espines.
Santiago D'Elía, Horacio Ceva.

Determinación del diagrama de fases del Hamiltoniano RCHB mediante la técnica del Monte Carlo.
Santiago D'Elía, Horacio Ceva.

Interacción cuadrupolo-cuadrupolo y transiciones orden-desorden en redes bidimensionales, con aplicación a N_2 sobre grafito.
V. Massida , J. Hernando.

Invariantes dinámicos de 2°orden.
E. Duering, D. Otero, A. Plastino, A.N. Proto.

Interacción cuadrupolar dinámica en el oscilador armónico.
E. Düering, D. Otero, A. Plastino, A.N. Proto, M.S. Torre.

Cálculo de intensidades Raman e infrarrojas del acetileno cristalino.
Z. Gamba, H. Bonadeo.

Variación de resolución en ensanchamiento Doppler.
E. Carpintero, D. Otero, A.N. Proto, A.H. Somoza.

Correlaciones angulares y ensanchamiento Doppler en aniquilación de positrones.
D. Otero, A.N. Proto, A.H. Somoza.

Análisis local de defectos por aniquilación de positrones.
E. Carpintero, D. Otero, A.N. Proto, R. Romero.

Influencia de impurezas sustitucionales e irradiación en las transiciones de fase del $Pb_8V_2O_{13}$.
M. Benyacar, B. Blum, H. Dussel, G. Polla, L. Schmirgeld.

Validez de los primeros ordenes de la NFT en el problema de cuatro partículas en una capa-j.
N. Scoccola, D.R. Bes.

Cálculo de elementos de matriz a partir del principio variacional dependiente del tiempo.
M.C. Cambiaggio, G.G. Dussel, M. Saraceno.

Aproximación de Hartree constreñida a un valor promedio dado del momento angular para sistemas compuestos de muchos bosones.
J. Dukelsky, G.G. Dussel, R.P.J. Perazzo, H.M. Sofía.

Cálculo de las cabezas de bandas de energía en sistemas de muchos bosones utilizando la aproximación de fases al azar.
J. Dukelsky, G.G. Dussel, R.P.J. Perazzo, H.M. Sofía.

Tratamiento perturbativo de un sistema de fermiones deformado.
D.R. Bes, R.J. Liotta, M.T. Mehr.

Distribución de carga en el punto de escisión en fisión fría.
D.R. Napoli, D. Otero, A. Plastino, A.N. Proto.

International Conference on Nuclear Physics (1983 : Florence, Italy)
Proceedings. v. 1. Contributed papers

Calculation of matrix elements from the time dependent variational principle.
M.C. Cambiaggio, G.G. Dussel, M. Saraceno.

Towards a geometric theory of collective motion.
P. Kramer, M. Saraceno, Z. Papadopolos , W. Schweizer.

Hartree-Bose and RPA for many bosons systems .
J. Dukelsky, G.G. Dussel, R.P.J. Perazzo , H.M. Sofía.

Decoupling phenomena in doubly odd deformed nuclei: structure of $^{186}_{Ir}$.
A.J. Kreiner, D.E. Di Gregorio, A.J. Fendrik, J. Davidson , M. Davidson.

Search for two octupole phonon states in ^{208}Pb.
M.A.J. Mariscotti, D. R. Bes, S.L. Reich , H.M. Sofía, W. F. Davidson, P. Hungerford, W.R. Kane , S.A. Kerr, W. Gelletly.

IBA description of the ^{218}Ra Spectrum.
J. Dukelsky, J. Fernández Niello, H.M. Sofía, R.P.J. Perazzo.

The contribution of one an two-step processes to inclusive (p,d) reactions.
A.O. Gattone, O. Dragún, A.M.J. Ferrrero.

Time dependent variational calculation of α-^{16}O scattering.
M. Saraceno, L.F. Canto, R. Donangelo.

Resonances of surface waves and of geometrical rays in ion-ion scattering from an optical potential.
A.R. Farhan, A. Nagl, B. Stoyanov, H. Überall, M. de LLano, Olga Dragún, E. Maqueda, J. R. Seaborn.

Form factors for many nucleon transfers.
S.Lenzi, O. Dragún, E.E. Maqueda.

Spectroscopy of ^{217}Ra.
C. Mittag, H. Puchta, F. Riess, J. Fernández Niello.

Workshop nuclear collective states (1983 : Suzhou, China)
Proceedings. Contributed papers.

Self consistent solutions of many bosons Hamiltonians.
J. Dukelsky, G.G. Dussel, R.P.J. Perazzo, H. Sofía.

International Conference on Highly Excited States of Nuclei (1983 : Orsay, Francia)
Proceedings

The second moment of the stregth function in the RPA.
G.G. Dussel, R.P.J. Perazzo, S.L. Reich, H.M. Sofía.

International Symposium on Nuclear Quadrupole Resonance Spectroscopy (7. : 1983 : Queen's University, Kingston, Canada). Proceedings.

Crystal field and charge transfer in mixed salts of TCNQ.
J. Murgich, J.A. Hernando, V. Massida, H. Soscun.

European Meeting on Ferroelectricity (5.: 1983 : Benalmádena, España)

Phase transitions and physical properties of $Pb_8V_2O_{13}$ single crystals.
R.Baggio, M.A.R. de Benyacar, H.L. de Dussel, G. Polla, L. Schmirgeld.

On the influence of different parameters on the phase transition temperatures and ferroelectric domain structure in $H(UO_2)(AsO_4).\ 4H_2O$.
R. Baggio, M.A.R. de Benyacar, H.L. de Dussel, P.K. de Perazzo, L. Schmirgeld.

Congreso Iberoamericano de Cristalografía (8.: 1983 : Buenos Aires)

Estructura del formiato de Cu y Sr hidratado ($(CO_2H)_6\ CuSr_2 8H_2O$).
R. Baggio, P.K. de Perazzo, G. Nievas.

International Symposium on Nuclear Quadrupole Resonance Spectroscopy (7: 1983 : Kingston, Canadá)

Crystal field and charge transfer in mixed salts of TCNQ
J. Murgich, J. Hernando, V. Massida, H. Soscun.

Congreso del Programa Nacional de Electrónica (1983 : Buenos Aires, Argentina)

La norma CAMAC. Desarrollo locales.
D. Camín.

Controlador de TRC en norma CAMAC.
D. Camín, T. Schmukler.

Controlador autonomo para norma CAMAC.
M. Satinosky, T. Schmukler.

Asociación Argentina de Tecnología Nuclear. Reunión Científica (11. : 1983 : Buenos Aires, Argentina)

Diseño de un espectrómetro magnético para partículas cargadas.
M.C. Berisso, A. Etchegoyen, J.J. Rossi.

El Acelerador de Iones Pesados TANDAR; estado actual del proyecto.
E. Pérez Ferreira.

Sistema de control del acelerador TANDAR.
D.V. Camín, S. Tau.

Pruebas de tensión del acelerador TANDAR.
C. Bolaños, A. Ceballos, N. Fazzini, A. Filevich, H. González, J. Rossi, S. Tau, J. Testoni.

Calibración del voltímetro generador del acelerador TANDAR de 20 Mv.
D. Camín.

Sistema de control del proyecto Nave.
J. Mónico, M. Satinosky.

El Inyector: estado actual y posibilidades futuras.
A. Tersigni, M. González.

Montaje del Acelerador Electrostático de Iones Pesados TANDAR.
A. Binda, N. Fazzini, E. Garay Ramos, H. González, B. Ietri, J. Laffranchi, E. Lolago, C. Míguez, A. Morales, C.A. Palacio, M. Professi, J.C. Rodríguez, J. Vidallé.

Congreso Argentino de Reumatología (26. : 1983 : Mendoza, Argentina) Simposio Internacional de Enfermedades del Tejido Conectivo (2.: 1983 : Mendoza, Argentina)

Estudio cristalográfico de calcificaciones heterotópicas en pacientes con enfermedades del tejido conectivo.
R.O. Toubes, M.A.R. de Benyacar, O. Hüsbscher.

Reuniao de Trabalho de Fisica Nuclear (6. : 1983 : Itatiaia, Brasil)

Aceleradores de Iones Pesados.
M.A.J. Mariscotti.

Asociación Física Alemana. Jornadas (1983: Münster, Alemania)

Lifetime measurements in ^{218}Ra
C.Mittag, J. Fernández Niello, F. Riess.

Spectroscopy of ^{217}Ra.
C. Mittag, J. Fernández Niello, H. Puchta, F. Riess.

Symposium on Panamerican Collaboration (2. : 1983 : Rio de Janeiro, Brasil)

Nuclear Physics in Argentina.
M.A.J. Mariscotti.

Panamerican Workshop on Condensed Matter Theories (7 : 1983 : Altemberg, Alemania)

Classical phase space description of quantum effects in nucleus-nucleus scattering.
M. Saraceno

International Colloquium on Group Theoretical Methods in Physics (12. : 1983 : Trieste, Italy)
Proceedings.

Quantum effects in classical phase space: sympletic structures associated to the scattering on nuclear fragments.
P. Kramer, M. Saraceno.

Tandem Conference (6. : 1983 : Daresbury, England)

The Buenos Aires tandem accelerator facility.
E.Pérez Ferreira, E.Achterberg, D.Camín, A.Ceballos, N.Fazzini, A.Filevich, H.Gonzalez, A.Jech, M.A.J.Mariscotti, J.Milberg, J.Nicolai, R.Requejo, R.Ribarich, J.J.Rossi, S.Tau, A.Tersigni, J.Testoni, E.Ventura.

The SF6 gas handling system for the Buenos Aires 20MV accelerator
N.Fazzini, H.Gonzalez, J.Nicolai, R.Requejo, E.Ventura, G.Feimberg, G.Gidekel, P.Goldschmidt.

Asociación Argentina de Energía Solar. Reunión de Trabajo (8. : 1983 : La Pampa, Argentina)
Actas. (in press)

Utilización de concentradores de radiación solar para la generación de calor para uso industrial en la Argentina.
C. Franciulli, J.A. Moragues.

Instalación térmica para ensayo de concentradores.
E. Mezzabolta, J. Di Santo, C. Franciulli, H. Bajano, C. Bruno, J.M. Kesque, J.A. Moragues.

Pautas para el llamado a concurso de anteproyectos para un edificio administrativo con aprovechamiento de energía solar y diseño para el ahorro de energía.
J.C. Fucaraccio, J. A. Moragues, R.O. Nicolás, A. Rapallini, W. Scheuer, A.A. Elisei

Sistema de seguimiento para concentradores de foco lineal.
C.J. Bruno, J.J. Nicolás.

Reunión de Trabajo de Física Nuclear (6.: 1983 : Buenos Aires)
(in press)

Fenómenos de desacoplamiento en nucleos doblemente impares.
A.J. Kreiner.

Espectroscopía de deformaciones y vibraciones octupolares.
J. Fernández Niello.

Nuevas técnicas experimentales aplicadas al estudio de nucleos muy deficientes en neutrones.
G.G. Bermúdez.

Reacciones de fusión con iones pesados-livianos.
D. E. Di Gregorio.

Aspectos macroscópicos de reacciones con iones pesados. (abstracts)
A. Pacheco.

Principio de máxima entropía en procesos de fisión.
A. Proto.

Dispersión anómala a ángulos traseros.
J. Rossi.

Anisotropía de los fragmentos de fisión.
D. Otero.

La fusión nuclear en función de Z_1Z_2.
D. Otero.

Introducción a las sesiones de sólidos.
M. Benyacar.

Estructura y fases inconmensuradas en los compuestos de la serie M_2XH_4.
M. Benyacar.

Comportamiento dielectrico en compuestos de la serie M_2XH_4.
L. Schmirgeld.

Metaestabilidad en transiciones de fase de primer orden.
J. A. Hernando.

Algunos aspectos sobre irradiación de sólidos no metálicos.
B. Blum.

Propiedades de transporte, ondas de densidad de carga y cargas fraccionarias. Efectos de la radiación.
H. Ceva.

Descripción fenomenológica de las transiciones: N-I E I-LOCK-IN de L Rb2ZnBr4.
H.L. de Dussel.

Dos casos de metaestabilidad en transiciones de fase de primer orden.
P. K. de Perazzo.

Introducción a la sesión de transuránicos.
M.A.J.Mariscotti .

Estado actual de la espectroscopía de transuránicos y propuesto experimental.
A.J. Kreiner.

Blancos de interés para la producción de nucleos muy pesados (A 256) y su posible obtención.
M.A.J. Mariscotti.

Informe sobre la síntesis de elementos muy pesados.
A. Pacheco.

Los NAVE, antecedentes históricos y panorama internacional.
M.L. Pérez.

La facilidad actual. Del Tandem a la computadora.
A. Jech.

Resultados obtenidos en el IALE. Resultados esperables con los NAVE. Otras posibilidades futuras.
H. Huck.

Sistema de control del acelerador 20 UD.
S. Tau.

Estado actual del montaje del acelerador TANDAR.
N. Fazzini.

Sistema de trasvase y recirculación de SF6.
H. González.

El inyector: estado actual y posibilidades futuras.
A. Tersigni.

Estudio de la excitación de bandas rotacionales y vibracionales en nucleos deformados utilizando el formalismo de la matriz S dependiente de las coordenadas intrínsecas.
O. Dragún, J. Testoni, H. Massmann.

The use of a modified DWBA for the study of direct reactions in deformed nuclei.
H. Massman, G. Ramírez, O. Dragún.

Efecto Josephson nuclear.
H. Huck, D. Bes, O. Dragún, A. Jech, N. Scoccola, J.J. Rossi.

Cámara de dispersión multipropósito línea experimental, situación actual.
A. Ceballos.

Reacciones de pre-equilibric inducidas por iones livianos.
A.M.J. Ferrero.

Presentación de las propuestas experimentales de reacciones de transferencia inducidas por proyectiles semipesados.
C. Berisso.

Códigos de análisis de reacciones directas.
E.E. Maqueda.

Aspectos de la física a estudiar.
G. Dussel.

Instrumentación experimental.
A. Filevich.

Informe para el sistema de adquisición de datos.
E. Achterberg.

Ph.D. THESIS

Berisso de Etchegoyen, María Cristina
Nuclear structure, nuclear reactions. University of Oxford, 1982.

Di Gregorio, Daniel
Estudio de reacciones de fusión con iones pesados. Facultad de Ciencias Exactas y Naturales, UBA, 1983.

Gattone, Anibal Osvaldo
Estudio de la contribución a la sección eficaz en el regimen de preequilibrio de los procesos en una y dos etapas. Facultad de Ciencias Exactas y Naturales, UBA, 1983.

Massidda, Victor
Cálculo de sumas reticulares electrostáticas por el método de "suma por planos". Facultad de Ciencias Exactas y Naturales, UBA, 1983.

Pacheco, Alberto
Momento angular en reacciones entre iones pesados. Facultad de Ciencias Exactas y Naturales, UBA, 1983.

Spina, M.E.
Collectivity and statistics in duply-inelastic heavy ion collisions. Heidelberg, Ruprecht -Karls-Universität, 1983.

LICENCIATURA THESES

Bernath, Martín D.
Cálculo de las funciones de onda distorsionadas paramétricas para aplicar al estudio de la transferencia de partículas alfa entre nucleos deformados. - Facultad de Ciencias Exactas y Naturales, UBA, 1983.

Blum, Bárbara
Influencia de defectos en las transiciones de fase del $8PbO.V_2O_5$, Facultad de Ciencias Exactas y Naturales, UBA, 1983.

Cardona, María Angélica
Rendimientos independientes en la fisión de uranio con neutrones térmicos y rápidos. Facultad de Ciencias Exactas y Naturales, UBA, 1983.

Carpintero, Eladio
Códigos de computación para análisis de perfil Compton. Facultad de Ciencias Exactas, Universidad Nacional del Centro, Tandil, 1983.

Curutchet, Patricia
Cálculo de anarmonicidades de estados colectivos de núcleos esféricos. Facultad de Ciencias Exactas y Naturales, UBA, 1982.

Figliola, María Alejandra
Coeficiente de viscosidad, tensor de tensiones y algebra de operadores. Facultad de Ciencias Exactas y Naturales, UBA, 1983.

Gonzalez, Alejandro Daniel
Extensión del formalismo de máxima entropía en sistemas tridimensionales y problemas de perturbaciones. Facultad de Ciencias Exactas y Naturales, UBA, 1983.

Jáuregui, Nélida Marcela
Estudio teórico de la adsorción de iones sobre superficies metálicas. Facultad de Ciencias Exactas y Naturales, UBA, 1983.

Lenzi, Silvia
Cálculo autoconsistente de los factores de forma para transferencia de varios nucleones. Facultad de Ciencias Exactas y Naturales, UBA, 1983.

Mota, Virginia de la
Evolución temporal de variables dinámicas y principio de máxima entropía. Facultad de Ciencias Exactas y Naturales, UBA,1982.

Nievas, Graciela Viviana
Determinación de la estructura cristalina y atómica del formiato de cobre y estroncio hidratado, Instituto Nacional de Profesorado Técnico, 1983.

Rocco, Carmelo J.
Generador de un haz de neutrones rápidos para experiencias en física nuclear. Facultad de Ciencias Exactas y Naturales, UBA, 1983.

Salem, Lázaro
Relevancia del estado de momento angular en el análisis de reacciones de transferencia entre iones pesados. Facultad de Ciencias Exactas y Naturales, UBA, 1983.

Scoccola, Norberto N.
Aplicación del esquema perturbativo de diagramas plegados a la teoría de campos nucleares. Instituto J.A. Balseiro, Universidad Nacional de Cuyo, 1982.

INTERNAL REPORTS

Identificación de minerales radiactivos mediante rayos X.
R. Toubes Spinelli
CNEA-NT 7/82, 1982

Nuclear Physics Workshop (5. : 1982 : Chapadmalal, Prov. de Buenos Aires, Argentina)
CNEA-NT 20/82, 1982

Aprovechamiento directo de la energía solar. Estado actual y perspectivas.
W. Scheuer, J.A. Moragues.
CNEA-NT 1/83, 1983

Sistema a torre central para el aprovechamiento de la energía solar. Estado actual de su desarrollo.
J. A. Moragues.
CNEA-NT 19/83, 1983

Collector for intermediate temperature application.
J. A. Moragues
CNEA-AC 39/82, 1982

TABLE OF CONTENTS

Introduction i

I. TANDAR

I.1 HEAVY ION ACCELERATOR

I.1.1 Electromechanical installation for the Tandar Project..... 1

I.1.2 Assembly of the 20 UD heavy ion accelerator 2

I.1.3 The injector..... 4

I.1.4 SF6 Gas handling plant, assembly and start up 7

I.2. LABORATORIES

I.2.1 Target laboratory 9

I.2.2 ΔE-E telescope for the identification of heavy ions 10

I.2.3 The design and construction of a system to evaluate Lithium precipitation in germanium detectors 11

I.2.4 Generating voltmiter calibration using a capaciting divider . 14

I.2.5 Analog to digital converter for nuclear spectroscopy 16

I.2.6 CAMAC CRT controller 18

I.2.7 Particle identifier 19

I.2.8 Temperature proportional controller 20

I.2.9 CAMAC autonomous crate controller 21

I.2.10 Control electronics for the ion source of the NAVE Project .. 22

I.3 NUCLEAR FACILITIES

I.3.1 Magnetic espectrometer 25

I.3.2 Experimental line for the all purpose scattering chamber ... 25

I.3.3 Nuclei far away for the stability valley (NAVE) 26

I.3.4 The heavy ion scattering chamber 27

I.3.5 Facilitie for on line gamma-ray and electron spectroscopy.... 27

II. NUCLEAR PHYSICS

II. NUCLEAR ESTRUCTURE

II.1.1 Multi-step shell-model description of the Sn isotopes 29

II.1.2 Multi-step shell-model calculation of even-even nuclei 29

II.1.3 Multiplet structure in ^{205}Pb and ^{203}Pb 31

II.1.4 Multi-step shell-model method in light nuclei 32

II.1.5 Perturbation treatment of the interaction between correlated many particle states 34

II.1.6 On the microscopic description of the discontinuity in Mallmann's plot 38

II.1.7 Quantal description of the discontinuity in Mallmann's plot 39

II.1.8 Calculation of matrix elements for the time dependent variational principle 40

II.1.9 Configuration mixing calculations in soluble models. 40

II.1.10 Maximum overlap and critical phenomena..... 40

II.1.11 On an iterative scheme for the solution for the constrained variational equations 41

II.1.12 Methods for describing the coexistence of competing degrees of freedom in a many body system 41

II.1.13 Pair correlations in bosons systems 41

II.1.14 An interacting quartet-boson model 44

II.1.15 The nucleus as a condensate of a monopole pairing vibrations. 44

II.1.16 Search for two octupole phonons in ^{108}Pb 45

II.1.17 Two correlated quasi-particle states in the Principal Series Aproximation 45

II.1.18 Separable interactions and excited states in open-shell nuclei 46

II.1.19 The RPA calculations of bandhead energies in many-boson systems 46

II.1.20 Connection in one body operators in fermion and boson spaces 46

II.1.21 The moments of strength functions 47

II.1.22 Crancked Hartree approximations for systems with many interacting bosons 47

II.1.23 On the assignment of high-spin cascades in ^{98}Rh and ^{98}Pd isotopes 47

II.1.24 Equation of motion approach to the neutron-proton pairing problem 48
II.1.25 The structure of the ^{100}Rh high spin states 48
II.1.26 New data for the controversial ^{100m}Rh scheme 49
II.1.27 High spin states in ^{218}Ra 51
II.1.28 Evidence of g bosons in the ^{218}Ra spectrum 53
II.1.29 High spin states study in ^{217}Ra 51
II.1.30 Deformations of the ^{75}Kr nucleus 52
II.1.31 Band structure in ^{76}Rb 54
II.1.32 New method to interpret decoupled rotational bands 56
II.1.33 Double decoupling in doubly odd deformed nuclei: Structure of ^{186}Ir 57
II.1.34 Excited states of ^{188}Ir populated by the reaction (α,3n) 59
II.1.35 Isovector collective states with K $=1^+$ in deformed nuclei .. 59
II.1.36 Perturbative treatment of rotational motion 60
II.1.37 Validity of the NFT lower orders 61
II.1.38 The structure of the S and D pairs of the interacting boson model from the Hartree-Fock-Bogoliubov approximation... 63
II.1.39 The quenching of $2p_{1/2}$ - $2p_{3/2}$ proton spin-orbit spliting in the Sr-Zr region 63
II.1.40 OXBASH: The Oxford-Buenos Aires shell model code 63
II.1.41 Giant resonances in ^{208}Pb 64

II.2 NUCLEAR REACTIONS

II.2.1 Cross sections calculations based on the intrinsic coordinates dependent collision matrix 66
II.2.2 An investigation of nuclear reactions leading to charge exchange between heavy ions 66
II.2.3 Spin determination via alpha-d angular correlations and α-transfer DWBA analysis in ^{18}F high energies states..... 67
II.2.4 Free particle transfer in ^{14}N 68
II.2.5 A study of the ^{26}Mg(^{12}C,^{12}B)^{26}Al charge-exchange reaction 68
II.2.6 ^{10}B+^{17}O fusion cross sections 69

II.2.7 Fusion, direct and total reaction cross sections of the $^{10}B+^{14}N$ system up to E_{14N} = 180 MeV 69
II.2.8 $^{14}N+^{13}C$ fusion cross sections and compound nucleus limitation in ^{27}Al 70
II.2.9 Fusion cross sections for the $^{12}C+^{15}N$ system 70
II.2.10 Fusion and peripheral processes in the collisions of $^{20}Ne+^{20}Ne$ and $^{20}Ne+^{16}O$ 71
II.2.11 Charge distribution and pairing effects in cold fission processes 71
II.2.12 Prediction of anomalous large angle scattering of heavy ions . 72
II.2.13 Pair-exchange or double-charge-exchange reactions 72
II.2.14 Form factors for many nucleon transfers 72
II.2.15 The (p,d) reaction: a good test to elucidate the strength of large energy loss one-step processes 73
II.2.16 The contribution of one and two-step processes to inclusive (p,d) reactions 73
II.2.17 Alpha particle emission from the reaction 1354 MeV $^{165}Ho+^{181}Ta$ 73
II.2.18 Angular momentum, statistical equilibrium and sequential fission in very asymmetric systems 74
II.2.19 Defected of statistical fluctuations on the measurement of the total energy and multiplicity of gamma-rays following deep-inelastic reactions 74
II.2.20 Intrinsic fragment spins generated in the reactions of ^{20}Ne with ^{197}Au and ^{238}U at 12.6 MeV nucleon 75
II.2.21 Equilibrium treatment of spin-depolarizing modes in mass asymmetric heavy ion system 75
II.2.22 Evidence for spin fluctuation in the deep-inelastic reaction $^{165}Ho+^{165}Ho$ at 8.5 MeV/amu 76
II.2.23 Angular momentum transfer and alignment in deep-inelastic reactions for nearly symmetric heavy ion systems 76
II.2.24 The characteristics of electric dipole strength built on highly excited continuum states 77
II.2.25 Time-Dependent Variational Description of alpha-alpha scattering 77
II.2,26 Study of the $\alpha-^{16}O$ reaction 78
II.2.27 Some physical quantities of interest in nuclear reactions and their dependence upon the projectile-target system: characteristic curves for the TANDAR accelerator..... 78

III. SOLID STATE PHYSICS

III.1 VIBRATIONAL SPECTROSCOPY

III.1.1 Polarized Raman spectra of a single crystal of Bromine 79

III.1.2 Lattice dynamics and crystal stability of Bromine 79

III.1.3 A cryostatic cell for polarized Raman studies 79

III.2 CRYSTAL STRUCTURE AND PHASE TRANSFORMATIONS

III.2.1 The crystal structure of copper strontium formate hydrate $CuSr_2 (COOH)_6 . 8H_2O$ 80

III.2.2 Topotactic transformations in $CuSr_2 (COOH)_6 . 8H_2O$ 80

III.2.3 Phase transitions in $8PbO.V_2O_5$ 81

III.2.4 Phase transitions and physical properties of $Pb_8V_2O_{13}$ 82

III.2.5 On the influence of different parameters on phase transition temperatures and ferroelectric domain structure in $H(UO_2) (AsO_4).4H_2O$ 82

III.2.6 Ferroelectricity in phase II of synthetic troegerite 82

III.2.7 Crystalochemical study of calcinosis from connective-tissue deseases 83

III.2.8 Crystalographic study of heterotypic calcifications present in connective-tissue deseases 84

III.2.9 Identification of radiactive minerals by X-rays..... 84

III.2.10 First mention of Kirovite for the Argentine Republic 84

III.2.11 Zinciferus alumnicopiapite from Santa Elena Mine, La Alcaparrosa Gorge, San Juan Province 85

III.3 CRYSTAL GROWTH

III.3.1 Hydrogen uranyl hydrate single crystals $H_2(UO_2)_2(AsO_4)_2.8H_2O$ gel growth and characterization..... 86

III.3.2 Synthesis of bismuth oxalates single crystals using two different techniques 87

III.3.3 Nucleation of new orientations in water droplets frozen on an ice sustrate 87

III.3.4 Grain growth in ice 88

III.3.5 Effects of growth temperatures and surface roughness on crystal orientation in ice accreted in a dry regime 88

III.3.6 Crystal size and orientation in ice grown by dropled accretion in wet and spongy regimes 89

III.4 MÖSSBAUER SPECTROSCOPY

III.4.1 Analysis argentine biotites samples by Mössbauer spectroscopy 91

III.4.2 Mössbauer studies of the corrosion reactions in arc-furnace refractories. Part I 92

III.4.3 Mössbauer studies of the corrosion reactions in arc-furnace refractories. Part II 93

III.4.4 Quantitative studies of thalassemic red blood cells with Mössbauer spectoscopy 93

III.4.5 Study of clays minerals from Córdoba province, Argentina, with Mössbauer spectroscopy 94

III.5 THEORETICAL SOLID STATE PHYSICS

III.5.1 Cluster calculation on the interaction and discharge of ions on a silver surface..... 95

III.5.2 Calculation of the density of states of NbN_x by the recursion method 95

III.5.3 Electronic density of a state of incommensurate-disordered systems 96

III.5.4 Vibrational density of states of rare-gas crystals doped with impurities 96

III.5.5 Phason and amplitudon-like vibrations of one dimensional incommensurate systems 97

III.5.6 Localization in differents models for one dimensional incommensurate systems 97

III.5.7 Specific adsorption of halogen ions on silver surfaces 98

III.5.8 Analytical calculation of a class of integrals containing exponential and trigonometric functions 98

III.5.9 Order-disorder transtions for two-dimensional lattice of reorientable quadrupoles in the mean-field approximation 98

III.5.10 A numerical method and general discussion of integral equations for the primitive model of the electrical interface.... 99

III.5.11 A program for the evaluation of two-dimensional lattice sums. 99

III.5.12 Nonuniversality in a model hamiltonian with four-spin interactions 100

III.5.13 Dual transforms in a model hamiltonian with four-spin interactions 100

III.5.14 Montecarlo determination of the phase diagram of a model hamiltonian with four-spin interactions 101

III.5.15 A new model hamiltonian with four-spin interactions: phase diagrams and formation of domains and walls..... 101

III.5.16 Magnetic susceptibility of a model for valence fluctuations between two magnetic configurations: renormalization group approach 102

III.5.17 Crystal structure and lattice dynamics of chlorine. The role of electrostatic and anisotropic atom-atom potentials .. 102

III.5.18 The effects of anistropic atom-atom interactions on the crystal structure and lattice dynamics of solid CS_2 103

III.6 GEOLOGICAL APPLIED

III.6.1 Geology of the Bertrab nunatak, Argentine Antartic sector.... 104

III.6.2 Potasium-argon dating of some rocks from Sierra de Valle Fértil, San Juan Province 104

III.6.3 What is a mineral? 105

IV. SOLAR ENERGY

IV.1 Experimental and theoretical studies on solar radiation..... 107

IV.2 Photovoltaic conversion 108

APPENDIX

Perssonel 109

Publications 115

Table of Contents 139

IMPRESO EN CNEA - MARZO 1984